The northern Cache Creek terrane: a record of Middle Triassic arc activity and Jurassic-Cretaceous terrane imbrication

by

Luke Bickerton

B.Sc., St. Francis Xavier University, 2011

Thesis Submitted in Partial Fulfillment of the
Requirements for the Degree of
Master of Science

in the
Department of Earth Sciences

SIMON FRASER UNIVERSITY

Spring 2014

Approval

Name: **Luke Bickerton**

Degree: **Master of Science**

Title of Thesis: ***The northern Cache Creek terrane: a record of Middle Triassic arc activity and Jurassic-Cretaceous terrane imbrication***

Examining Committee: **Chair:** Dr. Andrew Calvert
Professor, Department of Earth Sciences

Dr. Dan Gibson
Senior co-Supervisor
Associate Professor _____

Dr. Maurice Colpron
Senior co-Supervisor
Yukon Geological Survey _____

Dr. Derek Thorkelson
Supervisor
Professor _____

JoAnne Nelson
External Examiner
British Columbia Geological Survey _____

Date Defended/Approved: January 24th, 2014

Partial Copyright Licence

Abstract

The northern termination of the Cache Creek terrane in the Cordillera contains oceanic crustal lithologies including subalkaline mafic intrusive rocks with an arc geochemical signature, mafic volcanics with arc to back-arc signatures, and an arc-flanking volcaniclastic succession informally termed the Michie formation. This formation contains unimodal zircon populations with U-Pb dates of 245.85 ± 0.07 and 244.64 ± 0.08 Ma. These dates differ from the dominant detrital zircon age population of ca. 190 Ma found in the adjacent Whitehorse trough, but are similar to igneous crystallization ages of the Kutcho arc of northern British Columbia. Two main faults record oppositely verging deformational events: 1) The Judas Mountain thrust, a west-verging structure that emplaced Cache Creek terrane rocks above Stikinia and the Whitehorse trough, and 2) the Mount Michie thrust, an east-verging second phase structure that imbricated Stikinia and Whitehorse trough rocks onto and replaced them over the Cache Creek terrane.

Keywords: Cache Creek terrane; Canadian Cordillera; Kutcho arc; Whitehorse trough; U-Pb geochronology; lithogeochemistry

Acknowledgements

I would like to thank Dan Gibson and Maurice Colpron for giving me the opportunity to map the bedrock geology of the Marsh Lake area in Yukon Territory. Thank you for all of your support, mentorship and intellectual insight. I am very thankful to Derek Thorkelson and Don Murphy for taking the time to make suggestions and provide discussions which have greatly improved this thesis. I have also gained considerably from having had the opportunity to work with the entire staff at the Yukon Geological Survey.

I am very grateful to have joined lab mates such as Reid Staples, Ivanka Mitrović and Kirsti Medig, who were very willing to help and were patient with me during my time at SFU and transition to Canada's west coast. I am very thankful to Kevin Cameron and Kevin Gillen for numerous stimulating discussions and for giving me great labs to TA. Vince, Jaap, Flavien, Andrea, Nancy, Joanna and others have made my time at SFU enjoyable and a lot of fun.

I would like to thank Jim Crowley from Boise State University for providing me with U-Pb geochronology results in a timely manner despite welcoming a new family member at the time; his insight to the geochronology aspect of my thesis was very helpful. I am also very appreciative to the staff at the Earth Sciences department of SFU; particularly the assistance of Glenda, Tarja, Matt, and Rodney. I would like to thank my parents, as well as my brothers, for their support and motivation while I pursue my studies.

Table of Contents

List of Tables

List of Figures

Chapter 1.

Introduction

The northern Cordillera of western North America is composed of oceanic and pericratonic terranes, most of which accreted to the continental margin during the Mesozoic (Helwig, 1974; Coney et al., 1980; Monger et al., 1982; Nokleberg et al., 2000). These terranes can be divided into a number of orogenic belts within the Cordillera. The divisions are based on geology, terrane paleogeographic affinity and accretionary events. The orogenic belts in the Canadian Cordillera roughly correspond to the morphogeological belts of Gabrielse et al. (2001; Fig.1, inset), which were defined for the entire Canadian Cordillera, but are perhaps best suited to the southern Canadian Cordillera. The most extensive belt of terranes within the Canadian Cordillera is the Intermontane belt. The Intermontane terranes are composed of the Cache Creek accretionary complex terrane together with the Stikinia and Quesnellia volcanic arc terranes (Fig. 1).

The nature and timing of the accretion of these terranes to one another and to the North American margin are loosely constrained and widely debated. The debate is centered on the enigmatic envelopment of the Cache Creek terrane by the allochthonous island arc terranes, Stikinia and Quesnellia. Components of the Cache Creek terrane contain Tethyan fauna that are exotic with respect to Ancestral North America (Orchard et al., 2001). On the other hand, Stikinia and Quesnellia are island arc terranes partially built upon the mid- to late Paleozoic allochthonous Yukon-Tanana terrane (and correlatives) and contain fauna that have North American affinity (Belasky and Stevens, 2006). Considering the exotic and far traveled elements of the Cache Creek terrane relative to the more endemic terranes of Quesnellia and Stikinia raises the question of how the Cache Creek terrane became surrounded by Quesnellia and Stikinia. Previous models which have been proposed for the mechanism of enclosure include: westward obduction of oceanic crust (Tempelman-Kluit, 1979), northward

dextral displacement and shuffling of terranes (e.g. Packer and Stone, 1974; Beck, 1976; Wernicke and Klepacki, 1988), and eastward "megathrusting" leaving a klippe of Stikinia-Quesnellia and Cache Creek terrane (e.g. Coney, 1989; Samson et al., 1991; Gehrels et al., 1991). The models for enclosure of the Cache Creek terrane listed above each have supporting evidence as well as inherent shortcomings. The first model of Tempelman-Kluit (1979) describes the Cache Creek terrane as evolved from a back-arc basin to the Stikine arc and does not explain the exotic elements of the terrane. The second model of dextral displacement and shuffling of terranes uses paleomagnetic evidence showing a much more southerly paleogeographic location for accreted terranes of the Cordillera (e.g. Packer and Stone, 1974; Beck, 1976); however, accommodation necessary for the northern displacement of these terranes is difficult to confirm along major structures in the Cordillera (e.g. Price and Charmichael, 1986). The "megathrusting" model (e.g. Coney, 1989; Samson et al., 1991; Gehrels et al., 1991) suggests the Cache Creek, Stikinia, and Quesnellia terranes were thrust over the Yukon-Tanana terrane and the western margin of North America. The "megathrusting" model, however, does not correspond to the isotopic signature of postkineamatic Middle Jurassic plutons that intrude the western margin of northern Cache Creek terrane and show no evidence for inheritance from an older, isotopically evolved basement (e.g. Fourth of July Batholith; Mihalynuk et al., 1992). This model is also contradictory to the 3D seismic image of the Canadian Cordillera which shows the deeply rooted terranes accreted to one another (Slave-Northern Cordillera Lithospheric Evolution; Cook et al., 2004; Evenchick et al., 2005). A more recent model for entrapment argues for the impingement of the once-continuous Stikinia/Quesnellia arc by outboard Cache Creek oceanic seamounts, which is interpreted to have triggered oroclinal bending of the arc followed by entrapment of the Cache Creek terrane and its exotic components (Nelson and Mihalynuk, 1993; Mihalynuk et al., 1994).

The purpose of this study is to further describe and interpret the tectonic history of rocks at the northern end of the Cache Creek terrane, located in southern Yukon and compare it with its southeastward continuation in northern British Columbia. The rocks at this northern termination include the aforementioned Intermontane terranes, as well as syn- and post-accretionary basinal rocks. The study area provides an opportunity to examine a mechanism which was proposed to have triggered oroclinal bending and

terrane entrapment in the Mihalynuk et al. (1994) model; this is because the northern end of the Cache Creek terrane lies in the hinge of the proposed orocline. Prior to this study, the relationships between the Cache Creek and enclosing Stikinia and Quesnellia

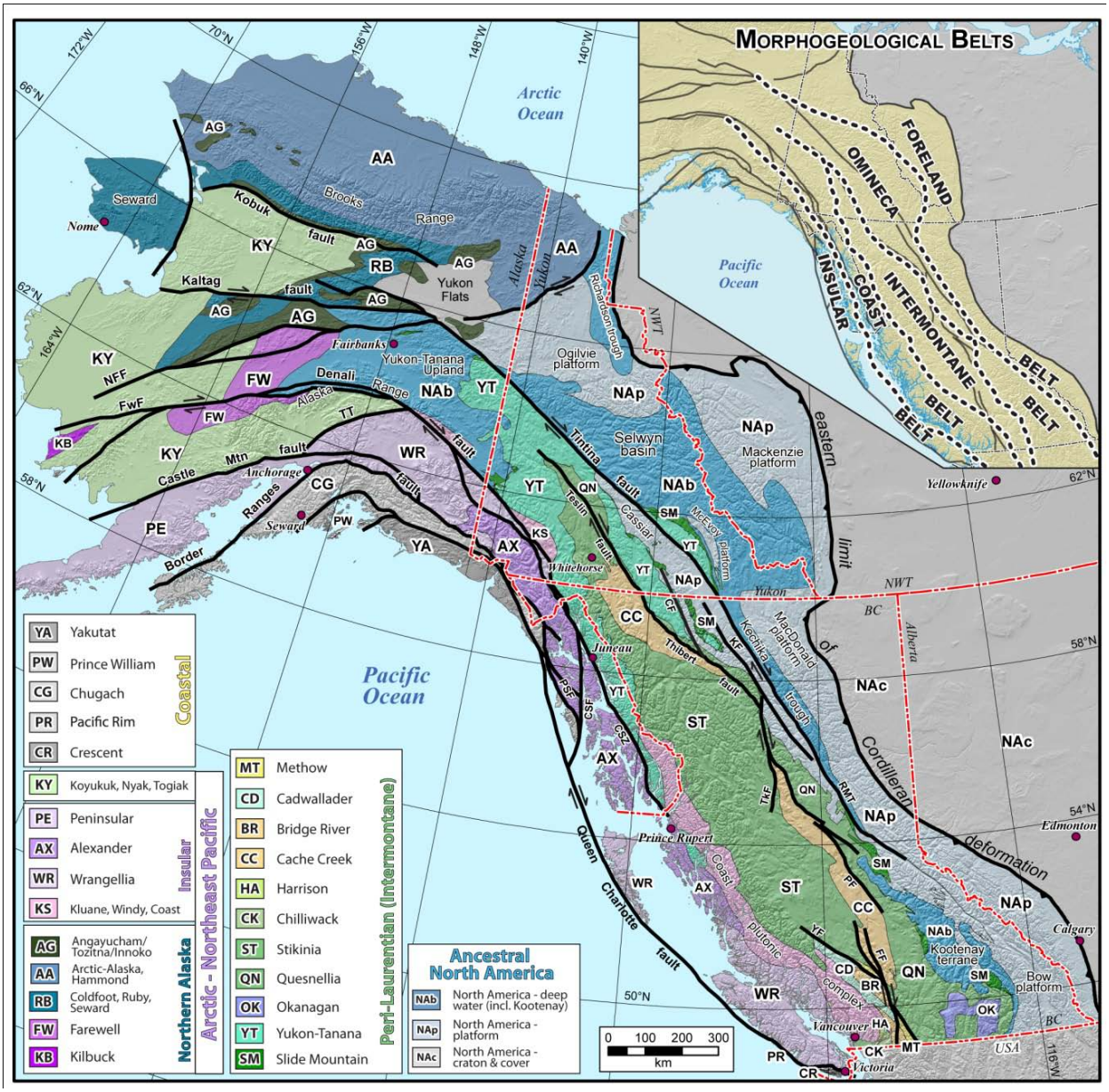

Figure 1. Terranes of the Canadian-Alaskan Cordillera

After Colpron and Nelson (2011), terranes are grouped in the legend according to paleogeographic realms. Inset shows morphogeologic belts of the northern Cordillera after Gabrielse et al. (1991). Fault abbreviations: CF = Cassiar fault, CSF = Chatham Strait fault, FF = Fraser fault, FwF = Farewell fault, KF = Kechika fault, NFF = Nixon Fork-Iditarod fault, PF = Pinchi fault, PSF = Peril Strait fault, NRMT = northern Rocky Mountain trench, TkF = Takla-Finlay-Ingenika fault system, TT = Talkkeetna thrust, YF = Yalakom fault.

terranes at the northern end of the Cache Creek terrane are better understood within British Columbia than in southern Yukon due to a lack of detailed geologic mapping and limited exposure, making geological interpretation difficult.

Previous mapping by Wheeler (1961) at a scale of 1:250 000 covers most of the study area. Wheeler identified many of the lithologies present and their respective stratigraphic relationships. In south-central Yukon, Wheeler (1961) was the first to define the Whitehorse trough, a sedimentary basin which overlaps both Stikinia and the Cache Creek terrane. According to Mihalynuk et al. (1994; 2004), the Whitehorse trough represents a forearc basin that formed during the subduction of Panthalassic oceanic lithosphere (piece of Panthalassic crust) beneath a continuous Stikinia-Quesnellia arc. Cordilleran terrane accretion has led to the development of a number of syn-orogenic depositional basins. Studying these sedimentary basins may provide clues to both the timing of accretion and to the tectonic environment during deposition. Therefore, studying the Whitehorse trough may provide clues to the timing and nature of envelopment of the Cache Creek terrane. Undertaking a more detailed analysis of the Yukon portion of Cache Creek terrane, as well as the associated arc terrane, Stikinia, and sedimentary basin, the Whitehorse trough, can contribute to understanding how the final terrane configuration was achieved.

In this study, mapping at a 1:50 000 scale was conducted on geology and structural relationships of the Marsh Lake area, where rocks of the Cache Creek terrane, Stikinia, and the Whitehorse trough are exposed (Fig. 2). The study documents the nature of the Cache Creek terrane boundaries; in particular, the western boundary north of the Crag Lake fault which was previously interpreted as a southwest-verging thrust fault and northern extension of the Nahlin fault within northern British Columbia (Fig. 2; Gordey and Makepeace, 2001; Colpron, 2011). Additional analyses conducted in this study include U-Pb zircon geochronology and detailed petrography of sedimentary and volcano-sedimentary sequences belonging to the Stikinia and Cache Creek terrane and the Whitehorse trough. Complete descriptions of these units and age populations of zircon grains were used to determine depositional setting for the rocks, as well as sedimentary provenance (and/or time of deposition). Detailed geochemical and petrographic analysis of intrusive rocks in the area was also conducted, particularly those of the extensive pyroxenite and gabbro complex found along the northeastern

shore of Marsh Lake, where they intrude the Cache Creek terrane. Comparing the collected data of Cache Creek terrane rocks within the study area to previous works in north-central British Columbia provides evidence that supports an arc affinity for the rocks of the northern Cache Creek terrane. Geochemical analyses of rocks belonging to the Cache Creek terrane in this area has helped to distinguish the tectonic setting in which they formed as well as helped contribute to constraining age relationships and paleogeographic reconstructions.

Chapter 2.

The northern termination of the Cache Creek terrane near Marsh Lake, Yukon Territory: Evidence for Middle Triassic arc activity and Jurassic-Cretaceous structural imbrication

2.1. Abstract

The northern termination of the Cache Creek terrane lies in south-central Yukon Territory and records accretion of arc and back-arc oceanic crust to the margin of the Stikine terrane. Bedrock mapping in this study has identified a previously unknown siliciclastic to volcaniclastic package informally named the Michie formation, a gabbroic intrusive complex named the Marsh Lake intrusive complex, as well as oceanic crustal volcanic assemblages. The Marsh Lake intrusive complex has a subalkalic geochemical signature indicative of a juvenile arc subduction zone setting. The siliciclastic Michie formation yielded $^{206}Pb/^{238}U$ dates of 245.85 ± 0.07 and 244.64 ± 0.08 Ma from two samples analyzed, similar ages to those of the Kutcho arc assemblage of the western Cache Creek terrane further south. This study proposes that introduction of arc crust into the Stikinia-Quesnellia subduction zone could have led to early Mesozoic cessation of subduction, contributing to oroclinal bending and entrapment of the Cache Creek terrane. The U-Pb zircon age populations obtained from the Laberge Group of the Whitehorse trough include a dominant age population at ca. 190 Ma. Two main phases of compressional deformation have been identified: 1) an initial phase of west-verging thrusting that placed Cache Creek terrane rocks over those of Stikinia and the Whitehorse trough along the Judas Mountain thrust, a northern extension of the Nahlin fault; and 2) a second, phase of east-verging thrusting placed Stikinia and Whitehorse trough rocks back over Cache Creek terrane along the Mount Michie thrust.

2.2. Introduction

Accretionary orogens evolve at plate margins where long-lived subduction promotes continental growth through construction of volcanic arcs and accretion of pieces of lithosphere (terranes) such as micro-continents, remnant ocean basins, and oceanic plateaux (Cawood et al., 2009). The evolution of the western margin of North America in the Mesozoic involved a complex history of terrane growth and accretion that resulted in development of the Cordilleran orogenic collage (Helwig, 1974; Coney et al., 1980; Monger et al., 1982; Nokleberg et al., 2000), one of the archetypical accretionary orogens on Earth (Cawood et al., 2009). In the early Mesozoic, the concurrent growth of regionally extensive allochthonous volcanic arc terranes, Quesnellia and Stikinia, was followed by their accretion to the western margin of North America that resulted in a configuration where the predominantly oceanic Cache Creek terrane was enveloped by these two arc terranes (Mihalynuk et al., 1994; Fig. 2, inset). These island arc terranes were partially built upon mid- to late Paleozoic Yukon-Tanana terrane and correlatives (e.g. Colpron et al., 2006; Nelson et al., 2006). Quesnellia and Stikinia have similar lithological characteristics and geochemical signatures and are thought to have developed while flanking the continental margin (e.g. Mihalynuk et al., 1994).

The Cache Creek terrane is primarily a fore-arc accretionary complex composed of pelagic sedimentary rocks, pieces of oceanic crust, oceanic seamounts with limestone caps, pieces of arc crust, as well as synorogenic clastic rocks (Mihalynuk, 1999). Parts of the Cache Creek accretionary complex have Lower Permian rocks which contain fusulinid fauna of Tethyan affinity that are truly exotic to western North America (Monger and Ross, 1971; Orchard et al., 2001). In contrast, strata of the Quesnellia and Stikinia terranes contain Permian rocks that have McCloud faunal affinity, thought to represent fauna in a northeast Pacific fringing-arc system which lay offshore of western Laurentia during the late Paleozoic (Miller, 1987). The Permian faunal affinity is an indication that the once continuous Stikinia-Quesnellia arc held a proximal position outboard of the western Laurentian margin, and thus, are categorized as peri-Laurentian (Nelson and Colpron, 2007; Nelson et al., 2013). The Cache Creek terrane developed as a fore-arc accretionary complex above an east-dipping subduction zone along the outer,

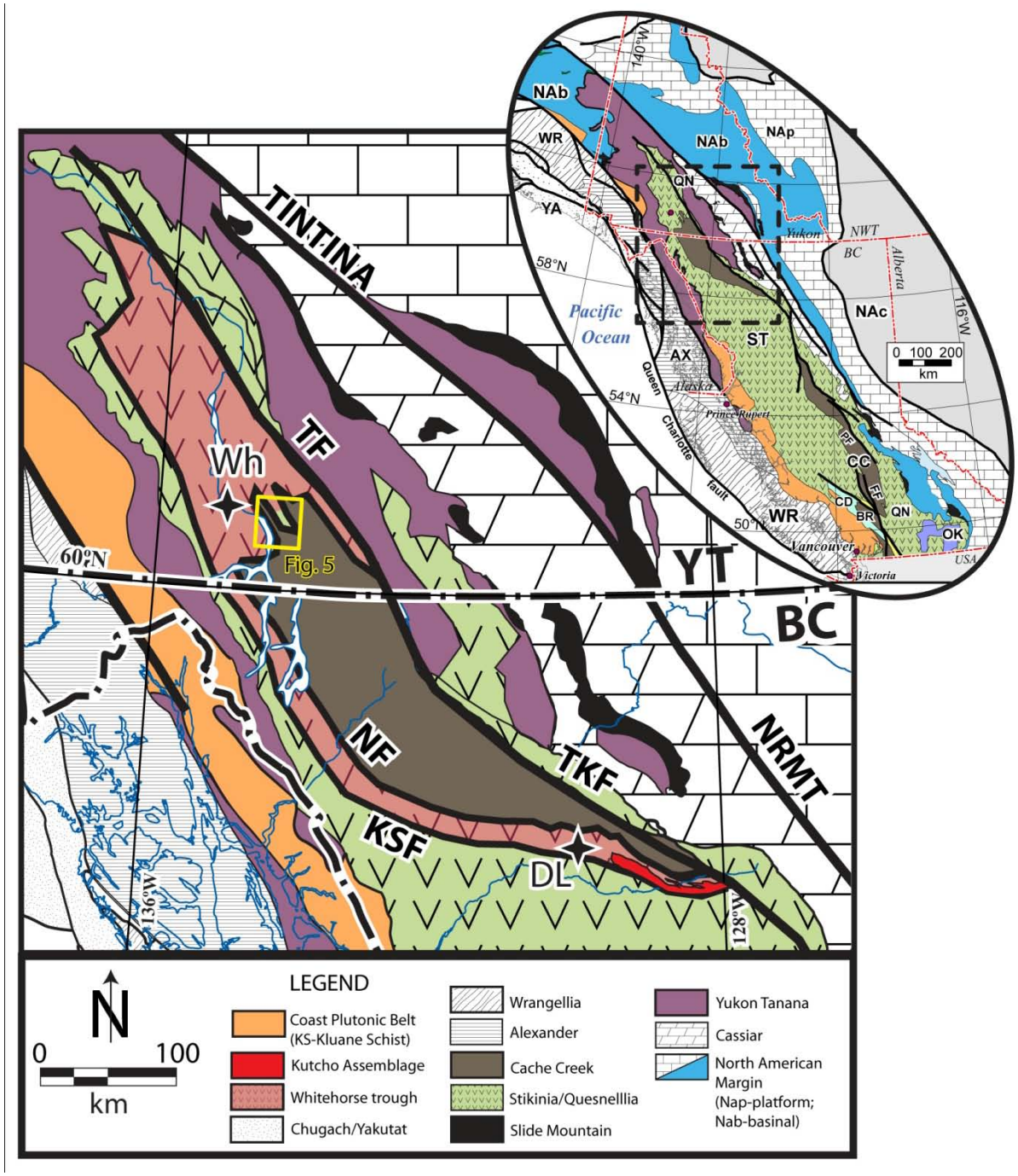

Figure 2. Modified terrane map of the northern Canadian Cordillera

Terrane map modified after Colpron and Nelson (2011), English et al. (2010), and Schiarizza (2011). Inset shows Cordilleran terrane map (Fig.1) at a smaller scale, dashed black box outlines Figure 2. Outline of study area and Figure 5 are also shown. Abbreviations: NRMT –Northern Rocky Mountain Trench fault; TKF-Thibert-Kutcho fault; TF – Teslin fault; NF – Nahlin Fault; KSF – King Salmon Fault; DL – Dease Lake; Wh – Whitehorse; YT – Yukon Territory; BC – British Columbia. See legend in Figure 1 for inset abbreviations.

oceanward side of the Stikinia-Quesnellia arc (Monger and Nokleberg, 1996; Struik et al., 2001).

The Tethyan affinity of parts of the Cache Creek indicates that a portion of the terrane originated far outboard of both western Laurentia and the Stikinia-Quesnellia volcanic arc. The current geometry that has Cache Creek terrane with its exotic Tethyan components enclosed by the peri-Laurentian Quesnellia, Stikinia and Yukon-Tanana terranes, therefore, remains an enigma. The tectonic model to solve this enigma is debated, and thus, studies which examine terrane boundaries between the Cache Creek, Stikinia, and Quesnellia are important contributions to this debate. The terrane boundaries at the northern termination of the Cache Creek has recently been studied in the Atlin and Dease Lake areas of northern British Columbia (e.g. Mihalynuk, 1999; English and Johnston, 2005; Schiarizza, 2012), however, research of similar terrane boundaries in Yukon prior to this study have not been investigated since detailed bedrock geological mapping of Wheeler (1961).

The northern apex of the Cache Creek terrane should contain evidence for the event which ceased subduction of the Panthalassic crust beneath the Stikinia-Quesnellia arc and enclosed the accretionary complex. The Cache Creek terrane has long been recognized as of oceanic-floor and oceanic seamount provenance (Struik et al., 2001). Recent work near the northern termination of the Cache Creek terrane (*e.g.*, English et al., 2010; Schiarizza, 2011) and further south in British Columbia (Schiarizza, 2013), however, indicates that assemblages of early Mesozoic arc affinity are far more abundant within Cache Creek terrane than previously known. This finding has important implications that help explain the partial preservation of seamounts and oceanic plateaux in the Cache Creek terrane. The seamount and oceanic plateau components of the Cache Creek terrane would need to have been underlain by a 30+ km-thick basaltic crust to cease subduction upon collision with the Stikinia-Quesnellia arc (e.g. Cloos, 1993). The accretion of buoyant intra-oceanic arc crust, however, would require ~15 km thickness to have slowed subduction and impact the geometry of the Stikinia-Quesnellia subduction zone prior to arrival of the remaining of Cache Creek terrane components (e.g., Lallemand et al., 1989; Cloos, 1993; Boutelier et al., 2003).

This study presents new data that provide a more complete picture of the geology at the northern termination of the Cache Creek terrane in south-central Yukon. The study area is the Marsh Lake region, which lies approximately 50 km south-east of the city of Whitehorse and roughly 50 km north of the British Columbia – Yukon border at 60^{o} N latitude. Marsh Lake falls within the 1:250 000 scale Whitehorse map sheet produced by J.O. Wheeler (1961; National Topographic System (NTS) 105D). This study proposes that the rocks in this region record the presence of arc crust which was introduced to the Stikinia-Quesnellia subduction zone and could have led to early Mesozoic cessation of subduction. This cessation of subduction could have contributed to the current Stikinia-Quesnellia terrane geometry and entrapment of the Cache Creek accretionary complex.

2.3. Regional Geology

The Stikinia and Quesnellia terranes of the Canadian Cordillera have been interpreted to be a contiguous arc system because of their similarities in lithologies, age range, contact relationships, and isotopic signatures (e.g. Souther, 1977; Dostal et al., 1999). The Quesnellia terrane stretches from the 49^{th} parallel to central Yukon Territory and is dominated by Upper Triassic augite and/or plagioclase-phyric volcanogenic units throughout (Fig. 1; Mortimer, 1986; Dostal et al., 1999). The Stikinia terrane spans a similar length of the Canadian Cordillera but is wider at nearly all intervals from south-central British Columbia to central Yukon (Fig. 1). The oldest exposed rocks in both the Stikinia and Quesnellia terranes are Paleozoic “basement” assemblages which correlate, in part, to the peri-Laurentian Yukon Tanana terrane (Jackson et al., 1991; McClelland, 1992; Mihalynuk et al., 1994; Nelson and Friedman, 2004). In Stikinia, these assemblages are defined by Devonian to lower Permian volcanic, sedimentary and plutonic rocks at the base of the successions, and thick limestone sequences with McCloud faunal affinity at the tops (Gunning et al., 2006; Nelson et al., 2006). Sequences similar to this occur in Quesnellia within the Lay Range of central British Columbia and Harper Ranch Group of southern British Columbia (Simard et al., 2003). Triassic to Jurassic similarities in the Quesnellia and Stikinia terranes include the widespread predominantly augite (-plagioclase) phyric arc volcanic sequences (Takla-Nicola of Quesnellia; Takla-Stuhini of Stikinia) and a suite of Triassic to early Jurassic

plutons which cut both terranes and merge at the northern apex within the Yukon-Tanana terrane (Wheeler and McFeely, 1991). The geochemical and isotopic evidence connecting the Stikinia and Quesnellia terranes throughout the late Paleozoic and early Mesozoic include a similar juvenile $^{87}Sr/^{86}Sr$ signature, negative Nb anomalies, as well as +6 to +8 ε_{Nd} values (Armstrong, 1988; Dostal et al., 1999; 2009).

The Cache Creek terrane is a fault-bounded accretionary complex which lies between Stikinia to the west and Quesnellia to the east (Fig. 1). The Cache Creek terrane includes a mixture of Mississippian to Jurassic lithologies in variable proportions. The terrane extends from the Marsh Lake area of southern Yukon to the Cache Creek area (the terrane's namesake) of southern British Columbia, along strike of the Cordilleran orogen (Fig. 1). The Cache Creek accretionary complex comprises components of oceanic crust including ultramafic rocks (primarily harzburgite, dunite, peridotite and pyroxenite), gabbro, basalt, ribbon banded chert, and massive limestone (e.g. Monger, 1975; Gabrielse, 1991; Struik et al., 2001). The complex also includes forearc sedimentary rocks such as greywacke, siltstone and slate. The age range of ultramafic rocks in the Cache Creek terrane is loosely constrained to be Permian to Triassic in central British Columbia (e.g. Struik et al., 2001) and Early Triassic in southern Yukon based on a U-Pb zircon age of 245.4 ± 0.8 Ma (Gordey et al., 1998). The volcanic rocks are best described in the Nakina River area of northern British Columbia where they consist of fine-grained, massive black basaltic flows and mint green basaltic tuff and flows (Mihalynuk, 1999). Intrusive rocks occur both as lozenges in mélange and as undeformed bodies which have been dated by U-Pb zircon at 261.4 ± 0.3 Ma in the Atlin area of British Columbia (Devine, 2002; Mihalynuk et al., 2003). The Kedahda formation of the Cache Creek terrane in northern British Columbia comprises radiolarian chert as well as siliciclastic rocks consisting of argillite and fine-grained wacke (Mihalynuk, 1999). The radiolarian chert of the Kedahda formation ranges from Guadalupian (middle Permian) to Lower Jurassic in age (Cordey et al., 1991; Jackson, 1992; Mihalynuk, 1999). The Cache Creek terrane also locally contains blueschist grade rocks in areas such as the French Range (Mihalynuk et al., 2004) and the Fort St. James area (Struik et al., 2001).

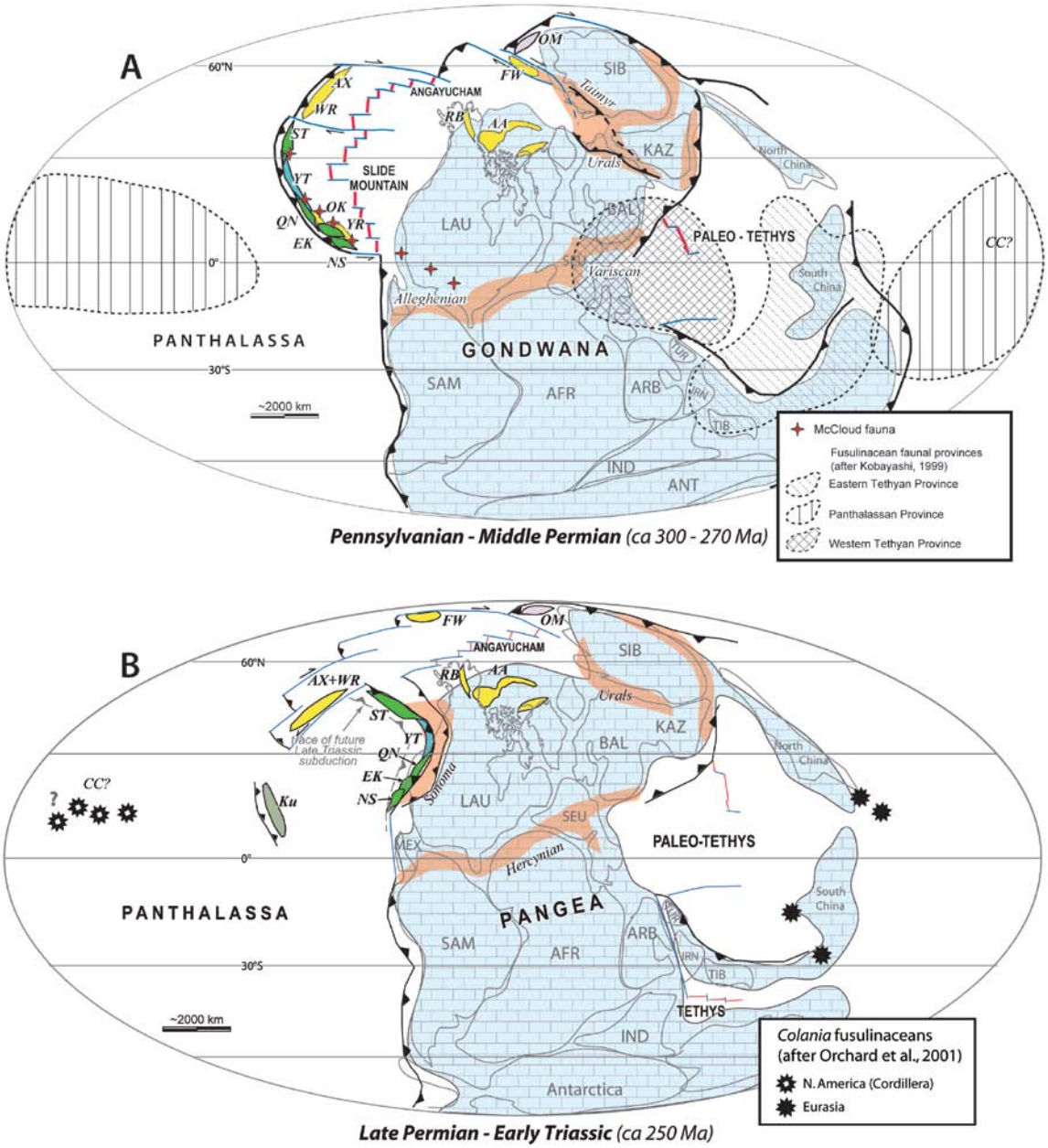

Figure 3. Late Paleozoic paleogeographic reconstructions

Reconstructions are modified after Scotese (2002) and Nelson et al. (2013). (A) Shows paleogeographic distribution of fusulinid faunal provinces in the Middle Permian as defined by Kobayashi (1999), as well as the distribution of McCloud fauna at this time. Symbols in (B) show the Permo-Triassic positions of Middle Permian fusulinid samples from both Eurasia and the North American Cordillera. Note: position of North American fusulinids at this time is loosely constrained but thought to be within the Panthalassic Ocean. AA = Arctic Alaska, AX = Alexander, CC = Cache Creek, EK = Eastern Klamaths, FW = Farewell, Ku = Kutcho arc, NS = Northern Sierras, OM = Omulevka, QN = Quesnellia, RB = Ruby, ST = Stikinia, WR = Wrangellia, YT = Yukon-Tanana. Craton abbreviations: AFR = Africa, ARB = Arabia, BAL = Baltica, IND = India, KAZ = Kazhakstan, LAU = Laurentia, MEX = Mexico, SAM = South America, SEU = Southern Europe, SIB = Siberia.

The thick limestone of the Cache Creek locally contains Early Permian Verbeekinid fusulinid with distinctive Tethyan affinity (*e.g.*, Monger and Ross, 1971). The distribution of Early Permian fusulinids with Tethyan affinity range in provinciality and the genera found in the Cache Creek terrane is restricted to the Permian tropical to sub-tropical Panthalassa (Fig. 3A; Monger and Ross, 1971; Kobayashi, 1999; Orchard et al., 2001). The paleogeographic reconstruction in Figure 3B shows where Middle Permian Tethyan fusulinids recovered from present-day Eurasia and the North American Cordillera (including those of the Cache Creek terrane) are inferred to have been located by Upper Permian to Triassic (Orchard et al. 2001). Although the paleogeographic location of the North American samples is speculative, all samples show evidence for an origin far outboard of the western Laurentian margin and the Stikinia-Quesnellia volcanic arc. In contrast, the Permian limestone within the Quesnellia and Stikinia terranes contain McCloud fauna with Laurentian affinity (Monger, 1977; Miller, 1987). Figure 3A displays the contrast in paleogeographic location for McCloud fauna of Stikinia, Quesnellia, and the southwest United States relative to the possible longitude for parts of the Cache Creek terrane at this time within the Panthalassan province. The McCloud fauna is best described from the fusulinids and corals of the McCloud Limestone of the allochthonous eastern Klamath terrane in the western United States (Skinner and Wilde, 1965).

The presence of limestone with exotic Tethyan fauna in the Cache Creek terrane, as well as the local occurrences of blueschist within mélange in the eastern parts of the terrane suggest protracted subduction of Panthalassic lithosphere beneath a contiguous north-south trending Quesnellia-Stikinia arc. Development of the Cache Creek accretionary complex occurred, at earliest, during the Permian and continued into the Jurassic, as indicated by the preservation of Permian limestone (Paterson and Harakal, 1974; Gabrielse, 1991; Struik et al., 2001) and exposure of Triassic and Lower Jurassic blueschist (ca. 173 Ma, Mihalynuk et al., 2004).

The northern end of Cache Creek terrane terminates in south-central Yukon and extends into northern British Columbia as a southeastward tapered wedge (Fig. 2). This wedge is overlapped by, and imbricated with, the Lower to Middle Jurassic basinal sedimentary rocks of the Whitehorse trough (Laberge Group). Clastic strata of the Whitehorse trough unconformably overlie the upper Paleozoic and lower Mesozoic arc

rocks of Stikinia (e.g. White et al., 2012); these include volcanic, volcaniclastic, silicilcastic and carbonate rocks of the Lewes River Group, originally thought to belong to the Whitehorse trough (Wheeler, 1961). The Lewes River Group is now correlated with the Stuhini Group of Stikinia in British Columbia (Hart, 1997). Whitehorse trough strata also unconformably overlie the Semenof and Shonektaw formations of Quesnellia, which have similar characteristics to that of the Lewes River and Stuhini groups (Gordey and Stevens, 1994; Simard, 2003; Colpron, 2011; Fig. 4). Post-Jurassic imbrication of the Cache Creek terrane, Stikinia, and the Whitehorse trough is documented by southwest-verging folds and thrusts that placed the Cache Creek onto Stikinia by early Bajocian (ca. 175-171 Ma, Mihalynuk et al., 2004; Evenchick et al., 2001). The Cache Creek terrane in northern British Columbia is bounded to the west by the Nahlin fault, which thrust Cache Creek rocks over strata of Whitehorse trough and Stikinia (Gabrielse, 1991; 1998; Mihalynuk, 1999; Mihalynuk et al., 2004; Evenchick et al., 2005; Fig. 2). The juxtaposition of Cache Creek rocks over strata of the Whitehorse trough resulted in detrital input from the Cache Creek terrane into the trough, contributing chert clasts to the Tantalus (Yukon; Long, 2005; Fig. 4) and Inklin formations (British Columbia; Thorstad and Gabrielse, 1986). Imbrication and uplift of the Cache Creek terrane also led to the onset of deposition into another syn-orogenic basin, the Upper Jurassic – Lower Cretaceous Bowser Basin, which overlies Stikinia in central British Columbia (e.g., Ricketts et al., 1992; Gabrielse, 1998). In northern British Columbia, the Cache Creek terrane is bound on the east by the Thibert-Kutcho strike-slip fault system (e.g., Gabrielse, 1985; 1991; Evenchick et al., 2005; Gabrielse et al., 2006) and by the Teslin fault in southern Yukon, the northern extension of the Thibert fault (e.g., Gabrielse et al., 2006; White et al., 2012; Fig. 2). These faults separate the Quesnellia and Yukon-Tanana terranes in the east from the Cache Creek and Stikine terranes to the west. The southwest-verging folds and thrust faults were subsequently dissected by northwest-striking strike-slip faults by mid-Cretaceous (Mihalynuk et al., 2004; English and Johnston, 2005; Colpron, 2011; White et al., 2012).

During the Early Jurassic, the northern apex of the Stikinia/Yukon-Tanana/Quesnellia arc collage was rapidly exhumed and was accompanied by the onset of marine deltaic sedimentation into the Whitehorse trough (Fig. 4; Laberge Group; Lowey, 2004; Lowey et al., 2009; Colpron et al., 2007, White et al., 2012; Nelson et al.,

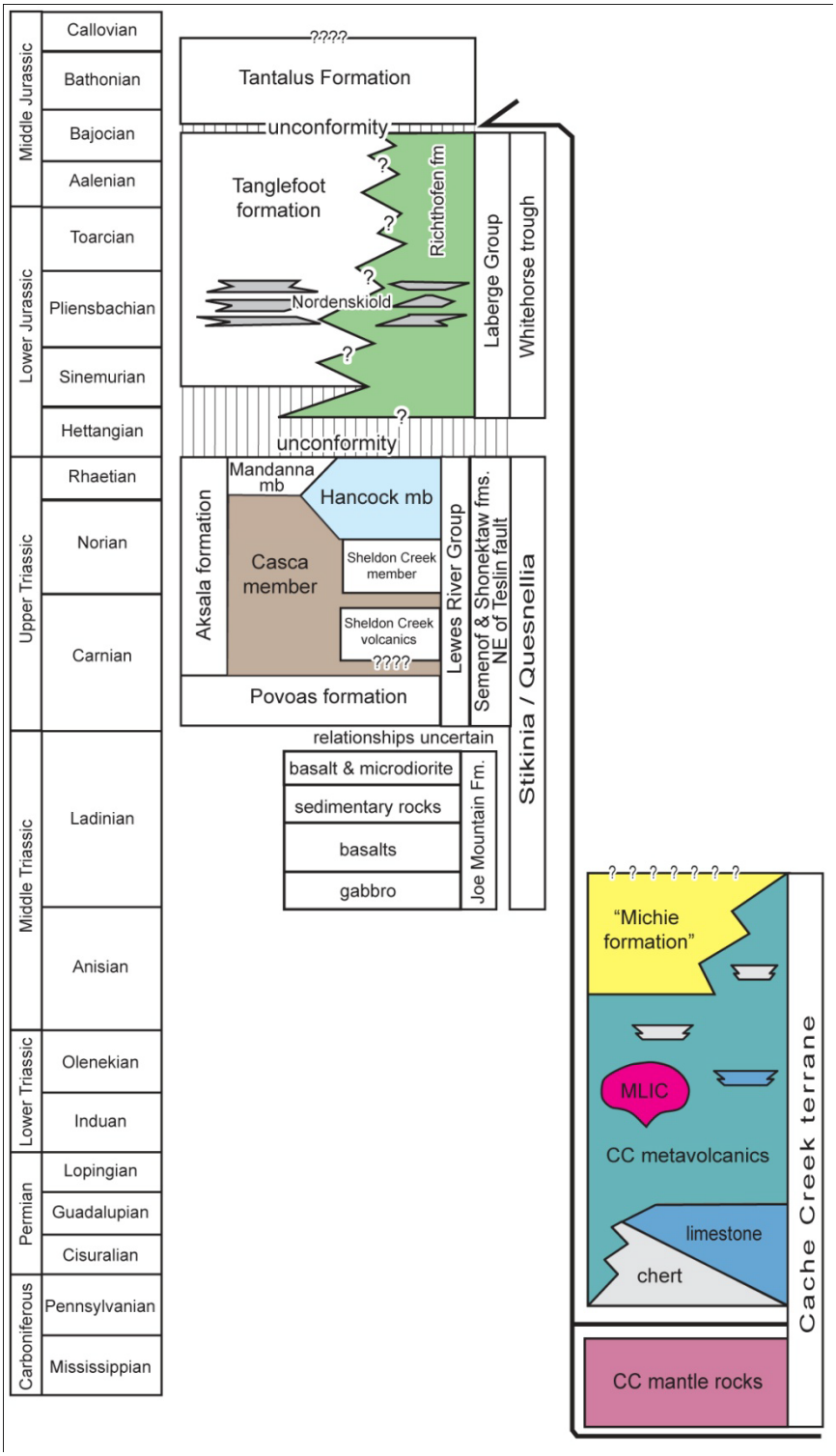

Figure 4. Stratigraphic chart for the study region

Composite stratigraphic section for the Cache Creek terrane, Stikinia, and Whitehorse trough in southern Yukon (modified after Hart, 1997; Lowey, 2004; White et al., 2012). The coloured units are those observed in the study area. CC = Cache Creek, MLIC = Marsh Lake intrusive complex.

2013). The Whitehorse trough is interpreted to record deposition in a forearc setting during the subduction of Panthalassic oceanic lithosphere beneath the Stikinia-Quesnellia arc (Mihalynuk et al., 1994; English and Johnston, 2005; Canil et al., 2006). The basin evolved into a synorogenic piggy-back basin overlaying the accreted terranes by Middle Jurassic (Fig. 2; White et al., 2012).

In the Dease Lake area of British Columbia, southeast of the Nahlin fault, metabasalt and serpentinite occurs at the structural base of the Cache Creek terrane, near the King Salmon fault and is spatially associated with Permo-Triassic bimodal volcanic and volcaniclastic rocks of the Kutcho assemblage (Schiarizza, 2011; Fig. 2). Schiarizza (2011) describes the Kutcho assemblage as a juvenile oceanic arc sequence within the Cache Creek terrane that forms part of the basement to strata of the Whitehorse trough. The U-Pb zircon ages in felsic volcanic rocks within the Kutcho assemblage range from 255.13 ±0.96 to 242 ±1 Ma (Childe and Thompson, 1997; Schiarizza, 2012). The Kutcho assemblage may also correlate with the volcanic Sitlika and Wineglass assemblages located along strike to the south (e.g. Schiarizza, 2013). This correlation is based on overlapping ages, similarities in lithologies and structural relationships at the western boundary of the Cache Creek terrane.

2.4. Geology at the northern termination of the Cache Creek terrane

At its northern termination, near Marsh Lake in south-central Yukon, the Cache Creek terrane comprises five main lithologies which crop out with limited exposure: (*i*) metavolcanic rocks, (*ii*) pyroxenite and gabbro intrusives, (*iii*) hemipelagic chert and shale, (*iv*) tectonized and serpentinized ultramafic rocks, and (*v*) volcaniclastic and clastic rocks informally defined as the Michie formation (Bickerton et al*.,* 2013; Fig. 4). Here, the Cache Creek terrane is structurally imbricated with carbonate and clastic rocks of the Lewes River Group of the Stikinia terrane and the Laberge Group of the Whitehorse trough. This western boundary of the northern termination is represented by the Nahlin fault in northern British Columbia and extends northwards, to southern Yukon, where it is cut by the north-east striking Crag Lake fault near the town of Carcross (Hart and Radloff, 1990). The trace of the cross-cutting fault relationships in this area is

partially obscured by the intrusion of post-accretionary mid- to Late Cretaceous granitoid rocks. The mid-Cretaceous age is based on a single K-Ar date of 104 ± 4 Ma from a diorite stock near the north-eastern shore of Marsh Lake (Fig. 5; Hart, 1995).

2.4.1. Cache Creek Terrane

Metavolcanic rocks

Metavolcanic rocks mainly composed of plagioclase and clinopyroxene within a chloritic matrix are the most widespread unit in the Cache Creek terrane near Marsh Lake (Fig. 5). The basaltic rocks are typically massive, extensively chloritic, and range from dark grey, medium-grained to aphanitic basalt to light grey, fine-grained andesite. They are commonly thoroughly fractured and silicified, and locally contain amygdules filled with both calcite and quartz. The metavolcanic rocks locally show pillows and a hyaloclastic texture. The mafic metavolcanic succession in the map area locally contains metre- to decimetre-scale lenses of limestone and chert. In the eastern part of the map area (105D/9, Fig. 5), the andesite and basalt are intercalated with green-grey volcaniclastic rocks, particularly in proximity to the Michie formation, containing a significant amount of carbonate and chert lithic clasts.

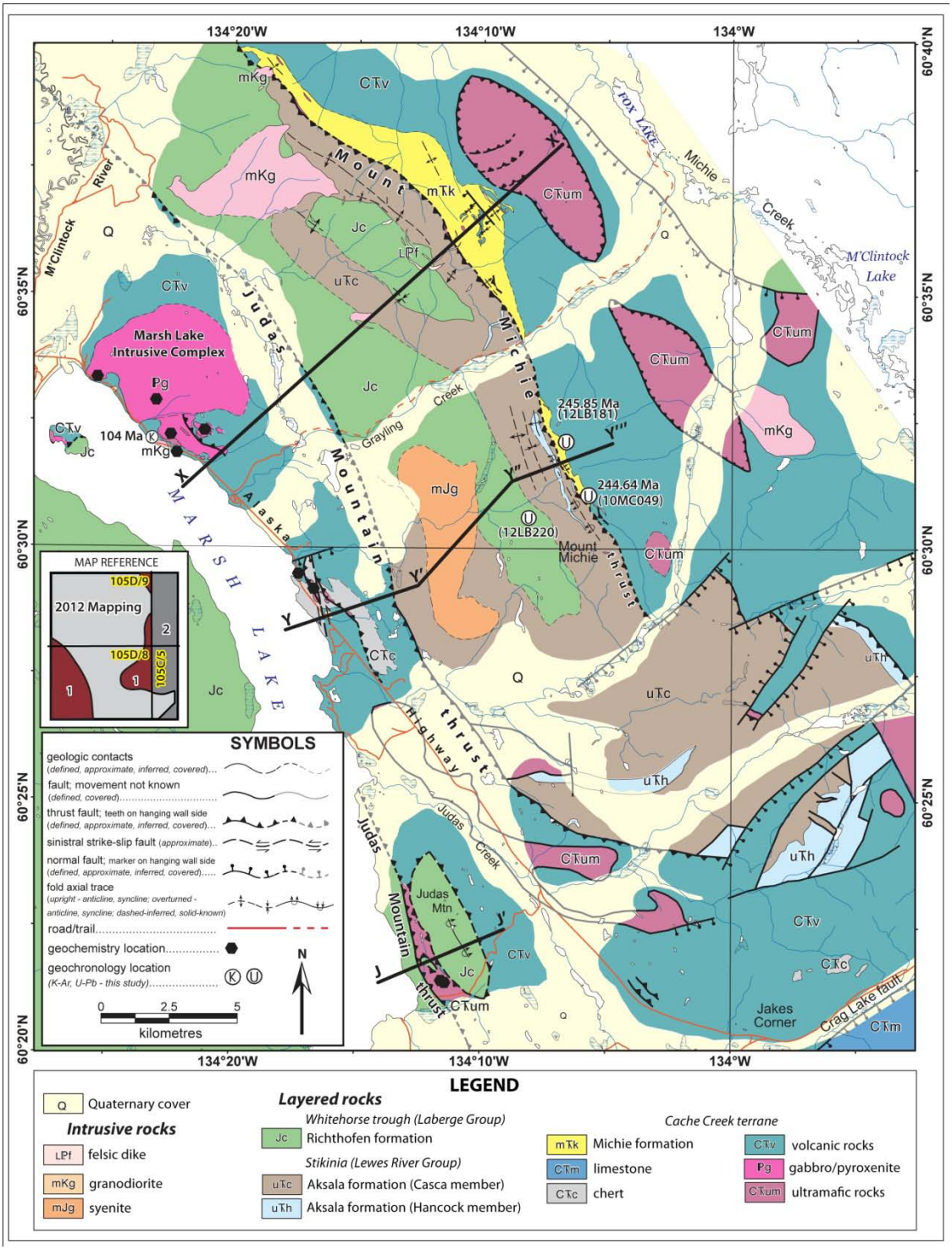

Figure 5. Simplified bedrock geology map of the study area.

Map reference inset shows parts of the map area compiled from 1) Wheeler (1961); and 2) Gordey and Stevens (1994); the author's more detailed mapping straddling the Michie Creek (105D/9), Tagish (105D/8), and Squanga Lake (105C/5) map areas is indicated in light grey. A 1:50 000 scale version of this bedrock geology map is found in Appendix A.

Marsh Lake intrusive complex

A gabbroic complex crops out in the south-central part of the Michie Creek map area, near the north end of Marsh Lake (105D/9; Fig. 5). The complex intrudes exclusively mafic plutonic and volcanic rocks of the Cache Creek terrane. These rocks have extensive chlorite alteration and, locally, are intensely foliated. Compositions range from gabbro to pyroxenite. Olivine-phyric diabase crosscuts the gabbro throughout the intrusive complex. Plagioclase, clinopyroxene and, less commonly, olivine-bearing gabbroic intrusive rocks locally grade into clinopyroxene-dominant pyroxenite (Fig. 6).

Figure 6. Outcrop photo of Marsh Lake intrusive complex

Pyroxene gabbro of the Marsh Lake intrusive complex.

Chert

Chert is one of the more characteristic lithologies of the Cache Creek terrane in British Columbia, but is less extensive at the northern termination of this terrane. Massive chert is locally intercalated with metavolcanic rocks (Fig. 5). The chert commonly crops out as ribbon-banded sections, grey-red-brown in colour and is locally

contorted by soft-sediment deformation (Fig. 7). Bed thicknesses in the chert normally range from 5 to 10 cm with 1 to 3 cm fine-grained argillite interbeds. Hemipelagic chert also appears as subordinate lenses within the metavolcanic rocks and as clasts in volcanic breccia of the Cache Creek.

Figure 7. Outcrop photo of Cache Creek terrane ribbon-banded chert

Outcrop in the Marsh Lake area along the Alaska Highway; rock hammer for scale.

Ultramafic rocks

Ultramafic rocks in the Cache Creek terrane near Marsh Lake are characterized by two main compositions with distinct geographic distribution. The ultramafic rocks exposed in the western part of the study area are typically clinopyroxenite, whereas in the eastern part of the area they have the composition of harzburgite to dunite and typically form larger exposures as thrust sheets structurally above the metavolcanic rocks (Fig. 5). Typical pyroxenites in the western part of the map area, near Judas Mountain and Judas Creek, occur near fault contacts with volcanic rocks, chert and

Laberge Group clastic sedimentary rocks. They are commonly altered to serpentinite and listwaenite (quartz-carbonate-fuschite) and locally brecciated (Fig. 8).

The large harzburgite-dunite bodies in the eastern part of the Michie Creek map area (Fig. 5) are coarse-grained and contain abundant magnetite. Locally, harzburgite shows a subtle cumulate texture of olivine with interstitial orthopyroxene. These rocks also occur as rounded blocks in a sheared ultramafic matrix that has been extensively carbonatized. Veins of antigorite and chrysotile occur throughout these bodies. The large ultramafic bodies are in fault contact with volcanic rocks of the Cache Creek terrane, but unlike those in the western part of the map area, listwaenite alteration is not a prominent feature near these contacts.

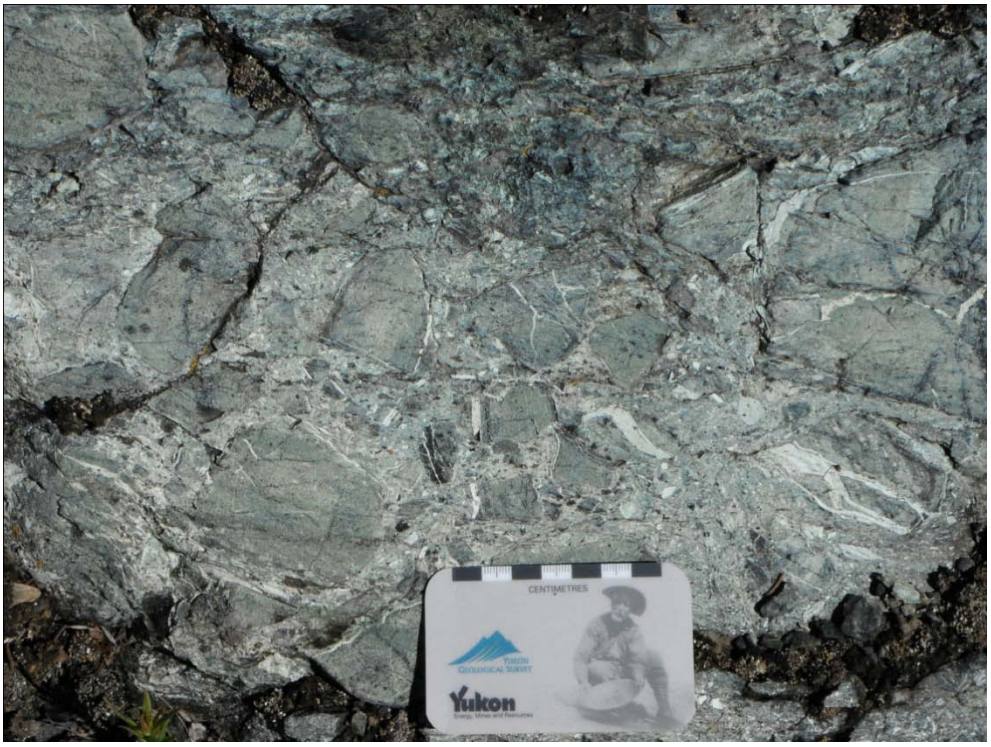

Figure 8. Outcrop photo of ultramafic rock near Judas Mountain

Brecciated serpentinite found west of Judas Mountain.

Michie formation (informal; new unit)

The Michie formation is a previously undocumented stratigraphic unit referring to clastic rocks which overlie mafic metavolcanic rocks in the eastern part of the study

area, from east of Mount Michie extending northwest to the area southwest of Fox Lake (Fig. 5, Appendix A). This formation is composed of a variety of lithologies with no complete section identified. The lithologies include beige, coarse-grained sandstone to wacke, pebble orthoconglomerate, and dark grey siltstone (Fig. 9 a,b and Fig. 10 a). The subrounded to angular clasts in the conglomerate include both mafic and felsic volcanic clasts, limestone, chert, and very fine-grained siltstone (Fig. 10a). Siltstone is

Figure 9. Photos of example lithologies within the Michie formation (I)

a) Coarse-grained wacke; c) overturned, fining-upward sequence of conglomerate, sandstone, siltstone – photo looking north.

commonly coupled with sandstone beds, but locally forms massive sections up to 250 m thick. The siltstone is carbonaceous, giving the bed surfaces an iridescent sheen, and is locally interbedded with buff-weathering limestone beds that are 10 to 15 cm in thickness. Southwest of Fox Lake (Fig. 5), a carbonate-rich debris flow unit occurs near an outcrop of limestone interbedded with siltstone. The Michie formation is locally brecciated and has an intermediate volcanic matrix southwest of Fox Lake (Fig. 10b).

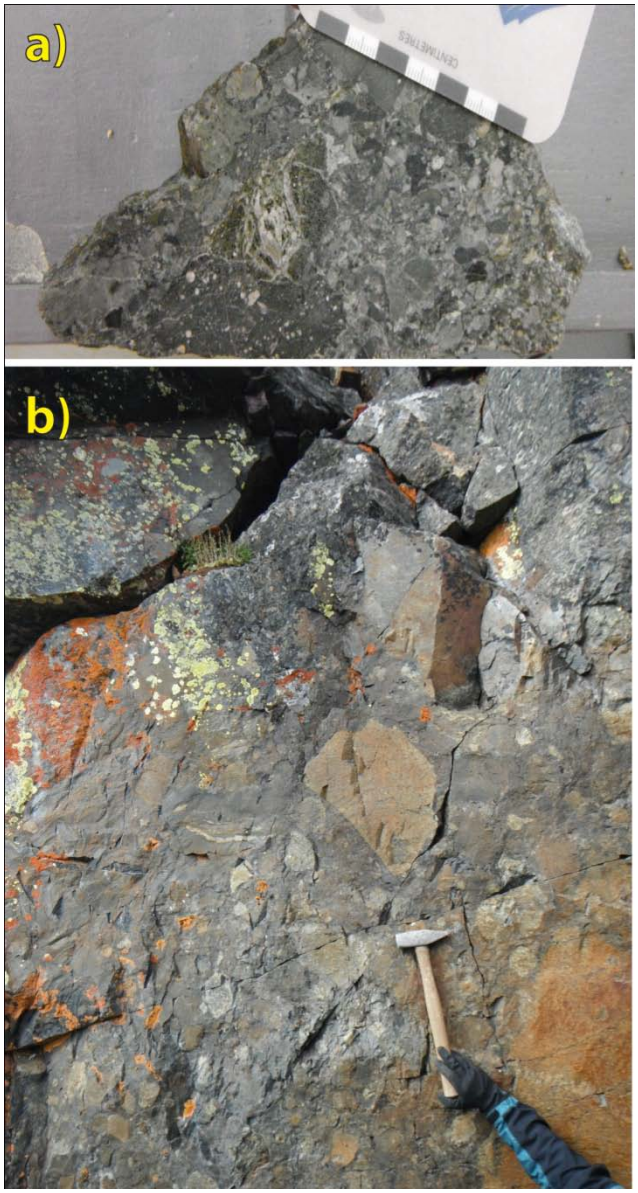

Figure 10. Photos of example lithologies within the Michie formation (II)

a) Slab photo of conglomerate; b) sedimentary clasts within volcanic breccia – photo looking north.

2.4.2. Stikinia

Lewes River Group

Regionally, the Lewes River Group is composed of a volcanic and sedimentary succession that consists of the Povoas formation and Aksala formation, respectively (Tempelman-Kluit, 1984). The Povoas formation is the lower formation and comprises augite-phyric basalt, andesite, and volcaniclastic rocks. The overlying Aksala formation is composed of epiclastic and carbonate rocks. In the study area, only the lower sedimentary units of the Aksala formation are exposed, and have been assigned to the Casca member. These strata vary from coarse-grained, black-grey sandstone to fine-grained, thinly laminated, dark grey argillaceous siltstone. Siltstone units occur as thick, monotonous sections with grey and tan-coloured, very fine-grained sandstone interlaminations. The siltstone beds are commonly graded (Fig. 11a) and contain scour marks, flame structures, rip-up clasts, and locally, trace fossils (Fig. 11b); all indicate that the section is upright. The sandstone of the Casca member has relatively immature grains which are angular to subangular and dominantly poorly sorted. The sandstone occurs as 10 to 20 cm-thick beds among the more dominant argillaceous siltstone.

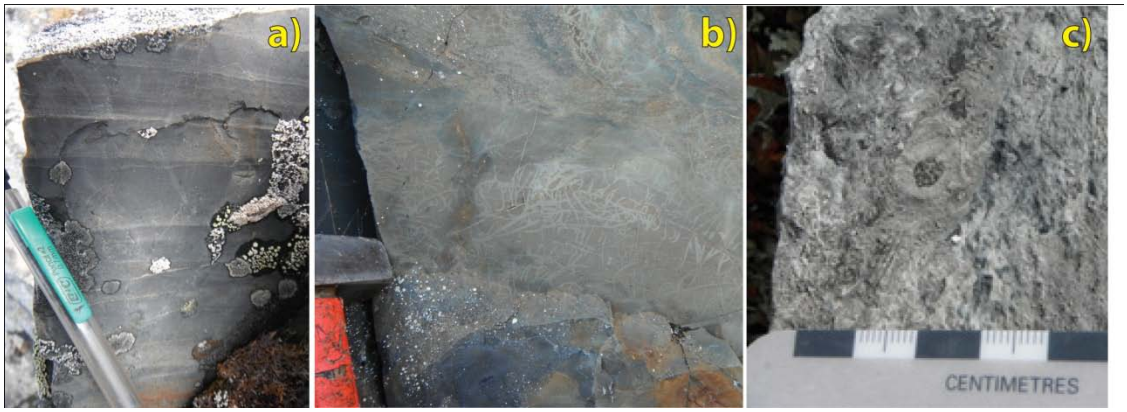

Figure 11. Outcrop photos of layered rocks of Stikinia

a) Graded siltstone of the Casca member in the Aksala formation; (b) trace fossils (*Chondrites*) found within the Casca member of the Aksala formation; (c) limestone interbed in Aksala formation containing coral and crinoid macrofossils.

The Casca member is interpreted as a clastic sequence that represents erosion of the Povoas arc (Fig. 4; Tempelman-Kluit, 1984; 2009; Long, 2005). Elsewhere in the Lewes River Group, the Casca member occurs with a unit of dominantly massive

limestone, the Hancock member. Lithologies similar to the Hancock member are locally interbedded with sedimentary rocks of the Casca member in the Marsh Lake area. These exposures of limestone locally contain mid-upper Norian microfossils and ammonoids with Tethyan affinity (Gordey and Stevens, 1994; Colpron, 2011; Fig. 11c). The Triassic Tethyan faunal affinity in this formation merely indicates a warm-water depositional environment because of the cosmopolitan distribution of marine realm species which followed the Permo-Triassic mass extinction that led to the loss of the provinciality seen in the Permian (e.g. Bambach, 1990; Brayard et al., 2006).

2.4.3. Whitehorse trough

The Whitehorse trough in the study area is represented by rocks of the Richthofen formation of the regionally extensive Laberge Group. These rocks are dominantly sub-greenschist facies and have similar characteristics to the siliciclastic rocks of the Lewes River Group.

Richthofen formation

The Lower to Middle Jurassic Richthofen formation includes black turbiditic siltstone, greenish-grey sandstone and thick matrix-supported polymictic conglomerate (Wheeler, 1961; Hart, 1997; Lowey et al., 2009). All of these units are present in the study area, however, rocks typical of the Richthofen formation crop out on the Marsh Lake shoreline, to the west of Judas Mountain, and trend parallel to the Mount Michie ridgeline in the north-central part of the area (NW-SE; Fig. 5). The medium to coarse-grained sandstone typically forms beds 5 to 15 cm thick and is coupled with fine-grained green-brown mudstone. Sandstone composition varies from quartz-dominant to having a strong volcanic-lithic component. The black siltstone forms monotonous strata up to an estimated 1200 m in thickness, locally showing partial Bouma sequences, ranging from C-D to A-D (Fig. 12a). The Richthofen conglomerate is matrix-supported and is polymictic, with grey, very fine-grained siltstone clasts, pebble- to boulder-sized limestone, felsic plutonic, and less commonly, felsic volcanic clasts (Fig. 12b)

Figure 12. Outcrop photos of layered rocks of the Whitehorse trough

a) Fining-upwards bedding of sandstone and siltstone in the Laberge Group; and b) polymictic paraconglomerate of the Laberge Group.

2.4.4. Post-Accretionary Intrusive Rocks

Granitoids

A number of post-accretionary intrusive rocks assigned to the mid-Cretaceous Whitehorse plutonic suite crop out throughout the study area and range in composition from granodiorite to quartz monzonite (Wheeler, 1961; Gordey and Makepeace, 2001; Colpron, 2011). One exception is a syenitic intrusive body, which crops out in the center of the map area within the Aksala and Richthofen formations.

The igneous bodies range in composition from granodiorite to quartz monzonite and are mostly coarse-grained, equigranular, with alkali-feldspar and plagioclase, as well as minor quartz and biotite. The largest body is approximately 6 km wide, east to west, and 3.5 km long, north to south, and occurs in the northern part of the map area. It intrudes both Casca member and Richthofen formation (Fig. 5). A small quartz monzonite pluton, located approximately 2 km north of the main granodiorite body, crosscuts the Mount Michie thrust which juxtaposes the Michie formation and sedimentary rocks of Stikinia against the Whitehorse trough (Fig. 5).

The syenite intrusion is intermediate in composition and ranges from coarse-grained to pegmatitic, is alkali-feldspar dominant, and contains small (5 to 10 mm) books of coarse-grained biotite and muscovite that are partially altered to chlorite. The body occurs north of the Judas Creek area straddling the Michie Creek and Tagish map areas; it extends approximately 6.5 km north to south, and 1.5 km east to west. The pluton is poorly exposed and its contact is rarely exposed, but it does appear to have intruded the sedimentary strata of the Laberge Group and the Casca member (Fig. 5) where minor hornfels is observed.

Rhyodacite

Rhyodacitic dikes and plugs occur throughout the map area and intrude all map units, making it the youngest unit observed. The rocks are typically medium- to coarse-grained, spherulitic, quartz and feldspar-phyric rhyolite to dacite. The dikes show a well-developed flow-banded texture near their margins and typically have a massive texture with spherulitic feldspar closer to the cores. These intrusive rocks occur as ring dikes, most commonly proximal to the peaks southwest of Fox Lake (Fig. 5). They are similar in character to those recognized in the Atsutla Range of northern British Columbia (Watson and Mathews, 1944; Mathews and Watson, 1953). Regionally, felsic to intermediate intrusive and volcanic rocks which resemble those seen in the map area include the early Tertiary Sifton Range volcanic rocks (e.g., Miskovic and Francis, 2004), the Mount Skukum intrusive rocks (e.g. Love et al., 1998) and Eocene Sloko Group volcanic rocks (Souther, 1991; Mihalynuk, 1999) in northwestern British Columbia and southern Yukon, west of the study area.

2.5. Analytical methods

Samples were collected for petrographic analysis, lithogeochemistry and geochronology in order to better characterize the Cache Creek terrane in southern Yukon, as well as the provenance and depositional setting of clastic rocks in the area.

2.5.1. Petrographic Techniques

Samples were collected and thin sections prepared for petrographic analysis from the Cache Creek terrane volcanic and intrusive rocks (27 samples), the Michie formation (12 samples), the Lewes River Group clastic rocks (5 samples), the Laberge Group clastic rocks (9 samples), and post accretionary intrusive rocks of the map area (7 samples). All sample locations and full petrographic descriptions are presented in Appendix B. A representative selection of medium-grained sandstone and wacke samples from the Michie formation (Cache Creek terrane), the Richthofen formation (Laberge Group, Whitehorse trough), and the Casca member (Aksala formation, Lewes River Group, Stikinia terrane) were chosen for detailed petrography to assist in determining depositional setting and proximity from a dominant detrital source. The general mineralogy of 21 samples was determined petrographically by counting 300-400 points per section using a mechanical stage, following the Gazzi-Dickinson point-counting method (Dickinson, 1970; Ingersoll, 1978; Ingersoll et al., 1984). Group means and standard deviations of general mineral content are shown in Table 1.

2.5.2. Lithogeochemistry

Representative samples were collected from gabbroic intrusive and mafic volcanic rocks of the Cache Creek terrane for whole-rock geochemical analysis (Fig. 5). The primary goal of the geochemical analyses is to characterize tectonic affinity of the mafic rocks of the Cache Creek terrane in south-central Yukon and to facilitate comparison of these rocks to those in the Atlin area of northern British Columbia (e.g. English et al., 2010).

Major and selected trace elements were analyzed by X-ray fluorescence at Activation Laboratories in Ancaster, Ontario. Rare-earth element (REE) analyses were also determined by inductively coupled plasma – mass spectrometry (ICP-MS). These data were combined with the unpublished results of seven samples from the same area collected by Stephen Piercey in 2005 (herein termed SJP samples; Table 2). Details of the analytical methods, precision, and accuracy for these samples are presented in Ruks et al. (2006) and Piercey et al. (2004).

2.5.3. Geochronology

In order to constrain the provenance of rocks in the Michie formation and the Richthofen formation of the Laberge Group, representative samples of coarse-grained sandstone from each unit were collected for U-Pb detrital zircon geochronology. One sample from the Richthofen formation (12LB220) was processed for geochronology, and of the six samples collected from the Michie formation, two samples yielded zircon grains (12LB181 and 10MC049). The geochronology was undertaken at Boise State University using two methods for the age analyses; laser ablation inductively coupled plasma mass spectrometry (LA-ICPMS) for rapid, reasonably precise reconnaissance dating of the detrital zircon and chemical abrasion isotope dilution thermal ionization mass spectrometry (CA-TIMS) when more precise results were sought for samples with a unimodal zircon population.

LA-ICPMS

Zircon grains were separated from rocks using standard techniques and annealed at 900^{o} C for 60 hours in a muffle furnace. They were mounted in epoxy, polished to the grain centers and imaged using cathodoluminescence (CL) on a JEOL JSM-1300 scanning electron microscope in order to characterize the internal zoning of the zircon grains. The LA-ICPMS consisted of a ThermoElectron X-Series II quadrupole ICPMS and New Wave Research UP-213 Nd:YAG UV (213 nm) laser ablation system. Data were collected from two samples during two analytical sessions conducted in May 2011 (session 1, sample 10MC049) and March 2013 (session 2, sample 12LB220). Laser ablation spot size was 25 microns, and a laser firing repetition rate of 10 Hz. Standard calibration uncertainties for $^{207}Pb/^{206}Pb$ dates are 0.7 and 0.5% (2σ) for experiments 1 and 2, respectively. Standard calibration uncertainty for $^{206}Pb/^{238}U$ dates are 2.0 and 3.2% (2σ for experiments 1 and 2, respectively). Errors on the $^{207}Pb/^{206}Pb$ and $^{206}Pb/^{238}U$ dates from individual LA-ICPMS analyses are given at 2σ, as are the errors on the weighted mean dates. A complete summary of the in-house analytical protocols, standard materials, and data reduction software used for acquisition and calibration of U-Pb dates and acquisition of a suite of high field strength elements (HFSE) and rare earth elements (REE) are provided in Appendix C. A summary of the

analytical results for all samples is provided in Table 3. Age interpretations are based on the $^{206}Pb/^{238}U$ chronometer.

CA-TIMS

Zircon grains extracted from the samples using standard separation techniques were mounted in epoxy and polished to grain centres. Prior to CA-TIMS analyses, CL images were obtained. Approximately 8-10 zircon grains or fragments from two samples of the Michie formation (10MC049; 12LB181) were selected for dating based on the CL images. The grains selected for analysis were removed from the epoxy mounts and subjected to a modified version of the chemical abrasion method of Mattinson (2005); a complete summary of the CA-TIMS method used in this study can be found in Appendix D.

Age interpretations based on the weighted mean $^{206}Pb/^{238}U$ ages were calculated using Isoplot 3.0 (Ludwig, 2003; Table 4). Errors given at the 2σ confidence interval on the weighted mean age reflect the internal errors based on analytical uncertainties only, including counting statistics, subtraction of tracer solution, and blank and initial common Pb subtraction. Errors on the $^{206}Pb/^{238}U$ dates from individual grains are also given at the 2σ confidence interval. A summary of the analytical results for the CA-TIMS analyses is provided in Table 4, where bolded samples are those which were used in the weighted mean age results.

2.6. Results

2.6.1. Petrography

Samples from the Michie formation were collected for petrographic analysis and, in order to compare these samples to fore-arc and syn-orogenic depositional basin facies of the Stikine terrane and Whitehorse trough, representative samples of the Casca member (Lewes River Group, Stikinia) and Laberge Group (Whitehorse trough) were collected for the same purpose. As the volcaniclastic rocks of the Michie formation are locally intercalated with volcanic rocks attributed to the Cache Creek terrane, characterizing the detrital source rock can constrain the depositional proximity to the

Stikinia-Quesnellia arc versus another detrital source for these clastic rocks. Further petrographic description of samples from the Marsh Lake intrusive complex was completed by transmitted-light microscopy and complete descriptions are found in Appendix B.

Table 1. Point-count data from clastic samples in study area

Formation		QFL%			LmLvLs%			Fr%	Fr%	Fr%
		Q	F	L	Lm	Lv	Ls	Bt	D	M
Richthofen	Mean	35.08	27.76	37.16	0.00	83.66	16.34	1.03	10.79	1.37
	SD	10.44	12.43	4.70	0.00	5.18	5.18	0.54	5.83	1.45
Aksala	Mean	31.06	62.16	6.78	0.00	66.75	33.25	1.93	7.10	5.32
	SD	9.34	9.47	5.87	0.00	23.64	23.64	1.35	4.50	3.26
Michie	Mean	16.81	15.85	67.34	4.46	78.82	16.73	9.54	2.80	6.71
	SD	6.54	7.44	8.08	7.95	12.65	6.61	5.34	2.25	5.31

Formation		QmFL%			QmPK%			QpLvmLsm%			
		Qm	F	Lt	Qm	P	K	Qp	Lvm	Lsm	P/F
Richthofen	Mean	27.29	27.76	44.95	76.67	23.33	0.00	16.41	69.99	13.59	0.93
	SD	8.94	12.43	8.17	25.88	25.88	0.00	7.36	8.25	4.06	0.07
Aksala	Mean	21.00	62.16	16.84	44.48	48.99	6.54	60.10	25.07	14.83	0.86
	SD	9.22	9.47	9.12	30.48	27.09	6.44	28.24	15.62	15.66	0.07
Michie	Mean	9.26	15.85	74.89	93.38	6.50	0.12	10.47	71.84	18.45	0.98
	SD	5.55	7.44	9.89	18.72	18.37	0.35	8.49	15.07	8.89	0.02

Notes:
Mean measures average number of points counted in all samples for a given formation, SD measures the standard deviation for the counts.
Q - quartz, F - Feldspar, L - Lithic clast, Lm - metamorphic lithic clast, Lv - volcanic lithic clast, Ls - sedimentary lithic clast; Fr% - percent of total fragments which is: Bt - biotite, D - dense minerals (i.e. hornblende, pyroxene, opaques), M - phylosilicates (i.e. biotite, chlorite, muscovite)

Michie formation

The Michie formation is characterized by immature volcaniclastic to polymictic sandstone and wacke which range in grain size from medium to coarse-grained. The grains are typically sub-rounded, of various compositions and moderately to poorly sorted. The rock units vary from calc-lithic to volcanic lithic arenite in composition. Among the 8 samples examined, a majority have a mineralogy with predominate lithic grains, particularly volcanic and fine grained mafic intrusive clasts, and to a lesser extent, chert and siltstone clasts. The grain counts in the Michie formation reveal a notable carbonate population relative to the other clastic units in the area (Table 1). Other accessory clasts include greenstone metamorphic clasts. The modal percentage of typical quartz-feldspar-lithic clast mineralogy in the Michie formation samples indicate provenance from an undissected to transitional arc (Fig. 13).

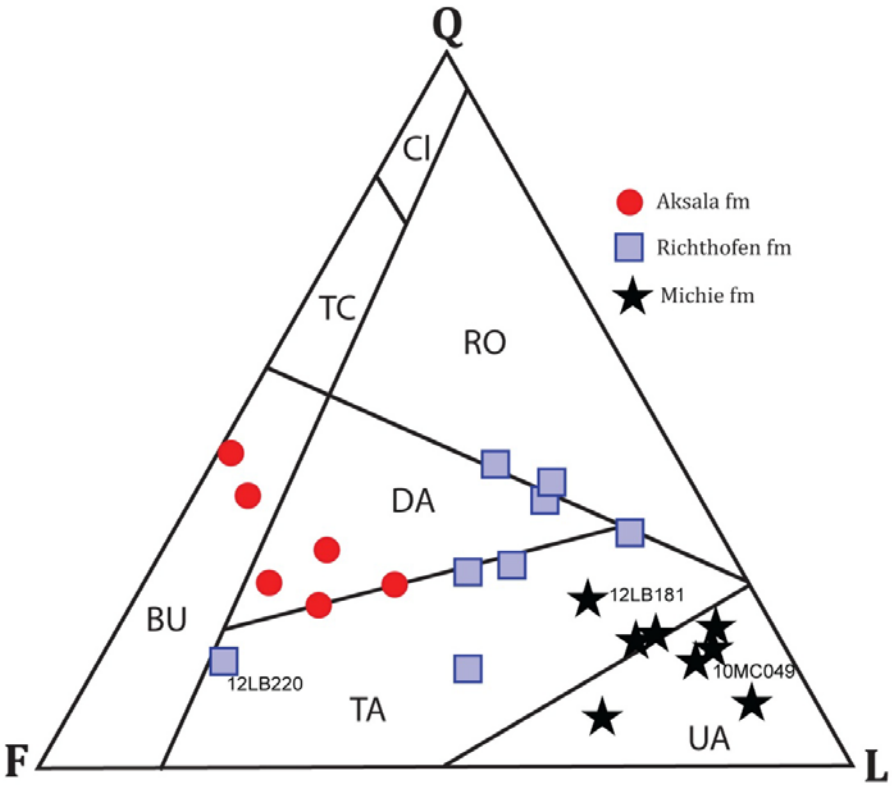

Figure 13. QFL (Quartz-Feldspar-Lithic clast) triangular plot
Plotted points represent spread of sample compositions for each formation. The template provenance fields of Dickinson et al. (1983) are abbreviated: CI, craton interior; TC, transitional continental; RO, recycled orogenic; BU, basement uplift; DA, dissected arc; TA, transitional arc; UA, undissected arc. In the arc-related provenance fields (UA, TA, DA), the degree of arc dissection increases from right to left.

Aksala formation, Lewes River Group

The siliciclastic rocks of the Casca member within the Aksala formation of the Lewes River Group are typically moderately to well-sorted, submature, subangular fine to coarse-grained lithic arkose to arkosic arenite. General mineralogical determinations show that the sandstone is dominated by feldspar with a high plagioclase-to-alkali feldspar ratio (P/F; Table 1).The mineralogy also includes quartz grains, volcanic lithic and chert grains, hornblende, with minor carbonate and chlorite. The feldspars show minor sericite alteration and mafic minerals are replaced by chlorite. Six samples of dominantly fine to medium-grained feldspathic arenite compositions were examined by point-counting and have an interpreted provenance straddling basement uplift and dissected arc tectonic settings (Fig. 13).

Richthofen formation, Laberge Group

The Richthofen formation contains subangular fine to coarse-grained, moderately to poorly sorted, immature feldspathic litharenite. The rock is dominated by lithic fragments, ranging from volcanic to chert, but also contains quartz and feldspar as major components and hornblende as a minor component. Accessory phases include opaques, zircon and apatite. The general mineralogy in the 8 samples examined showed a relatively even distribution of modal percentages, a lithic clast content dominated by volcanic clasts, and a P/F ratio of 0.93 (Table 1). The Richthofen samples, which were analyzed by point-counting, plot in the dissected to transitional arc field in Figure 13.

Marsh Lake intrusive complex

Nine samples of the Marsh Lake intrusive complex were collected for petrographic analysis to compliment whole-rock geochemistry and better characterize the pyroxenite and gabbro intrusive rocks. The complex contains medium and coarse-grained to porphyritic samples of gabbro, gabbronorite and pyroxenite. Groundmass in these samples typically is composed of very fine-grained plagioclase. Crystals of clinopyroxene are subhedral to euhedral and typically have embayment and sieve textures, as well as local cumulate textures. Samples in the Marsh Lake intrusive complex show weak epidote alteration throughout, with intense alteration locally. Accessory phases include magnetite and apatite.

2.6.2. Lithogeochemistry

Cache Creek mafic igneous rocks

Nine mafic rock samples from the Cache Creek terrane were selected for geochemical analysis. These are combined with the data of seven samples collected in the same area by Steve Piercey (noted as SJP). Five samples (11LB026, 11LB027, 11LB029, 11LB033, 11LB036) were collected from within the Cache Creek terrane along the Alaska Highway northwest of Jakes Corner and in the Judas Mountain area. The remaining four samples (11LB024, 12LB020, 12LB056, 12LB217) were collected from within the Marsh Lake intrusive complex at the northern end of Marsh Lake (Fig. 5). These samples have alteration which ranges from minor sericitization of feldspars to

extensive sericitic and epidote alteration throughout the samples, which were originally clinopyroxene and plagioclase-rich. Due to the alteration of a majority of these samples, the abundance of some major and trace elements may not be representative of their original chemistry. Accordingly, in order to understand the tectonic setting, magmatic evolution and chemical affinity of the corresponding plutonic and volcanic rocks, major element weight percents are recalculated to a volatile-free (anhydrous) basis (Table 2). The SiO_2 concentrations in the mafic samples range from 48.94 to 60.75 wt % on an anhydrous basis. Selected major elements are plotted against SiO_2 in the Harker plots of Figure 14. In addition to recalculating the major element weight percents,

Table 2. Major Element (wt %) and trace element (ppm) data

Sample	12LB020	12LB056	12LB217	11LB024	05SJP065-1-1	05SJP065-3-1	05SJP066-1-1	05SJP078-1-1	05SJP067-1-1	11LB027	11LB033	11LB027	11LB033	11LB029	11LB036	11LB026	05SJP065-2-1(1)	05SJP074-1-1
Rock Type	gabbro	gabbro	pyroxenite	gabbro	gabbro	gabbro	gabbro	gabbro	gabbro	gabbro	gabbro	gabbro	gabbro	pyroxenite	pyroxenite	basalt	basalt	basalt
Unit	MLIC	MLIC	MLIC	MLIC	MLIC	MLIC	MLIC	MLIC	CCT	CCT	CCT	CCT	CCT	CCT	CCT	CCT	CCT	CCT
SiO2	50.27	53.34	53.14	53.37	56.39	51.07	50.62	48.94	50.39	50.72	52.11	50.72	52.11	51.65	60.75	51.94	49.53	57.50
Al2O3	17.18	15.38	17.30	17.39	17.43	15.87	15.82	16.82	17.88	14.20	13.01	14.20	13.01	11.67	16.77	16.81	11.28	17.94
Fe2O3(T)	9.82	9.67	9.11	9.37	7.27	10.18	10.69	10.88	9.21	11.31	8.77	11.31	8.77	10.06	7.49	10.38	9.60	7.71
MnO	0.17	0.17	0.16	0.19	0.13	0.17	0.19	0.18	0.15	0.17	0.14	0.17	0.14	0.16	0.12	0.19	0.18	0.15
MgO	4.36	5.75	4.69	4.21	3.28	5.46	5.47	5.74	6.74	7.43	9.46	7.43	9.46	7.48	2.79	5.24	10.09	3.13
CaO	10.69	7.71	7.95	7.82	6.19	9.46	9.46	10.07	9.96	11.72	10.87	11.72	10.87	11.43	5.48	7.98	14.39	6.56
Na2O	3.24	3.19	3.72	3.41	4.40	3.79	2.63	1.86	3.67	2.83	2.19	2.83	2.19	1.90	4.03	3.59	1.86	3.53
K2O	3.10	3.54	2.92	3.04	3.69	2.63	3.94	4.34	1.03	0.30	2.18	0.30	2.18	3.78	1.55	2.47	2.02	2.51
TiO2	0.72	0.91	0.75	0.85	0.82	0.96	0.76	0.73	0.82	1.21	0.86	1.21	0.86	0.84	0.78	1.07	0.78	0.64
P2O5	0.46	0.35	0.28	0.35	0.41	0.39	0.42	0.43	0.14	0.11	0.42	0.11	0.42	1.02	0.25	0.32	0.28	0.32
FeO*	8.83	8.70	8.20	8.43	6.54	9.16	9.62	9.79	8.28	10.17	7.89	10.17	7.89	9.05	6.74	9.34	8.63	6.93
Total	94.228	97.949	96.019	95.624	95.092	96.517	97.523	97.217	97.009	96.14	89.073	96.14	89.073	96.826	94.788	95.762	97.857	97.079
Sc	24	36	28	29	12.4	22.1	21.6	21.6	24.4	42	32	42	32	39	17	37	42.9	13.3
Be	2	1	1	1	0.98	0.77	0.89	0.73	0.20	< 1	2	< 1	2	2	1	< 1	0.52	0.87
V	237	267	249	263	191	255	240	244	261	298	201	298	201	261	176	309	235	158
Cr	30	130	50	20	21	49	45	58	158	290	450	290	450	180	40	30	165	17
Co	29	29	25	22	16	27	31	30	29	40	30	40	30	32	12	24	33	14
Ni	< 20	< 20	< 20	< 20	-4	9	5	11	55	60	90	60	90	40	< 20	< 20	29	6
Cu	130	120	100	70	61	77	90	95	85	150	60	150	60	120	10	100	59	22
Zn	80	90	90	90	84	84	89	86	63	80	60	80	60	80	100	110	70	90
Ga	19	18	19	20	18	15	14	13	13	15	13	15	13	13	19	18	11	15
Ge	2.2	1.9	1.8	2						2.1	2.3	2.1	2.3	1.9	2.8	2.8		
As	5	< 5	< 5	5						< 5	< 5	< 5	< 5	< 5	< 5	< 5		
Rb	53	79	67	55	71.80	50.26	78.25	92.15	24.27	5	41	5	41	33	32	45	37.96	49.50
Sr	418	675	1210	873	888.2	792.5	867.0	681.7	267.9	140	1528	140	1528	244	601	852	676.2	656.1
Y	16.3	20.3	15	19	16.18	19.05	16.43	15.76	14.02	21.1	17.3	21.1	17.3	18.9	16.3	21.6	16.76	17.29
Zr	91	87	75	114	144.0	101.4	95.4	84.4	36.4	63	97	63	97	115	110	86	67.4	104.1
Nb	5	4.5	3.8	5.7	8.8	6.5	5.3	4.8	1.4	3.2	4.3	3.2	4.3	5.2	6.7	5	3.9	5.7
Mo	< 2	< 2	< 2	< 2	N.D.	N.D.	N.D.	86	N.D.	< 2	< 2	< 2	< 2	< 2	< 2	< 2	N.D.	N.D.
Ag	0.7	0.5	< 0.5	3						< 0.5	< 0.5	< 0.5	< 0.5	0.5	< 0.5	0.8		
In	< 0.1	< 0.1	< 0.1	< 0.1						< 0.1	< 0.1	< 0.1	< 0.1	< 0.1	< 0.1	< 0.1		
Sn	1	2	1	1						< 1	1	< 1	1	2	1	2		
Sb	0.7	0.5	5.9	2.5						0.3	0.8	0.3	0.8	< 0.2	0.5	1.8		
Cs	0.6	4.8	2.1	3						0.3	4	0.3	4	0.2	0.6	3.7		
Ba	1705	2973	2540	2589	>1400	1365	>1400	>1400	220	362	3293	362	3293	1308	1101	2971	1326	>1400
La	27.1	19	20	26.4	33.22	26.07	25.33	24.22	3.03	4.36	27.7	4.36	27.7	20.9	18.7	23.6	17.04	20.39
Ce	51.6	38.8	38.2	50.6	59.90	48.85	47.61	45.17	7.54	11.4	59.5	11.4	59.5	45.1	37.8	47.4	32.14	37.23
Pr	5.58	4.29	4.24	5.8	6.94	5.94	5.77	5.50	1.18	1.64	7.21	1.64	7.21	5.75	4.43	5.76	4.01	4.36
Nd	22.7	18.2	17.5	22.9	27.32	24.12	23.40	22.44	5.90	8.19	30.2	8.19	30.2	24.2	17.7	22.9	16.87	16.97
Sm	4.79	4.3	3.72	4.88	5.37	5.09	4.98	4.70	1.86	2.6	5.99	2.6	5.99	5.41	3.85	4.77	3.95	3.59
Eu	1.33	1.25	1.08	1.22	1.53	1.50	1.45	1.38	0.73	0.885	1.52	0.885	1.52	1.52	1.03	1.39	1.14	1.11
Gd	4.37	4.47	3.6	4.21	4.42	4.56	4.30	4.05	2.40	3.1	4.6	3.1	4.6	4.84	3.36	4.27	3.79	3.40
Tb	0.59	0.67	0.52	0.61	0.57	0.63	0.58	0.56	0.41	0.59	0.64	0.59	0.64	0.71	0.54	0.68	0.54	0.51
Dy	3.11	3.61	2.78	3.3	3.20	3.71	3.27	3.13	2.62	3.64	3.33	3.64	3.33	3.46	3.05	3.63	3.24	3.21
Ho	0.6	0.74	0.55	0.66	0.59	0.73	0.64	0.61	0.55	0.75	0.64	0.75	0.64	0.65	0.6	0.72	0.65	0.67
Er	1.67	2.15	1.61	1.84	1.65	2.03	1.76	1.69	1.60	2.16	1.68	2.16	1.68	1.76	1.66	2.13	1.81	1.96
Tm	0.244	0.301	0.23	0.268	0.23	0.29	0.25	0.24	0.23	0.313	0.236	0.313	0.236	0.235	0.232	0.295	0.26	0.29
Yb	1.63	2.07	1.53	1.78	1.55	1.90	1.60	1.54	1.52	2.02	1.48	2.02	1.48	1.56	1.56	1.91	1.74	1.99
Lu	0.268	0.345	0.259	0.283	0.227	0.277	0.235	0.225	0.229	0.324	0.236	0.324	0.236	0.241	0.254	0.314	0.253	0.301
Hf	2.3	2.2	2	2.7	3.70	2.60	2.40	2.20	1.10	1.7	2.5	1.7	2.5	3	2.8	2.2	1.90	2.70
Ta	0.3	0.29	0.23	0.27						0.2	0.22	0.2	0.22	0.27	0.4	0.21		
W	< 0.5	0.9	< 0.5	0.8	N.D.	N.D.	N.D.	N.D.	N.D.	< 0.5	0.6	< 0.5	0.6	< 0.5	0.6	0.7	N.D.	N.D.
Tl	0.38	0.37	0.47	0.39						< 0.05	0.47	< 0.05	0.47	0.23		0.33		
Pb	20	12	15	20						< 5	9	< 5	9	19	10	13		
Bi	< 0.1	< 0.1	< 0.1	< 0.1						< 0.1	< 0.1	< 0.1	< 0.1	0.1	< 0.1	< 0.1		
Th	7.63	5.42	5.73	7.39	10.03	7.28	7.33	6.92	0.30	0.41	4.9	0.41	4.9	5.08	3.94	4.95	4.62	5.99
U	3.62	2.67	2.99	3.12	4.25	3.17	3.08	2.97	0.16	0.14	1.85	0.14	1.85	2.12	1.4	1.81	2.00	2.98

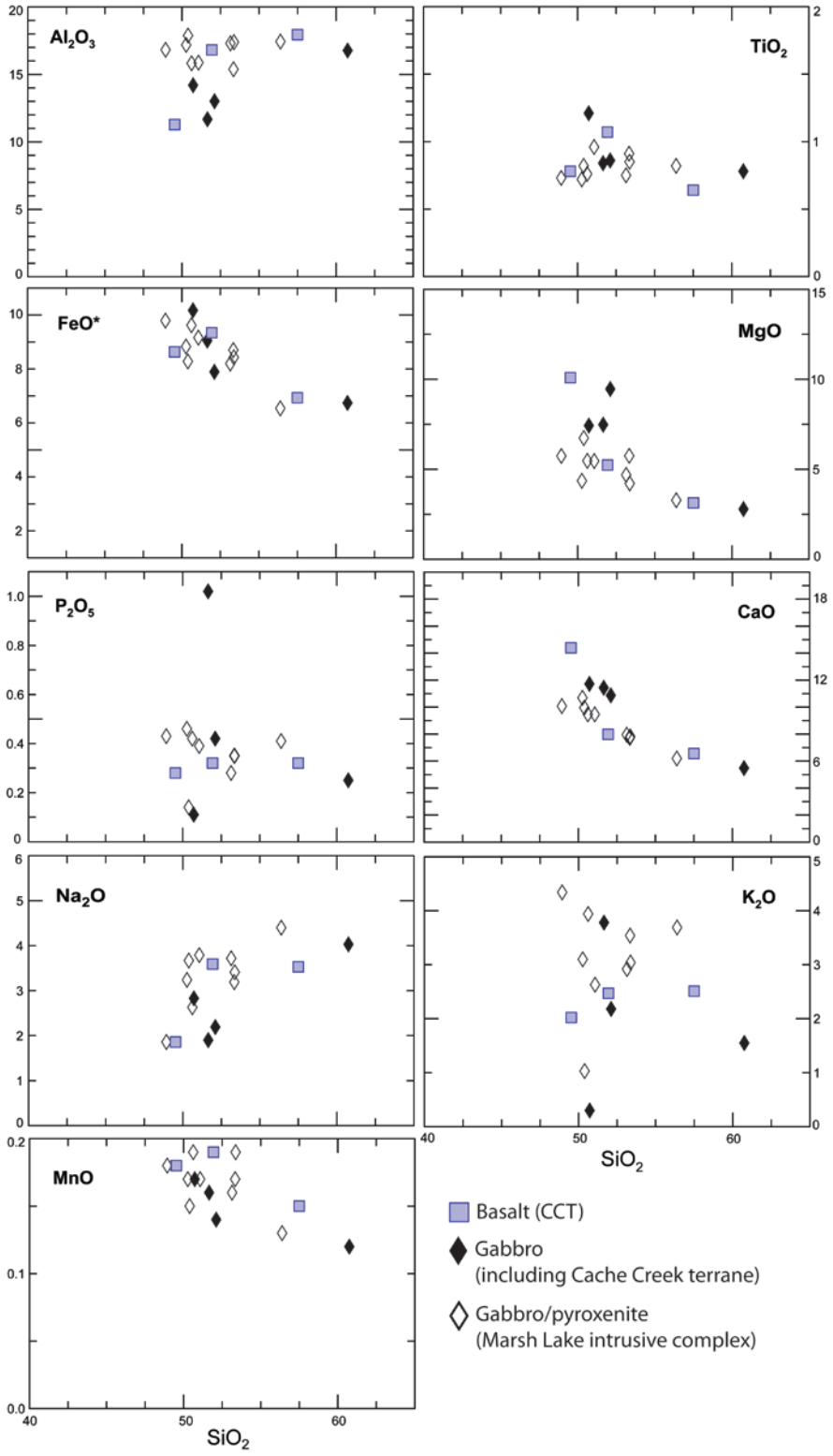

Figure 14. Major element variation (Harker) Diagram
Plots show relationship of Al_2O_3, TiO_2, FeO*, MgO, P_2O_5, CaO, Na_2O, K_2O, and MnO versus SiO_2 on an anhydrous basis.

emphasis was also placed on the least mobile high field strength (HFS) and rare earth elements (REE) in order to further minimize the influence of alteration. As Zr is considered immobile during the low grade metamorphism of mafic igneous rocks (e.g. Gibson et al., 1982), it is plotted against incompatible elements Nb, Ba, La, Sr, Th and U

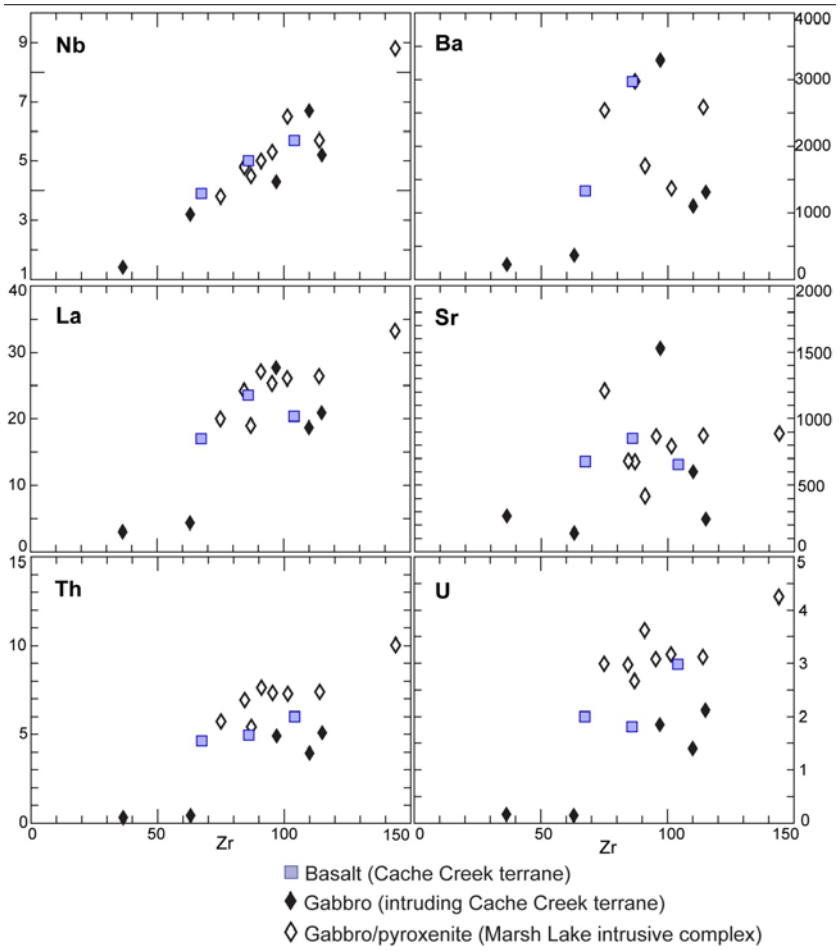

Figure 15. Lithogeochemical incompatible element variation diagrams
Plots of incompatible elements Nb, La, Th, Ba, Sr, and U versus Zr (in ppm)

in Figure 15. While Nb, La, Th correlate reasonably well with increasing Zr content in these rocks, the relationship with Ba and Sr (both large ion lithophile elements; LILEs) is more random. The scatter in Ba and Sr versus Zr indicates the LILEs were mobilized during alteration of these rocks.

A majority of samples collected from the mafic rocks of the study area plot as alkaline in the total-alkali versus silica (TAS) diagram of LeBas et al. (1985) and range

from basalt to basaltic trachy-andesite to andesite (Fig. 16A). However, the TAS plot in Figure 16A is subject to error based on mobility of alkali elements during metasomatism (e.g. Smith and Smith, 1976); therefore, the plot of Winchester and Floyd (1977) is used to discriminate incompatible element ratios Zr/TiO_2 and Nb/Y for determining rock classification (Fig. 16B). The dominant rock type according to the geochemical classification of these samples is basaltic andesite, with two samples from the Cache

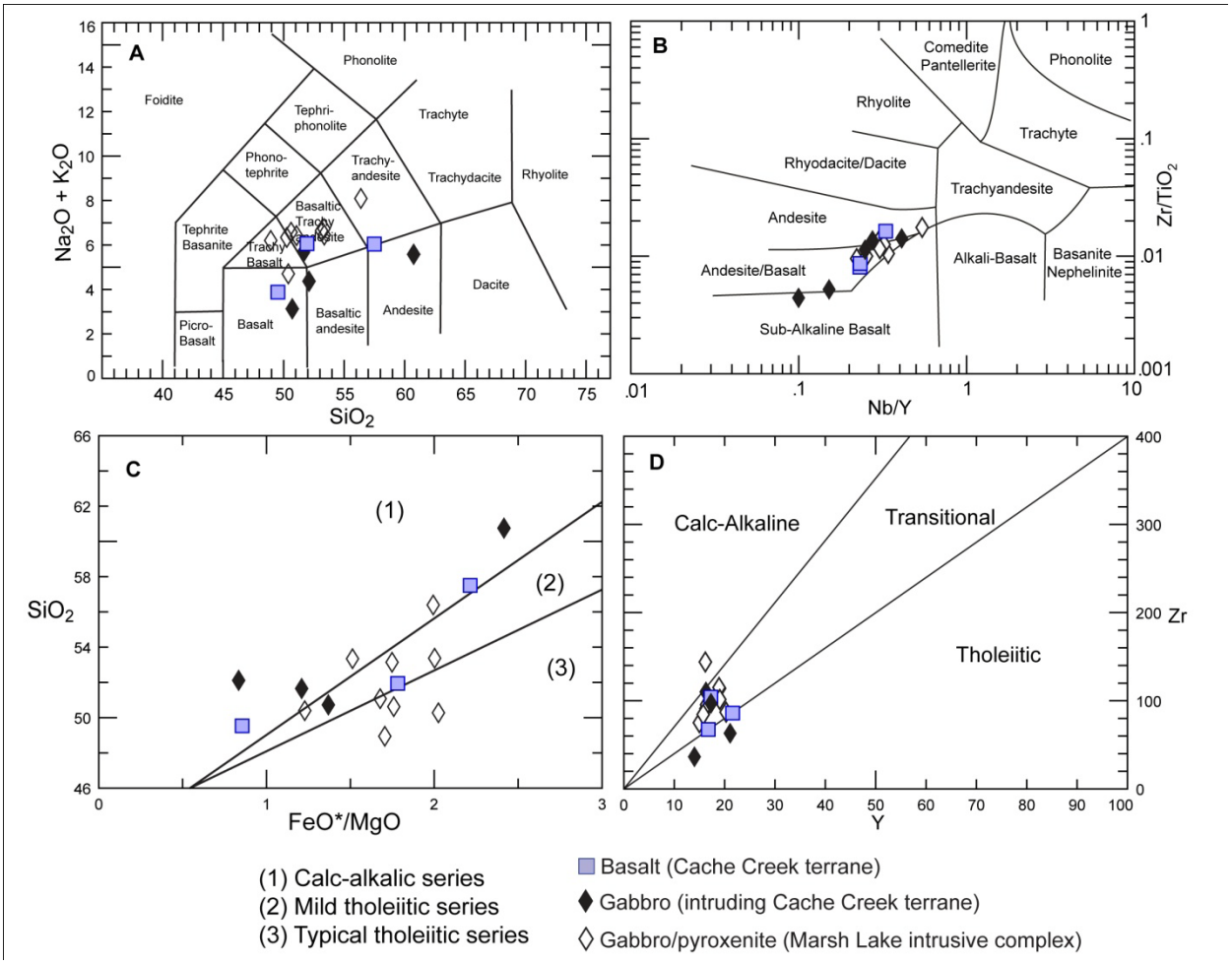

Figure 16. Lithogeochemical classification diagrams
Mafic igneous sample data plotted on (A) rock classification diagram using Na_2O+K_2O versus silica (TAS) abundances in weight percent (from LeBas et al., 1985), (B) rock classification diagram using immobile trace-element abundances (from Winchester and Floyd 1977), (C) SiO_2 versus FeO*/MgO for calc-alkalic and tholeiitic series (from Miyashiro and Shido, 1975), and (D) Zr-Y diagram of Barrett and MacLean (1999).

Creek volcanic unit (05SJP067-1-1 and 11LB027) plotting closer to sub-alkaline basalt. A majority of the basalt and gabbro samples from the Cache Creek volcanic unit and the

Marsh Lake intrusive complex have a calc-alkaline to transitional basaltic composition (Fig.16 C and D). The transitional to calc-alkalic basaltic composition is visible in plots of the major and immobile elements, however, the major element calc-alkaline/tholeiitic basalt series diagram, after Miyashiro and Shido (1975), has three samples from inside the Marsh Lake intrusive complex (12LB020, 05SJP066-1-1, and 05SJP078-1-1) being geochemically closer to tholeiitic basalt (Fig. 16C). The more reliable immobile element calc-alkaline/tholeiitic basalt series diagram, after Barrett and MacLean (1999), has two samples from outside the complex (05SJP067-1-1 and 11LB027) being geochemically closer to tholeiitic basalt (Fig. 16D).

Mid-ocean ridge basalt (MORB) normalized multi-element plots of the mafic rocks collected in the Cache Creek terrane are shown in Figure 17 (a and b). The more immobile, incompatible elements such as Th, Ta, Nb and Zr show a slight enrichment relative to the average calc-alkalic basalt pattern and high peaks of Ba and Rb could be another indicator of mobilization of LILEs during metasomatism. Chondrite normalized plots of REE's of the mafic rocks are shown in Figure 17 (c and d). The LREE enrichment is noticeable for a majority of the samples with a $(La/Lu)_n$ ratio ranging from 5.9 to 15.7 in rocks of the Marsh Lake intrusive complex, which define a slope slightly steeper than that of the average oceanic island basalt (OIB; Fig. 17c). The $(La/Lu)_n$ ratio is up to 12.6 in samples collected outside the intrusive complex, with the exception of two samples (05SJP067-1-1 and 11LB027) that are geochemically distinct, showing a flat chondrite normalized profile with a $(La/Lu)_n$ of 1.4; this ratio is similar, but more depleted in LREEs than that of the average E-type mid-ocean ridge basalt (EMORB; Fig. 17d). Europium anomalies in all samples are minor or absent, and heavy rare-earth element (HREE) profiles are relatively flat in both the Marsh Lake intrusive complex ($1.6 \leq (Gd/Lu)_n \leq 2.4$; Fig. 17c, inset) and in mafic rocks of the Cache Creek outside the complex ($1.2 \leq (Gd/Lu)_n \leq 2.5$; Fig. 17d, inset).

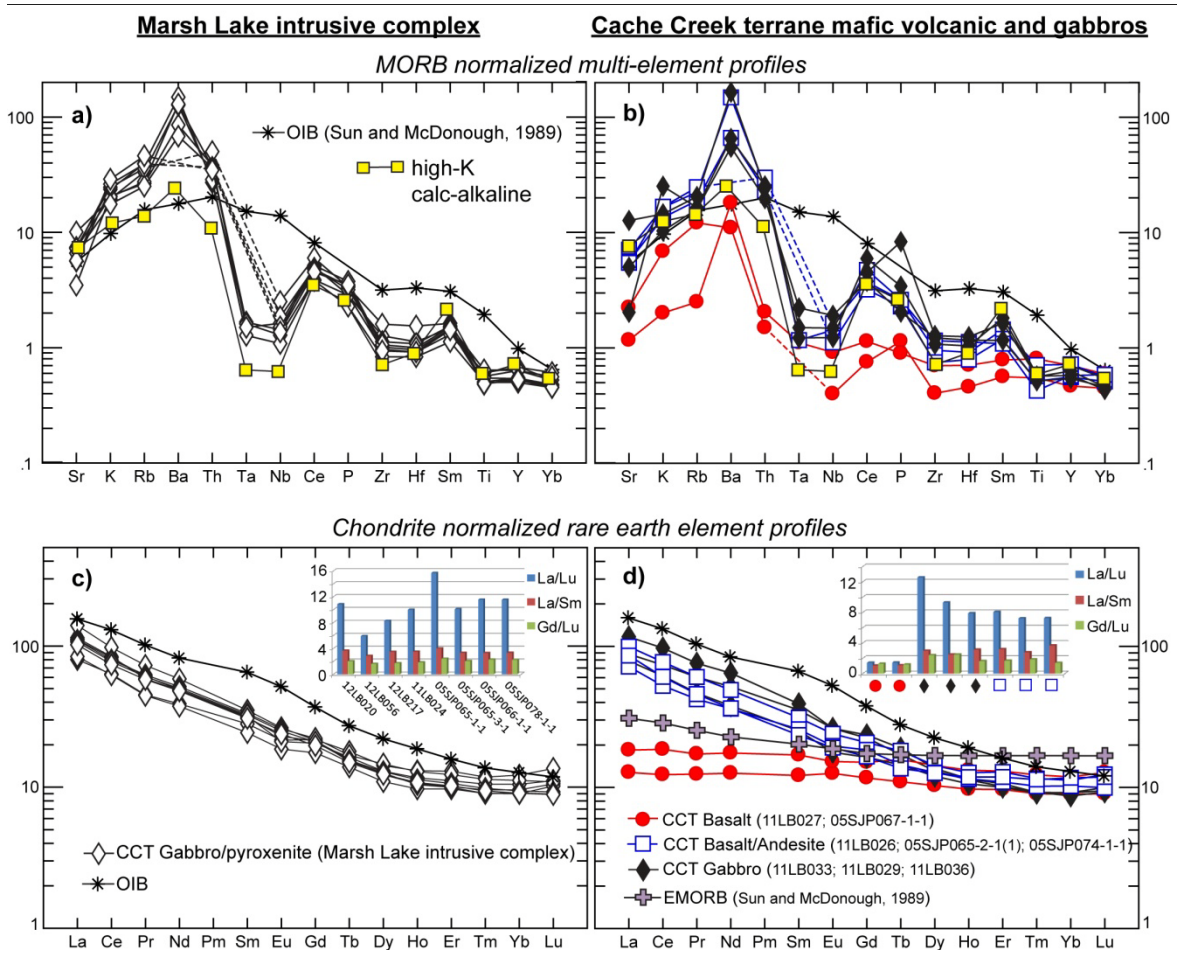

Figure 17. Multi-element profiles and rare-earth element (REE) profiles
(a and b) Mid-ocean ridge basalt (MORB) normalized multi-element profiles for (a) gabbros of the Marsh Lake intrusive complex and (b) mafic volcanic rocks and gabbros of the Cache Creek terrane. Normalizing values for (a) and (b) from Pearce (1983).
(c and d) Chondrite-normalized rare-earth element (REE) profile for (c) gabbros of the Marsh Lake intrusive complex and (d) mafic volcanic rocks and gabbros of the Cache Creek terrane. Inset figures of (c) and (d) show variations in light rare-earth elements (LREE) and heavy rare-earth elements (HREE) enrichment or depletion. Normalizing values for (c) and (d) from Sun and McDonough (1989).

The mafic samples collected in the field area have a predominant subalkalic signature and a tectonic setting of a destructive margin based on the tectonic discrimination diagrams of Figure 18. The enrichment of Th and, to a lesser degree, Nb relative to Yb indicates the rocks formed from magma with a significant subduction component, plotting further along the liquid-fractionation vector, and have an enriched mantle source relative to typical arc magmas (Pearce and Peate, 1995; Fig. 18a). The second tectonic discrimination diagram after Wood et al. (1980), shown in Figure 18b,

also indicates a majority of the collected samples formed in a subduction zone setting, with a Th enrichment relative to the mantle array (Fig. 18b). These observations are true for all samples from within the Marsh Lake intrusive complex and for a majority of those collected outside the complex, with the exception of two gabbro samples (11LB027 and 05SJP067-1-1) which show more of a back-arc to N-type MORB tectonic setting (Fig. 18 a and b).

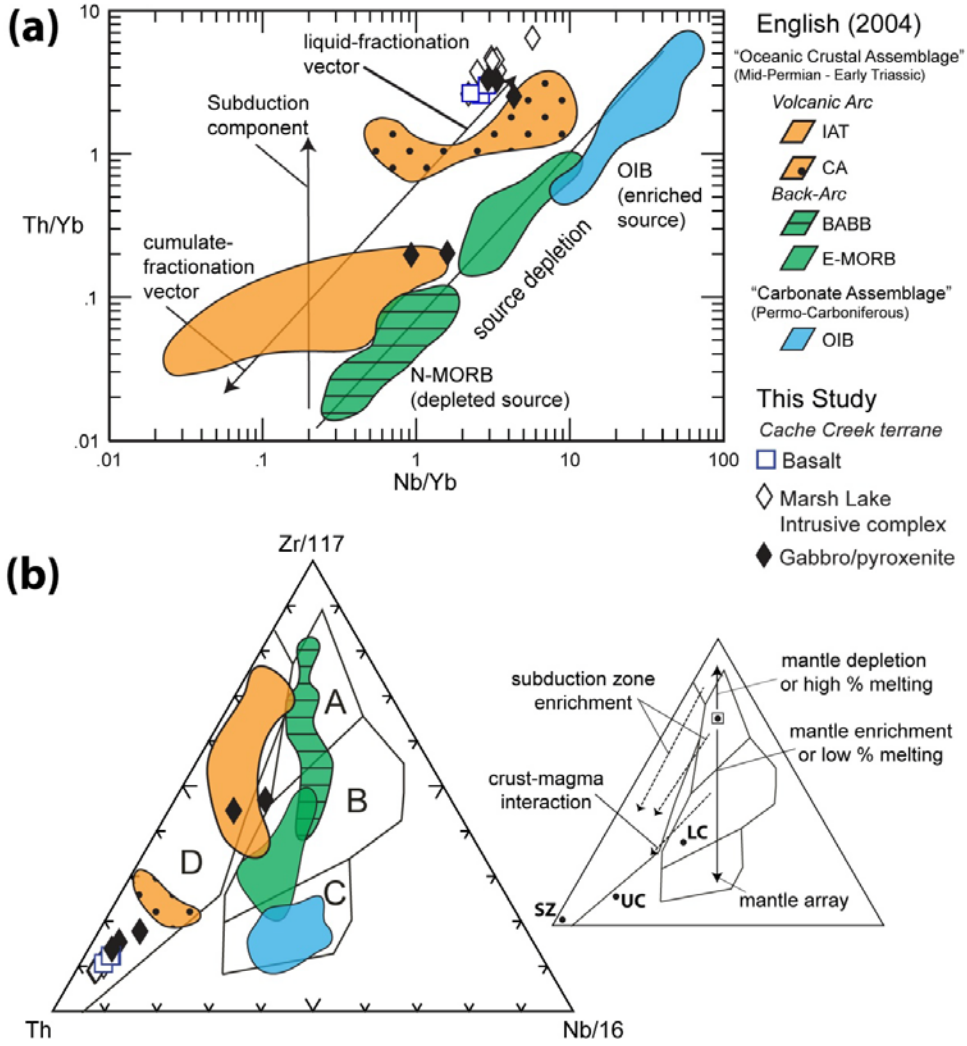

Figure 18. Tectonic setting discrimination diagrams
(a) after Pearce and Peate (1995), Th/Yb versus Nb/Yb showing influence of subduction zone and an enriched mantle source for rocks of this study, as well as from elsewhere in the Cache Creek terrane in the northern Cordillera (English, 2004; English et al., 2010); (b) after Wood (1980), showing tectonic settings in ternary discrimination diagram. Field abbreviations: A – N-type mid-ocean ridge basalt (MORB), B – E-type MORB and tholeiitic within-plate basalt (WPB) and differentiates, C – Alkaline WPB and WPB and differentiates, D – Destructive plate margin basalts and differentiates.

Interpretation

The mafic intrusive and volcanic rocks are part of an oceanic assemblage based on field characteristics and relationships; however, their geochemical composition is predominantly subalkalic basalt to andesite and gabbro to pyroxenite with magmatic arc signatures. Light rare earth element enrichments in the Marsh Lake intrusive complex, as well as high Th/Nb and Ce/Nb ratios, indicate these rocks formed in a subduction zone setting and could represent remnants of an intra-oceanic arc assemblage. The arc rocks were likely built upon rocks with back-arc to mid-ocean ridge basalt affinity that have an enriched mantle source; this possibility is shown by the two Cache Creek mafic volcanic samples collected near to the boundary zone of the Marsh Lake intrusive complex (11LB027 and 05SJP067-1-1; Fig. 16d and 18).

Tectonic discrimination diagrams shown in Figure 18, a and b, plot data from this study and compare it with the data of a previous geochemical study of the Cache Creek terrane in the Atlin area of northern British Columbia (English, 2004; English et al., 2010). Petrogenetic work done in the Cache Creek terrane of northern British Columbia identified two dominant intrusive and extrusive igneous rock types (English et al., 2010): alkaline volcanic rocks interbedded with carbonate which are compositionally identical to ocean island basalts (OIB), and subalkaline intrusive and extrusive rocks with mostly arc affinity. The OIB portion was thought to be part of an oceanic seamount and (or) plateaux which elevated the oceanic basement enough for shallow marine carbonate deposition. The remaining rocks in the English et al. (2010) study are mostly located along the western margin of the Cache Creek terrane and consist of island-arc tholeiites (IATs), calc-alkaline rocks, back-arc basin basalt (BABB), and E-MORB-type volcanic rocks which are all considered part of the “oceanic crustal package” (Fig. 18). It is likely that the “oceanic crustal package” was produced in an arc to back-arc setting (English et al., 2010). The basaltic rocks collected in this study, at the northern termination of the Cache Creek terrane, show influence of subduction and an enriched mantle source. They contain a high Th content, indicating a significant subduction component (Figure 18a), suggestive of a destructive plate margin setting (Figure 18b). The mafic intrusive and extrusive rocks in the study area, including the Marsh Lake intrusive complex, lie along the same trend of the “oceanic crustal complex” of English et al. (2010) in northern British Columbia, bordering the western edge of the Cache Creek terrane. The similar

structural position and geochemical correlation indicates the rocks in the study area, and those to the south, may be part of the same intra-oceanic arc or separate arcs that accreted to the Stikinia margin during the Permian to Triassic.

2.6.3. U-Pb isotopic data

Michie formation

Detrital zircon LA-ICPMS analyses were preformed on one sample from the Michie formation (10MC049). For sample 10MC049, seventy-seven grains were analyzed by LA-ICPMS, showing a narrow age range of $^{206}Pb/^{238}U$ ages from 263 ± 10 to 235 ± 12 Ma, with the largest peak at ca. 245 Ma (Table 3; Fig. 19). The zircon grains

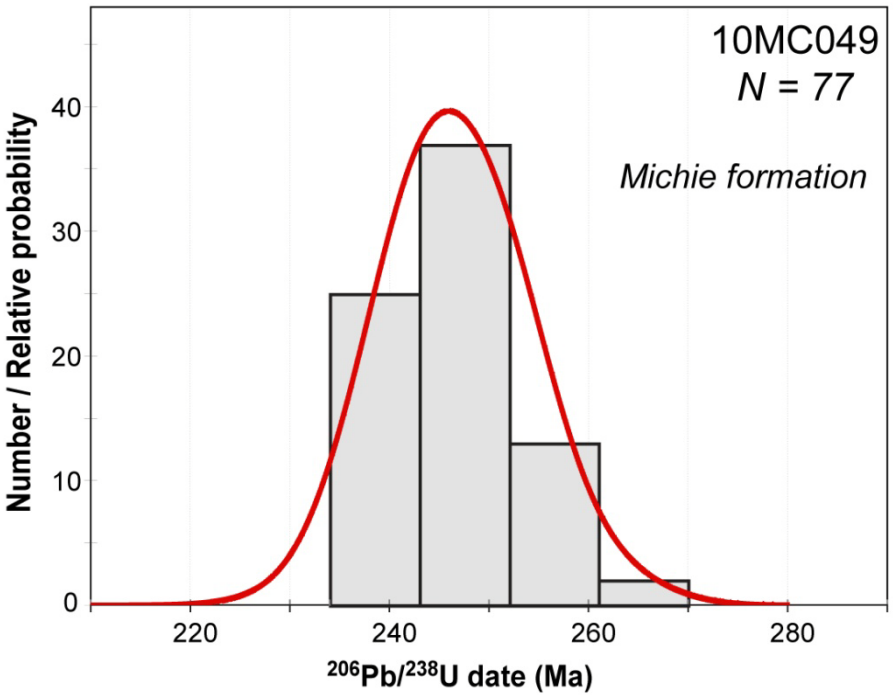

Figure 19. Detrital zircon U-Pb histogram and relative probability plot for sample 10MC049

Plot of LA-ICPMS $^{206}Pb/^{238}U$ ages for zircon grains in sample 10MC049 (plotted with Isoplot 3.0, Ludwig, 2003). See Figure 20A for example CL images for zircon grains. Bin width in the histograms is the average error on the dates. N – number of grains analyzed

in 10MC049 showed uniform, simple CL zoning patterns and sharply faceted morphology (Fig 20A). The other sample from the Michie formation, 12LB181, yielded only a few detrital zircon grains; the grains in this sample show similar morphology and

CL zoning patterns to those of 10MC049 (Fig. 20B). As a result of the CL similarities, the grains in 12LB181 were directly analyzed by CA-TIMS along with 10MC049 to establish a more precise age for the formation (Fig 20 C and D).

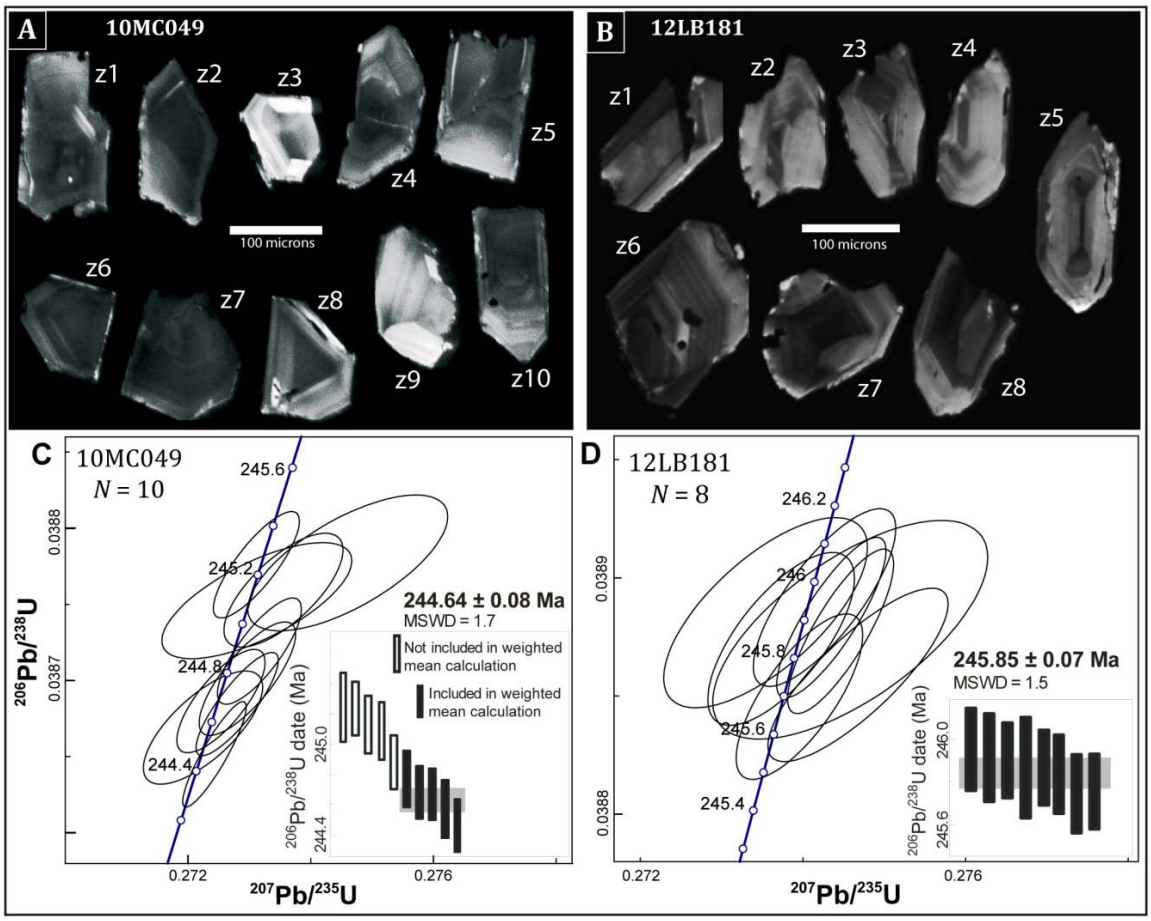

Figure 20. Cathodoluminescence images and U-Pb Concordia plots
(A) and (B) Cathodoluminescence (CL) images of zircon grains chosen from samples 10MC049 and 12LB181, respectively, for CA-TIMS analysis. Labels correspond to zircon analysis provided in Table 4); differences in brightness of CL images indicate differences in U concentration (low = bright; high = dark) and other trace element concentrations, as well as crystallinity of each grain. (C) and (D) U-Pb concordia plots; error ellipses are 2σ. Insets are ranked $^{206}Pb/^{238}U$ age plots with weighted mean ages represented by grey boxes behind error bars; errors are 2σ. Note that in (C), the weighted mean is calculated using the five youngest grains to achieve a maximum age constraint on volcaniclastic deposition of the Michie formation.

In sample 10MC049, 10 grains were analyzed by CA-TIMS. The five youngest zircon grains yielded equivalent $^{206}Pb/^{238}U$ dates with a weighted mean $^{206}Pb/^{238}U$ date of 244.64 ± 0.08 Ma (MSWD = 1.7; Fig. 20C). The other five grains yielded $^{206}Pb/^{238}U$ dates of 244.89 ± 0.18 to 245.25 ± 0.23 Ma. Eight zircon grains from 12LB181 yielded

equivalent $^{206}Pb/^{238}U$ dates with a weighted mean $^{206}Pb/^{238}U$ age of 245.85 ± 0.07 Ma (MSWD = 1.5; Fig. 21D).

Richthofen formation

A total of 69 LA-ICPMS spot analyses (one analysis per grain) were performed on zircon grains from sample 12LB220, of the Richthofen formation. Spots were targeted using CL imaging (e.g. Fig. 21A, inset). The $^{206}Pb/^{238}U$ ages range from 336 ± 24 to 181 ± 12 Ma, with the largest peak at ca. 190 Ma (Fig 21 A and B).

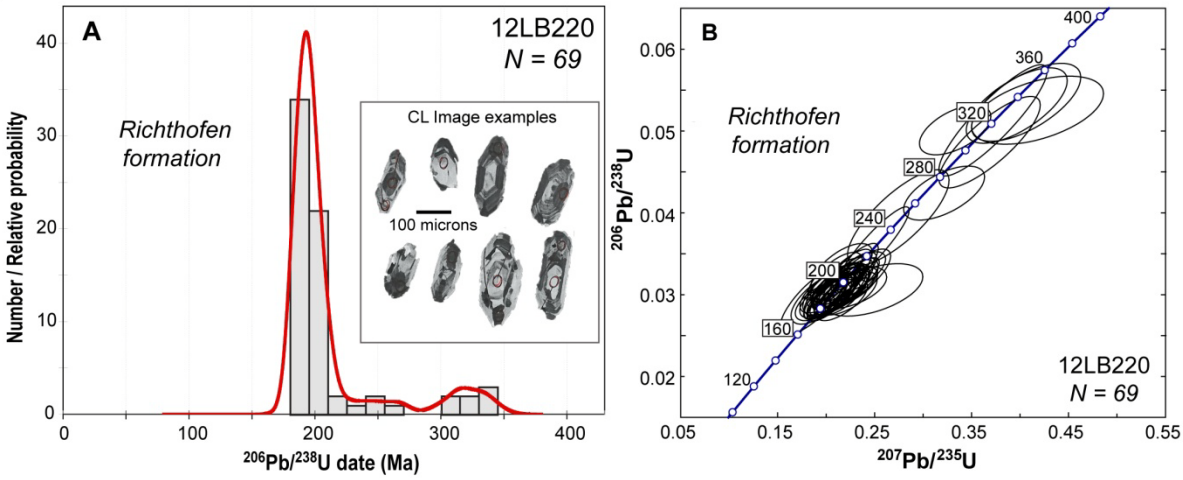

Figure 21. Detrital zircon U-Pb histogram and relative probability plot & Concordia plot for sample 12LB220

(A) Plot of LA-ICPMS $^{206}Pb/^{238}U$ ages for zircon grains in sample 12LB220 (plotted with Isoplot 3.0, Ludwig, 2003). See inset for example CL images for zircon grains. Bin width in the histograms is the average error on the dates. N – number of grains analyzed
(B) U-Pb concordia plot for 12LB220; error ellipses are 2σ.

Table 3. LA-ICPMS U-Pb Data

Table 3. U-Pb Isotopic LA-ICPMS Data

	Concentrations				Corrected isotope ratios						Age and 2σ absolute errors (Ma)						
Analysis	U ppm	Th ppm	Pb* ppm	Th/U	$^{207}Pb^*/^{206}Pb^*$	±2σ (%)	$^{207}Pb^*/^{235}U$	±2σ (%)	$^{206}Pb^*/^{238}U$	±2σ (%)	$^{207}Pb^*/^{206}Pb^*$	±2σ (Ma)	$^{207}Pb^*/^{235}U$	±2σ (Ma)	$^{206}Pb^*/^{238}U$	±2σ (Ma)	% Disc.
12LB220																	
S 59	50.016	29.878	3.3776	0.5974	0.05506	8.69	0.40628	11.33	0.05351	7.27	415	194	346	33	336	24	19
L 13	73.24	32.615	4.7543	0.4453	0.05415	8.07	0.39659	10.73	0.05311	7.08	377	181	339	31	334	23	12
L 5	38.26	19.122	2.498	0.4998	0.05770	11.61	0.41807	13.29	0.05255	6.47	518	255	355	40	330	21	37
L 2	126.54	63.696	7.9496	0.5034	0.05260	5.73	0.37210	12.25	0.05131	10.82	312	130	321	34	323	34	4
S 44	128.95	60.368	8.0343	0.4681	0.04819	7.56	0.33306	9.03	0.05012	4.94	109	178	292	23	315	15	195
S 58	198.83	160.36	13.199	0.8065	0.05496	6.78	0.36860	11.58	0.04864	9.39	411	152	319	32	306	28	26
S 62	103.18	40.549	6.0409	0.393	0.05834	6.21	0.39110	10.03	0.04862	7.88	543	136	335	29	306	24	45
S 38	74.811	39.047	4.0278	0.5219	0.05501	8.48	0.32168	10.60	0.04241	6.36	412	190	283	26	268	17	36
L 26	14.69	4.1414	0.6859	0.2819	0.03421	54.70	0.18617	55.38	0.03947	8.67	-772	1543	173	88	250	21	135
L 19	80.771	75.39	4.4995	0.9334	0.05050	9.76	0.27443	15.58	0.03942	12.14	218	226	246	34	249	30	15
S 67	399.11	84.489	16.26	0.2117	0.05028	5.04	0.24843	12.26	0.03584	11.18	208	117	225	25	227	25	9
S 42	226.8	121.45	9.8314	0.5355	0.04693	7.41	0.22817	13.39	0.03526	11.16	46	177	209	25	223	25	398
S 46	170.91	66.788	6.75	0.3908	0.04729	9.11	0.21607	11.90	0.03314	7.66	64	217	199	21	210	16	234
S 35	136.09	56.332	5.7095	0.4139	0.05955	14.45	0.26996	15.99	0.03288	6.86	587	313	243	35	209	14	66
L 22	149.6	77.599	6.0629	0.5187	0.05179	7.25	0.23412	9.49	0.03279	6.12	276	166	214	18	208	13	25
L 10	237.51	98.062	9.3123	0.4129	0.05067	5.65	0.22853	8.37	0.03271	6.18	226	131	209	16	207	13	8
S 41	241.45	97.555	9.4347	0.404	0.04978	6.02	0.22334	11.14	0.03254	9.37	185	140	205	21	206	19	12
S 64	197.14	130.14	8.1043	0.6602	0.05266	7.53	0.23405	11.33	0.03223	8.47	314	171	214	22	205	17	35
S 49	170.09	72.079	6.7044	0.4238	0.04717	7.85	0.20903	10.99	0.03214	7.69	58	187	193	19	204	15	258
S 43	210.66	91.522	8.3043	0.4345	0.04923	6.48	0.21799	10.87	0.03212	8.72	159	152	200	20	204	18	29
S 56	165.91	112.36	7.1846	0.6772	0.06281	8.33	0.27682	11.66	0.03197	8.16	702	177	248	26	203	16	72
S 52	208.19	66.237	7.6412	0.3182	0.05240	5.38	0.23088	8.48	0.03195	6.55	303	123	211	16	203	13	34
L 9	83.093	38.587	3.6092	0.4644	0.08864	7.53	0.38798	10.85	0.03174	7.82	1396	144	333	31	201	16	87
L 6	55.758	2.6252	1.9718	0.0471	0.05025	10.43	0.21870	13.09	0.03157	7.91	206	242	201	24	200	16	3
S 45	321.43	203.39	12.982	0.6328	0.05006	4.84	0.21764	7.65	0.03153	5.92	198	112	200	14	200	12	1
S 33	231.16	79.277	8.6328	0.343	0.05280	5.13	0.22930	8.39	0.03150	6.64	320	117	210	16	200	13	38
S 68	196.89	91.007	7.5775	0.4622	0.04987	6.76	0.21554	9.38	0.03135	6.50	189	157	198	17	199	13	5
L 20	137.6	56.525	5.1096	0.4108	0.05333	6.61	0.22855	8.81	0.03109	5.83	343	150	209	17	197	11	43
S 57	269.27	151.87	10.868	0.564	0.04907	6.45	0.21020	9.92	0.03107	7.53	151	151	194	17	197	15	31
L 16	202.22	104.07	7.877	0.5147	0.05086	7.97	0.21774	10.25	0.03105	6.44	235	184	200	19	197	13	16
L 3	150.21	74.832	5.6186	0.4982	0.04952	7.55	0.21198	10.42	0.03105	7.17	172	176	195	19	197	14	15
L 14	162.06	69.834	6.0869	0.4309	0.05126	6.81	0.21939	10.92	0.03104	8.53	253	157	201	20	197	17	22
L 21	192.9	107.96	7.5806	0.5597	0.05338	5.91	0.22795	8.65	0.03097	6.31	345	134	209	16	197	12	44
L 23	101.48	63.676	4.0052	0.6275	0.05265	12.17	0.22411	13.98	0.03087	6.88	314	277	205	26	196	13	38
L 8	139.42	63.206	5.2609	0.4533	0.04744	6.26	0.20157	8.80	0.03082	6.18	71	149	186	15	196	12	177
S 63	166.39	83.529	6.3629	0.502	0.05237	5.17	0.22149	8.21	0.03068	6.38	301	118	203	15	195	12	36
S 39	149.36	58.626	5.4917	0.3925	0.04975	10.24	0.21034	13.36	0.03066	8.57	183	239	194	24	195	16	6
S 51	151.42	101.17	6.3051	0.6682	0.05877	14.81	0.24786	17.10	0.03059	8.55	559	323	225	34	194	16	66
S 60	179.17	83.882	6.7869	0.4682	0.05230	6.02	0.22026	9.41	0.03055	7.22	298	137	202	17	194	14	36
S 48	392.93	120.3	14.114	0.3062	0.05160	3.65	0.21719	8.65	0.03053	7.84	268	84	200	16	194	15	28
S 66	196.34	86.085	7.3531	0.4384	0.05212	4.84	0.21856	8.51	0.03041	7.01	291	110	201	16	193	13	34
S 32	247.56	119.88	9.3876	0.4843	0.04961	5.74	0.20773	8.37	0.03037	6.09	177	134	192	15	193	12	9

Table 3, *cont'd.*

S 48	392.93	120.3	14.114	0.3062	0.05160	3.65	0.21719	8.65	0.03053	7.84	268	84	200	16	194	15	28
S 66	196.34	86.085	7.3531	0.4384	0.05212	4.84	0.21856	8.51	0.03041	7.01	291	110	201	16	193	13	34
S 32	247.56	119.88	9.3876	0.4843	0.04961	5.74	0.20773	8.37	0.03037	6.09	177	134	192	15	193	12	9
S 37	142.62	62.422	5.238	0.4377	0.05125	8.48	0.21434	10.57	0.03033	6.31	252	195	197	19	193	12	24
S 34	281.94	197.99	11.201	0.7022	0.05108	4.68	0.21316	7.80	0.03026	6.25	245	108	196	14	192	12	22
L 17	159.37	99.689	6.1291	0.6255	0.04747	7.79	0.19797	10.27	0.03025	6.69	73	185	183	17	192	13	166
L 7	165.29	76.271	6.1774	0.4614	0.04986	8.35	0.20793	10.66	0.03025	6.63	188	194	192	19	192	13	2
S 50	226.16	112.08	8.4469	0.4956	0.05191	4.92	0.21645	7.60	0.03024	5.80	282	112	199	14	192	11	32
L 15	182.13	72.807	6.6638	0.3997	0.05479	8.20	0.22827	11.87	0.03022	8.58	404	184	209	22	192	16	53
S 55	167.77	75.037	6.1797	0.4473	0.05350	8.46	0.22250	11.08	0.03016	7.16	350	191	204	20	192	14	46
L 11	122.09	57.936	4.4995	0.4746	0.05013	6.24	0.20783	10.83	0.03007	8.85	201	145	192	19	191	17	5
L 27	269.66	250	10.794	0.9271	0.05061	5.59	0.20963	8.68	0.03004	6.64	223	129	193	15	191	12	15
S 29	221.15	114.49	8.2024	0.5177	0.04905	4.17	0.20316	7.99	0.03004	6.81	150	98	188	14	191	13	27
L 25	163.56	79.93	5.9728	0.4887	0.04944	6.93	0.20369	10.56	0.02988	7.97	169	162	188	18	190	15	13
S 65	250.11	169.86	9.5749	0.6792	0.04975	6.39	0.20415	9.57	0.02976	7.12	183	149	189	16	189	13	3
S 36	210.78	95.872	7.7873	0.4548	0.05126	5.41	0.20974	8.63	0.02968	6.72	252	125	193	15	189	12	26
S 61	204.96	107.96	7.6332	0.5267	0.04889	5.98	0.19986	9.43	0.02965	7.29	142	140	185	16	188	14	33
L 18	134.62	53.634	4.8111	0.3984	0.05048	6.21	0.20626	10.05	0.02963	7.91	217	144	190	17	188	15	14
S 47	116.99	41.922	4.1495	0.3583	0.04785	9.74	0.19516	13.11	0.02958	8.79	92	231	181	22	188	16	107
L 4	132.67	32.856	4.4523	0.2476	0.05063	9.47	0.20639	11.41	0.02956	6.38	224	219	191	20	188	12	16
L 1	136	77.355	5.0557	0.5688	0.04917	8.74	0.19892	10.74	0.02934	6.24	156	205	184	18	186	11	20
S 54	174.06	122.87	6.6793	0.7059	0.05355	7.17	0.21642	9.97	0.02931	6.93	352	162	199	18	186	13	48
S 40	186.06	75.573	6.6068	0.4062	0.04634	9.61	0.18708	15.15	0.02928	11.71	16	231	174	24	186	21	1115
S 53	108.29	46.266	3.8745	0.4272	0.04810	8.42	0.19343	10.67	0.02916	6.55	104	199	180	18	185	12	79
L 12	423.5	267.05	15.759	0.6306	0.05049	6.16	0.20172	10.34	0.02898	8.30	217	143	187	18	184	15	16
S 69	280.92	214.17	11.012	0.7624	0.05015	4.60	0.19941	7.08	0.02884	5.38	202	107	185	12	183	10	9
S 30	267.88	102.87	9.2706	0.384	0.04944	6.67	0.19624	9.20	0.02879	6.35	169	156	182	15	183	11	9
S 31	142.31	53.462	4.9103	0.3757	0.05062	8.84	0.20064	10.81	0.02874	6.22	224	204	186	18	183	11	19
L 24	117.89	50.207	4.108	0.4259	0.05287	7.70	0.20900	9.86	0.02867	6.16	323	175	193	17	182	11	44
L 28	155.25	68.837	5.3436	0.4434	0.05298	8.49	0.20841	10.80	0.02853	6.69	328	193	192	19	181	12	45
10MC049																	
S 44	96.889	108.2	5.352	1.1168	0.04838	10.39	0.27827	11.15	0.04172	4.04	118	245	249	25	263	10	126
S 40	124.1	189.71	7.4755	1.5287	0.05582	6.49	0.31939	7.82	0.04150	4.37	445	144	281	19	262	11	42
S 99	117.51	159.07	7.0802	1.3537	0.05828	11.20	0.32887	12.00	0.04093	4.29	540	245	289	30	259	11	53
S 98	85.129	85.026	4.4967	0.9988	0.04655	11.19	0.26188	12.08	0.04080	4.56	26	268	236	25	258	12	903
S 43	194.24	210.45	10.57	1.0834	0.04907	6.95	0.27431	7.66	0.04054	3.21	151	163	246	17	256	8	71
S 63	119.13	152.39	6.7457	1.2792	0.05157	8.22	0.28811	9.29	0.04052	4.33	267	189	257	21	256	11	4
S 45	131.2	167.6	7.3316	1.2774	0.04837	8.20	0.26978	8.89	0.04045	3.44	117	193	243	19	256	9	120
S 66	119.37	140.51	6.5764	1.1771	0.04984	8.42	0.27674	9.29	0.04027	3.92	187	196	248	20	255	10	37
S 70	102	107.73	5.4042	1.0562	0.04875	8.79	0.27023	9.60	0.04020	3.87	136	206	243	21	254	10	89
S 35	196.86	189.55	10.29	0.9629	0.04953	7.62	0.27403	8.58	0.04013	3.95	173	178	246	19	254	10	48

Table 3., *cont'd.*

S 95	109.78	134.26	6.1495	1.223	0.05655	9.34	0.31203	10.12	0.04002	3.90	474	207	276	24	253	10	48
S 39	195.53	158.16	9.852	0.8089	0.05034	6.28	0.27771	7.33	0.04001	3.78	211	146	249	16	253	9	20
S 38	66.345	51.778	3.3521	0.7804	0.03974	21.55	0.21853	22.01	0.03989	4.47	-368	558	201	40	252	11	172
S 59	114.31	118.85	6.0257	1.0397	0.05433	6.54	0.29874	7.46	0.03988	3.59	385	147	265	17	252	9	35
S 24	128.05	140	6.8157	1.0933	0.04637	10.28	0.25495	10.97	0.03988	3.82	17	247	231	23	252	9	1428
S 83	61.548	58.676	3.1431	0.9533	0.03715	23.30	0.20401	23.66	0.03983	4.11	-546	626	189	41	252	10	149
S 25	188.86	310.06	11.042	1.6417	0.04864	6.49	0.26692	7.10	0.03980	2.87	131	153	240	15	252	7	94
S 62	248.8	204	12.519	0.82	0.05047	5.98	0.27693	6.90	0.03979	3.45	217	138	248	15	252	9	16
S 47	45.3	38.397	2.237	0.8476	0.03795	21.55	0.20817	22.11	0.03978	4.91	-489	573	192	39	251	12	154
S 48	98.971	106.45	5.2725	1.0755	0.05016	10.64	0.27510	11.38	0.03978	4.02	202	247	247	25	251	10	25
S 21	36.31	13.73	1.7224	0.3781	0.05070	14.33	0.27798	15.35	0.03976	5.51	227	331	249	34	251	14	11
S 60	127.15	170.41	7.0863	1.3402	0.04964	6.99	0.27198	7.76	0.03974	3.37	178	163	244	17	251	8	42
S 67	136.83	182.23	7.672	1.3318	0.05137	7.71	0.28122	8.63	0.03971	3.89	257	177	252	19	251	10	2
S 22	168.87	199.94	9.1102	1.184	0.04739	11.47	0.25946	12.19	0.03971	4.12	69	273	234	25	251	10	269
S 65	130.28	166.2	7.2373	1.2757	0.05208	6.99	0.28452	7.87	0.03962	3.63	289	160	254	18	251	9	14
S 32	140.2	156.97	7.6174	1.1196	0.06823	6.99	0.37269	7.83	0.03962	3.54	875	145	322	22	250	9	73
S 42	98.299	127.26	5.2796	1.2946	0.03848	15.65	0.21018	16.13	0.03962	3.92	-452	413	194	28	250	10	158
S 84	97.982	95.384	5.0642	0.9735	0.04835	10.00	0.26410	10.77	0.03962	3.99	116	236	238	23	250	10	117
S 86	370.2	220.23	17.562	0.5949	0.05182	4.97	0.28123	5.96	0.03936	3.29	278	114	252	13	249	8	11
S 34	120.36	120.64	6.2326	1.0023	0.05162	8.38	0.28004	9.47	0.03935	4.42	269	192	251	21	249	11	8
S 52	111.11	126.94	5.9442	1.1425	0.04465	9.19	0.24175	10.02	0.03927	3.97	-75	225	220	20	248	10	440
S 73	120.69	140.42	6.472	1.1635	0.05255	10.40	0.28447	10.92	0.03926	3.35	309	237	254	25	248	8	20
S 79	110.28	123.57	5.8712	1.1205	0.04562	9.86	0.24665	10.49	0.03922	3.58	-23	239	224	21	248	9	1220
S 46	145.36	210.23	8.0794	1.4462	0.05223	6.11	0.28223	6.92	0.03919	3.25	295	139	252	15	248	8	16
S 50	116.6	103.43	5.9247	0.887	0.04508	8.37	0.24338	9.13	0.03916	3.64	-51	204	221	18	248	9	593
S 72	127.31	165.75	6.89	1.302	0.04601	10.70	0.24740	11.19	0.03900	3.26	-2	258	224	23	247	8	12375
S 61	65.631	73.181	3.2882	1.115	0.04201	18.97	0.22583	19.47	0.03898	4.42	-226	478	207	36	247	11	213
S 41	219.51	338.72	12.373	1.543	0.05050	6.64	0.27143	7.27	0.03898	2.96	218	154	244	16	247	7	13
S 57	129.87	176.79	7.245	1.3613	0.04900	8.63	0.26307	9.44	0.03894	3.84	148	202	237	20	246	9	68
S 31	99.414	99.259	5.007	0.9984	0.05248	7.49	0.28137	8.63	0.03888	4.30	307	171	252	19	246	10	20
S 101	149.49	217.04	8.4307	1.4519	0.04768	9.28	0.25529	10.02	0.03883	3.76	84	220	231	21	246	9	197
S 33	68.9	81.412	3.5583	1.1816	0.04181	13.74	0.22377	14.44	0.03882	4.44	-238	347	205	27	246	11	207
S 91	75.864	69.873	3.7979	0.921	0.04955	12.88	0.26497	13.51	0.03879	4.07	174	301	239	29	245	10	42
S 54	170.91	218.34	9.2494	1.2776	0.05238	6.45	0.28007	7.26	0.03878	3.33	302	147	251	16	245	8	19
S 49	117.6	134.79	6.1416	1.1462	0.04553	11.87	0.24323	12.44	0.03874	3.72	-27	288	221	25	245	9	1028
S 51	110.2	97.352	5.6541	0.8834	0.05431	10.79	0.28990	11.44	0.03872	3.79	384	242	258	26	245	9	37
S 53	298.85	286.43	15.061	0.9584	0.05213	4.77	0.27774	5.80	0.03864	3.30	291	109	249	13	244	8	16
S 27	221.28	341.06	12.368	1.5413	0.05266	6.38	0.28022	7.27	0.03859	3.48	314	145	251	16	244	8	23
S 71	125.33	106.24	6.0719	0.8476	0.05116	8.30	0.27220	9.17	0.03859	3.89	248	191	244	20	244	9	2
S 96	255.48	192.36	12.16	0.7529	0.05043	6.10	0.26820	7.00	0.03857	3.43	215	141	241	15	244	8	14
S 74	172.64	205.43	9.2365	1.1899	0.05213	7.77	0.27639	8.48	0.03845	3.41	291	177	248	19	243	8	17
S 100	98.94	96.532	4.9634	0.9757	0.04783	10.16	0.25341	10.73	0.03842	3.43	91	241	229	22	243	8	170

Table 3., *concluded.*

S 64	122.8	161.19	6.5872	1.3126	0.04732	8.65	0.25056	9.68	0.03841	4.35	65	206	227	20	243	10	278
S 87	31.57	25.107	1.5207	0.7953	0.03961	24.90	0.20968	25.65	0.03839	6.16	-376	646	193	45	243	15	168
S 77	129.4	150.75	6.8748	1.1651	0.05458	7.02	0.28891	7.91	0.03839	3.65	395	157	258	18	243	9	39
S 58	141.97	218.74	7.7625	1.5407	0.04554	9.37	0.24087	10.20	0.03836	4.01	-27	227	219	20	243	10	1028
S 90	99.404	90.146	4.9096	0.9069	0.04784	7.71	0.25294	8.56	0.03835	3.73	91	183	229	18	243	9	169
S 88	136.47	111.18	6.5753	0.8147	0.04855	8.03	0.25644	8.88	0.03831	3.80	126	189	232	18	242	9	94
S 92	169.22	274.27	9.6585	1.6208	0.04792	7.58	0.25297	8.38	0.03829	3.56	95	180	229	17	242	8	157
S 55	110.26	104.37	5.5803	0.9465	0.05143	9.33	0.27133	9.94	0.03826	3.42	260	214	244	22	242	8	7
S 102	323.33	286.56	16.157	0.8863	0.04804	6.14	0.25321	7.03	0.03823	3.42	101	145	229	14	242	8	141
S 82	130.3	174.27	6.9546	1.3374	0.04718	8.39	0.24811	9.09	0.03814	3.51	58	200	225	18	241	8	320
S 26	140.91	161.3	7.3007	1.1447	0.04698	7.87	0.24668	8.66	0.03808	3.61	48	188	224	17	241	9	409
S 75	159.78	253.15	8.7253	1.5843	0.04839	8.98	0.25321	9.52	0.03795	3.16	118	212	229	20	240	7	105
S 23	149.72	210.59	8.1705	1.4066	0.05134	7.52	0.26859	8.39	0.03794	3.71	256	173	242	18	240	9	6
S 20	229.23	303.47	12.366	1.3238	0.05109	7.51	0.26682	8.28	0.03788	3.49	245	173	240	18	240	8	2
S 81	106.24	97.539	5.3119	0.9181	0.05340	9.63	0.27775	10.35	0.03772	3.79	346	218	249	23	239	9	32
S 69	17.885	9.6292	0.8078	0.5384	0.06811	66.22	0.35400	66.50	0.03769	6.12	872	1372	308	177	239	14	74
S 37	87.415	92.546	4.437	1.0587	0.04444	11.86	0.23070	12.58	0.03765	4.19	-86	291	211	24	238	10	384
S 85	191.95	347.93	10.827	1.8126	0.04490	8.97	0.23228	9.70	0.03752	3.69	-61	219	212	19	237	9	498
S 30	109.52	132.28	5.5996	1.2078	0.04369	11.44	0.22595	12.03	0.03751	3.72	-128	283	207	23	237	9	291
S 80	113.4	122.03	5.4811	1.0761	0.04845	7.10	0.25034	8.49	0.03747	4.65	121	167	227	17	237	11	97
S 36	315.59	313.17	15.682	0.9923	0.05295	6.15	0.27246	7.21	0.03732	3.76	327	140	245	16	236	9	28
S 28	138.14	194.5	7.2008	1.408	0.05016	7.77	0.25806	8.58	0.03731	3.64	203	180	233	18	236	8	17
S 76	104.83	85.34	4.9811	0.8141	0.05233	9.04	0.26858	9.81	0.03722	3.79	300	206	242	21	236	9	22
S 78	26.719	9.0532	1.174	0.3388	0.04741	19.75	0.24316	20.63	0.03720	5.93	70	470	221	41	235	14	241
S 89	36.702	24.608	1.6591	0.6705	0.04627	21.21	0.23690	21.84	0.03713	5.23	12	510	216	42	235	12	1901

Notes:

Isotope ratios and ages are NOT corrected for initial common Pb.

10MC049 isotope ratio and apparent age errors include systematic calibration errors of 3.926526% (208Pb/232Th), 0.353480% (207Pb/206Pb), 1.0073211% (206Pb/238U) (all 1-sigma).

12LB220 isotope ratio and apparent age errors include systematic calibration errors of 4.739689% (208Pb/232Th), 0.241029% (207Pb/206Pb), 1.6105264% (206Pb/238U) (all 1-sigma).

Sweep-by-sweep downhole fractionation of U/Pb ratios NOT corrected via Si/Zr fractionation factor.

10MC049 backgrounds were monitored between sweeps 8 to 18. Sample counts were integrated from sweeps 35 to 80.

12LB220 backgrounds were monitored between sweeps 10 to 20. Sample counts were integrated from sweeps 28 to 54.

Ablation used a laser spot size of 25 microns, and a laser firing repetition rate of 10 Hz.

Table 4. U-Pb isotopic CA-TIMS data.

Sample[a]	Concentrations					Radiogenic Isotope Ratios									Isotopic Ages		
	Th/U[b]	$^{206}Pb^*$ x 10^{-13} mol[c]	mol % $^{206}Pb^*$[c]	Pb^*/Pb_c[c]	Pb_c(pg)[c]	$^{206}Pb/^{204}Pb$[d]	$^{208}Pb/^{206}Pb$[e]	$^{207}Pb/^{206}Pb$[e]	% Err[f]	$^{207}Pb/^{235}U$[e]	% Err[f]	$^{206}Pb/^{238}U$[e]	% Err[f]	Corr. coef.	$^{207}Pb/^{206}Pb$[g]	$^{207}Pb/^{235}U$[g]	$^{206}Pb/^{238}U$[g]
12LB181																	
z1	0.453	0.5340	99.42%	51	0.26	3094	0.144	0.05107	0.222	0.27373	0.269	0.03887	0.077	0.699	243.97 ± 5.12	245.67 ± 0.59	**245.85 ± 0.19**
z2	0.415	0.3437	98.89%	26	0.32	1630	0.132	0.05102	0.322	0.27354	0.374	0.03889	0.084	0.687	241.71 ± 7.42	245.52 ± 0.82	**245.92 ± 0.20**
z3	0.436	0.4907	99.35%	45	0.26	2793	0.138	0.05115	0.206	0.27427	0.261	0.03889	0.079	0.778	247.43 ± 4.73	246.10 ± 0.57	**245.96 ± 0.19**
z4	0.419	0.3834	99.19%	36	0.26	2221	0.133	0.05127	0.270	0.27468	0.330	0.03886	0.077	0.817	252.81 ± 6.22	246.43 ± 0.72	**245.77 ± 0.19**
z5	0.476	0.3812	98.27%	17	0.56	1045	0.151	0.05122	0.445	0.27458	0.503	0.03888	0.097	0.662	250.88 ± 10.23	246.35 ± 1.10	**245.87 ± 0.23**
z6	0.449	0.9080	99.52%	61	0.37	3741	0.142	0.05114	0.184	0.27396	0.232	0.03885	0.074	0.742	247.31 ± 4.24	245.85 ± 0.51	**245.70 ± 0.18**
z7	0.513	0.9763	99.62%	79	0.31	4770	0.163	0.05120	0.141	0.27446	0.194	0.03888	0.073	0.818	249.93 ± 3.24	246.26 ± 0.42	**245.87 ± 0.18**
z8	0.507	1.0145	99.52%	62	0.41	3736	0.161	0.05117	0.146	0.27435	0.200	0.03888	0.071	0.832	248.62 ± 3.37	246.16 ± 0.44	**245.91 ± 0.17**
10MC049																	
z1	0.630	0.5832	99.61%	80	0.19	4660	0.200	0.05108	0.155	0.27311	0.210	0.03878	0.074	0.819	244.59 ± 3.58	245.18 ± 0.46	245.24 ± 0.18
z2	0.627	0.6116	99.65%	88	0.18	5104	0.199	0.05115	0.145	0.27280	0.201	0.03868	0.072	0.848	247.39 ± 3.35	244.93 ± 0.44	**244.67 ± 0.17**
z3	0.604	0.2105	98.82%	26	0.21	1527	0.192	0.05136	0.426	0.27460	0.485	0.03878	0.094	0.681	257.03 ± 9.80	246.37 ± 1.06	245.25 ± 0.23
z4	0.653	0.3678	99.22%	40	0.24	2303	0.207	0.05112	0.412	0.27312	0.463	0.03875	0.080	0.688	246.06 ± 9.48	245.19 ± 1.01	245.10 ± 0.19
z5	0.667	0.5114	99.38%	51	0.26	2928	0.212	0.05106	0.242	0.27224	0.292	0.03867	0.079	0.713	243.61 ± 5.58	244.49 ± 0.63	**244.58 ± 0.19**
z6	0.713	0.9642	99.59%	78	0.33	4422	0.226	0.05117	0.153	0.27316	0.205	0.03872	0.074	0.794	248.38 ± 3.52	245.22 ± 0.45	244.89 ± 0.18
z7	0.769	1.1581	99.52%	67	0.47	3745	0.244	0.05109	0.168	0.27254	0.215	0.03869	0.072	0.755	245.04 ± 3.87	244.72 ± 0.47	**244.67 ± 0.17**
z8	0.696	0.6268	99.05%	33	0.50	1890	0.221	0.05119	0.241	0.27356	0.290	0.03876	0.079	0.705	249.30 ± 5.54	245.53 ± 0.63	245.14 ± 0.19
z9	0.515	2.3123	99.81%	161	0.36	9648	0.163	0.05112	0.095	0.27243	0.155	0.03865	0.073	0.896	246.22 ± 2.19	244.63 ± 0.34	**244.47 ± 0.18**
z10	0.656	0.7393	99.48%	60	0.32	3484	0.208	0.05115	0.181	0.27297	0.235	0.03870	0.079	0.780	247.80 ± 4.16	245.06 ± 0.51	**244.78 ± 0.19**

(a) z1, z2, etc. are labels for analyses composed of single zircon grains that were annealed and chemically abraded (Mattinson, 2005). Labels in bold indicate analyses used in weighted mean calculation.

(b) Model Th/U ratio calculated from radiogenic $^{208}Pb/^{206}Pb$ ratio and $^{207}Pb/^{235}U$ date.

(c) Pb* and Pbc are radiogenic and common Pb, respectively. mol % $^{206}Pb^*$ is with respect to radiogenic and blank Pb.

(d) Measured ratio corrected for spike and fractionation only. Fractionation correction is 0.18 ± 0.03 (1 sigma) %/amu (atomic mass unit) for single-collector Daly analyses, based on analysis of EARTHTIME ^{202}Pb-^{205}Pb tracer solution.

(e) Corrected for fractionation, spike, common Pb, and initial disequilibrium in $^{230}Th/^{238}U$. Common Pb is assigned to procedural blank with composition of $^{206}Pb/^{238}U$ and $^{207}Pb/^{206}Pb$ ratios corrected for initial disequilibrium in $^{230}Th/^{238}U$ using Th/U [magma] = 3.0 ± 0.3.

(f) Errors are 2 sigma, propagated using algorithms of Schmitz and Schoene (2007) and Crowley et al. (2007).

(g) Calculations based on the decay constants of Jaffey et al. (1971). $^{206}Pb/^{238}U$ and $^{207}Pb/^{206}Pb$ dates corrected for initial disequilibrium in $^{230}Th/^{238}U$ using Th/U [magma] = 3.0 ± 0.3; see (f) for errors.

Interpretation

The uniform, concordant age population of zircon grains in the Michie formation samples, combined with the grain morphologies and CL zoning patterns, indicate that the grains record rapid deposition of the unit near an igneous source. Petrography of the Michie formation samples also suggests an active arc setting (Fig. 13). The weighted mean age of the five youngest grains, 244.64 ± 0.08 Ma, falls within the range of U-Pb crystallization ages in tonalite and rhyolite of the Kutcho Assemblage in northern British Colombia, which is 255.13 ±0.96 to 242 ±1 Ma (Fig. 2; Childe and Thompson, 1997; Schiarizza, 2012). This age correlation suggests the Michie formation is a sedimentary succession deposited on the flank of an arc which is correlative to the Kutcho arc, during the Early to Middle Triassic.

The youngest detrital zircon population in the Richthofen formation sample, 12LB220, is ca. 190 Ma (Fig. 21). This age is consistent with an erosional source region from both the Stikinia arc to the west and the Quesnellia arc to the east of the Whitehorse trough, where belts of batholiths yield U-Pb zircon crystallization dates ranging from Late Triassic to Early Jurassic (Tempelman-Kluit and Wanless, 1980; Hart and Radloff, 1990; Mortensen, 1992; Hart et al., 1995; Thorkelson et al., 1995; Johansson et al., 1997; Colpron, 2011). In addition, there are a number of older detrital zircon grains ranging in age from ca. 260-245 Ma and ca. 345-300 Ma (Fig. 21). The older, dominant population is most likely derived from a source in the uplifted Yukon-Tanana terrane, which is characterized by arc magmatism ranging from Late Devonian to Late Permian, including the “Little Salmon cycle” at ca. 342-314 Ma (e.g., Nelson et al., 2006). The younger ca. 260-245 Ma population may correlate to either, or both, the Yukon Tanana terrane’s “Klondike cycle” of magmatism (ca. 269-253 Ma; Nelson et al., 2006) or magmatism in the Kutcho assemblage and correlatives (ca. 255-242 Ma; e.g. Schiarizza, 2013).

2.7. Structure

Due to the lack of continuous outcrop, structural features in the map area are inferred primarily through cleavage-bedding relationships and changes in foliation intensity at isolated outcrops. A simplified bedrock geology map with structural readings and equal area lower hemisphere plots is shown in Figure 22. Other useful indicators

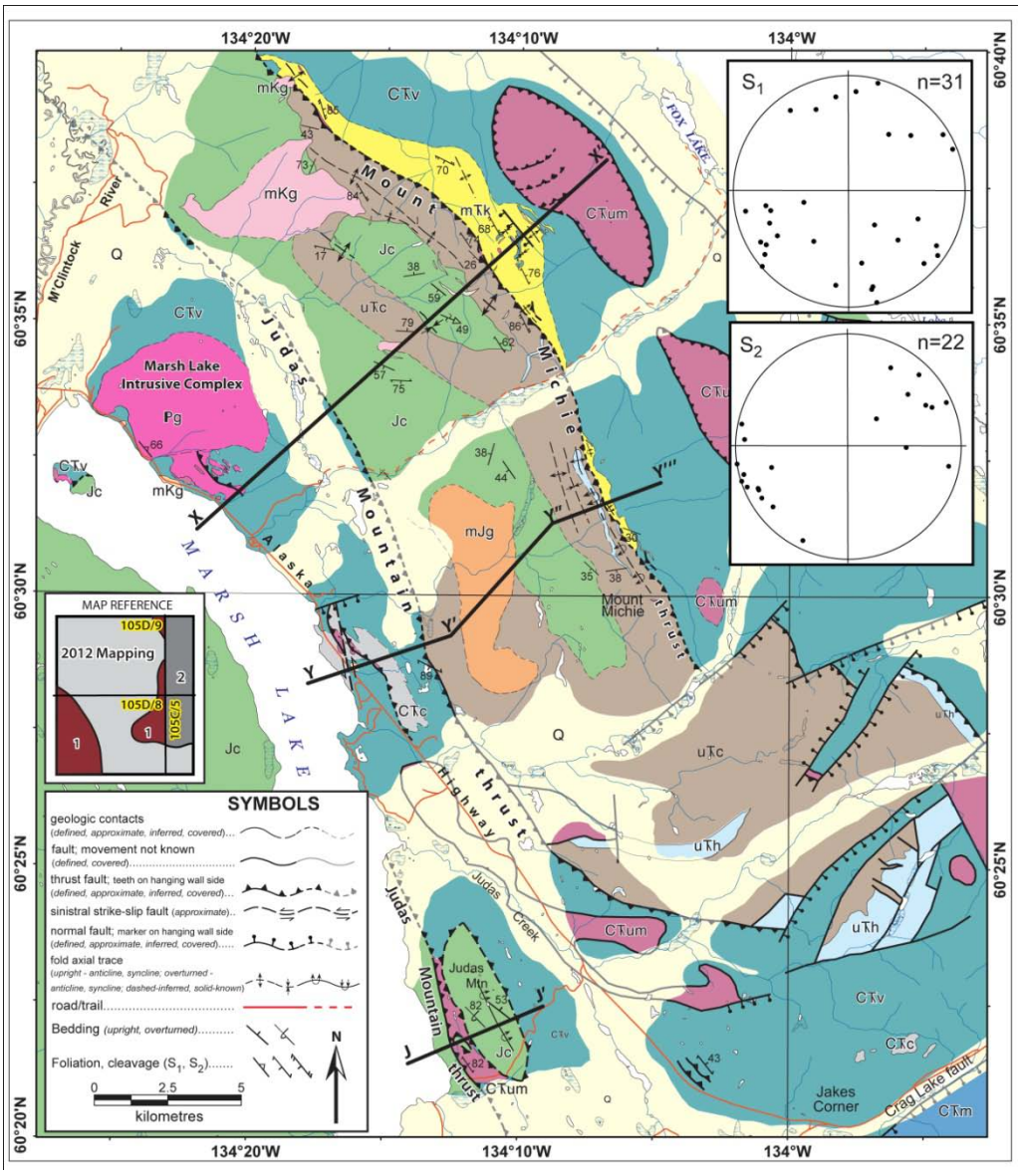

Figure 22. Simplified bedrock geology map of study area with structure

Poles to the axial surfaces for D1 (S_1) and D2 (S_2) throughout the study area shown in equal area lower hemisphere plot insets, legend is same as in Figure 5. A 1:50 000 scale version of this bedrock geology map is found in Appendix A.

include offsets of lithology on the map or the local presence of cataclasite and alteration of ultramafic rocks to listwaenite (Fig. 23a). The structural style of the Marsh Lake area is dominated by variable scale folding and foliation spacing from separate deformational events. The first deformational event (D1) is represented by thrusting of the Cache Creek terrane rocks onto rocks of the Whitehorse trough and Stikinia (Judas Mountain thrust) and was recorded through measurements of folded, spaced fracture cleavage in all stratigraphic units of the study area (S_1 foliation; Fig. 22). The second deformational event (D2) included reshuffling of the aforementioned units, thrusting Whitehorse trough rocks above those of the Cache Creek terrane (Mount Michie thrust). The D2 event is recorded through measurements of spaced fracture cleavage which cross-cut D1 features, affecting all stratigraphic units within the study area (S_2 foliation; Fig. 22). Both sets of foliations appear in outcrop as sets of parallel fractures within the stratigraphic units, without demonstrable mineral growth. When either S_1 or S_2 foliation appears in the volcanic and intrusive rocks proximal to the fault contacts, however, foliation can be defined by schistose fabric and growth of minerals such as fuchsite in the listwaenite bodies (Fig. 23 a and b).

Basinal Laberge Group and Lewes River Group sedimentary rocks throughout the study area preserve bedding and locally contain spaced S_1 fabric which has an average orientation of 290\87NE (Fig. 22). Foliation in the basinal rocks is more penetrative closer to fault contacts and typically follows the axial planar orientation of related folds. A penetrative foliation occurs in the volcanic rocks of the Cache Creek terrane, but it is difficult to discern its orientation except where it is more pervasive closer to fault contacts (e.g. Fig. 23 a and b). Hydrothermal brecciation of these units also occurs proximal to major fault contacts (Fig. 23c). Folding in the region was typically recognized through bedding-cleavage intersection relationships; however, outcrop-scale folding can be observed within 1-2 km of major fault contacts. The outcrop scale folds range from tight and upright (Fig. 24) to isoclinal and overturned. The folding recognized at outcrop scale typically becomes tighter and more inclined towards the fault contacts; this is particularly true for the D2 event, where S_2 orientations average a best fit at 154\31SW. Obtaining a sense of orientation for the fold inclination relative to fault emplacement aids interpretation on vergence for the faults if both features are related to the same deformational event.

Figure 23. Outcrop photos showing structural features

Photographs showing (a) strongly foliated listwaenite (altered from ultramafic) at Judas Mountain; (b) strongly foliated volcanic rocks near the Judas Mountain thrust; and (c) hydrothermally brecciated volcanic rock near Mt. Michie thrust.

The major features in the Marsh Lake area which are not immediately discernable at the outcrop scale include northwest-trending open folds and north-northwest striking thrust faults. Two major thrust faults have been identified in the map area: 1) the Judas Mountain thrust, a folded thrust fault striking north-northwest, which placed rocks of the Cache Creek terrane above sedimentary strata of the Whitehorse trough (D1; Fig. 25); and 2) the Mount Michie thrust, a south-southeast striking, steeply west-dipping reverse fault which brings rocks of the Whitehorse trough (Laberge Group) and underlying Lewes River Group (Casca member) above the Michie formation and Cache Creek volcanic rocks in the centre of the map area (D2; Figs. 22 and 26). In the southeast part of the map, north of Jakes Corner, Gordey and Stevens (1994) mapped a number of northeast-striking normal faults that delineate the contact between Stikinia and Whitehorse trough rocks to the north and Cache Creek rocks to the south. These

structures are similar in style and character to the Crag Lake fault mapped by Hart and Radloff (1990) southwest of the study area (Fig. 22; Appendix A).

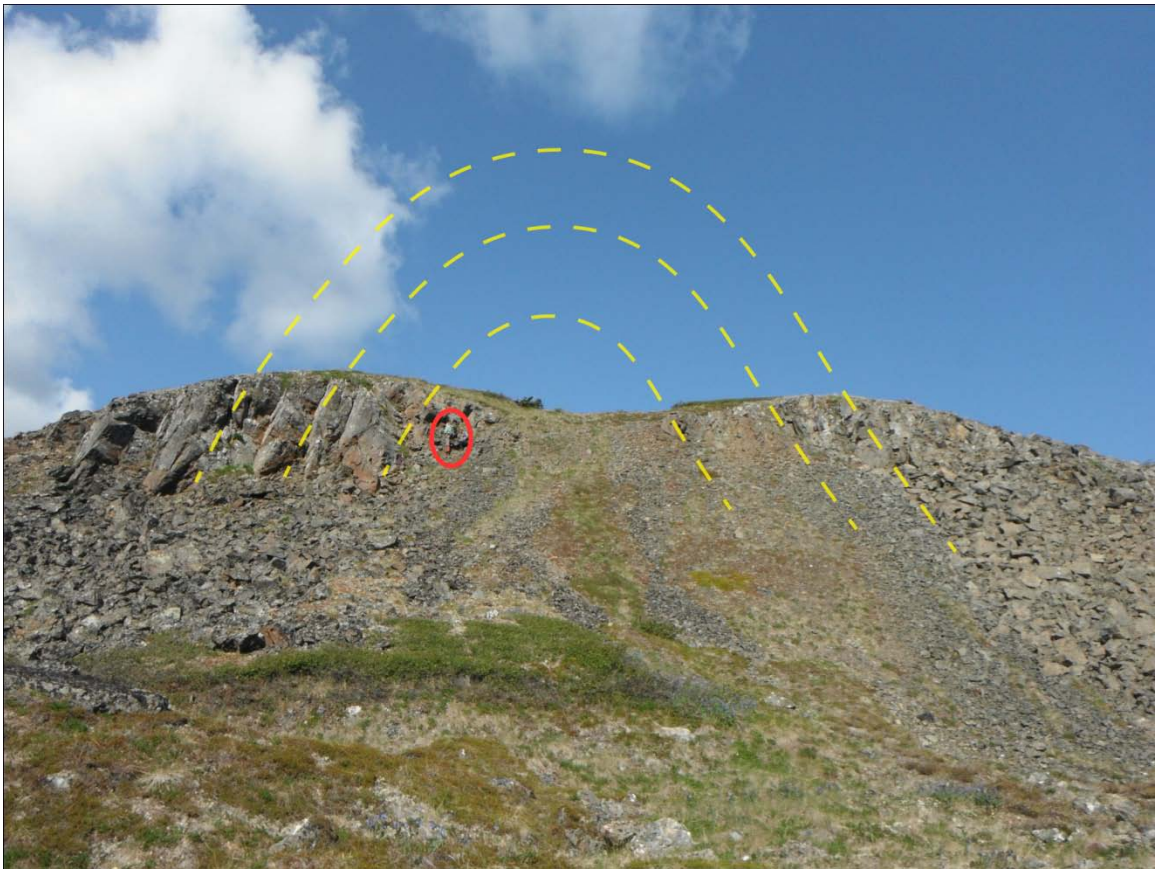

Figure 24. Photo of outcrop-scale upright F1 fold

See person circled in red for scale.

2.7.1. Judas Mountain thrust

The Judas Mountain thrust fault (D1) marks the structural boundary between the Cache Creek terrane and the sedimentary rocks of the Whitehorse trough in the western part of the study area (Fig. 5). The thrust is exposed in the Judas Mountain area where rocks of the Whitehorse trough in the footwall show tight, overturned, southwest-verging folds. In the immediate hanging wall at this location, mafic and ultramafic rocks are characterized by foliated listwaenite, serpentinite, and extensive hydrothermal veining. At Judas Mountain, directly east from the leading edge of the Judas Mountain thrust, rocks of the Laberge Group (Richthofen formation) are surrounded by Cache Creek

rocks which include intensely foliated ultramafic rocks to the west and metavolcanic rocks to the east (Fig. 22). This relationship is interpreted as a fenster of Laberge Group in the footwall of the Judas Mountain thrust, which was exposed through antiformal folding and erosion of the thrust contact (section J-J', Fig. 25). A fault surface with similar characteristics to the Judas Mountain thrust is recognized to the east-northeast of the Alaska Highway as a northwest-striking, steeply-dipping structure juxtaposing Cache Creek rocks to the west and sedimentary strata of Stikinia and Whitehorse trough to the east. This surface has little exposure, but is interpreted to be an eastern occurrence of the folded Judas Mountain thrust (Fig. 22). Folding of the Judas Mountain thrust is interpreted to result from a second phase of compression, which also led to the development of the northeast-verging Mount Michie thrust.

2.7.2. Mount Michie thrust

The Mount Michie thrust (D2) is characterized by intense foliation and tight to isoclinal, northeast-verging folds in the immediate hanging wall, as well as the local occurrence of listwaenite and hydrothermally brecciated rocks in the immediate footwall of the thrust. The Mount Michie thrust brings rocks of Stikinia, to the west, structurally above rocks of the Cache Creek terrane to the east. Open folds of sedimentary strata of the Lewes River and Laberge groups that crop out in the central part of the map area become progressively tight and overturned to the northeast, near the Mount Michie thrust (Fig. 25). The hinge lines of these folds typically have trends parallel to the strike of the Mount Michie thrust.

2.7.3. Interpretation

The structural evolution of the Michie Creek/Tagish area first involved a phase of southwest-verging folds and thrusts, D1, which emplaced rocks of the Cache Creek terrane over Stikinia and the Whitehorse trough. This phase is represented by the Judas Mountain thrust, which marks the westernmost extent of the Cache Creek terrane in the map area, and a probable northern equivalent of the Nahlin fault recognized in northern British Columbia and southern Yukon (Fig. 2; Hart and Radloff, 1990; Mihalynuk, 1999). This phase of thrust faulting may also be responsible for bringing the harzburgite/dunite bodies, interpreted to represent deeper levels of the arc assemblage, into contact with

relatively shallow level volcanic and volcaniclastic rocks of the Cache Creek terrane (Figs. 22, 25).

The Mount Michie thrust is interpreted to be part of a second compressional phase, D2, that brought rocks formerly in the footwall of the first phase Judas Mountain thrust (Stikinia and Whitehorse trough) over its hanging wall rocks (Cache Creek terrane). The second phase of compression also resulted in northeast-verging folds, including the folding of the Judas Mountain thrust that led to the exposure of a fenster of Laberge Group rocks at Judas Mountain (Figs. 22, 25). A series of late, northeast-striking normal faults locally disrupts this sequence.

2.8. Discussion

Based on the interpretations of mapping, petrography, geochemistry and U-Pb geochronology, the northern apex of the Cache Creek terrane: (*i*) records a complex structural history which includes emplacement of rocks of a Cache Creek terrane oceanic arc structurally above rocks of the Whitehorse trough to the west (D1), followed by folding of this contact and eastward thrusting of the Whitehorse trough and Stikinia sedimentary units, the footwall to the first thrust event, structurally above the Cache Creek terrane in the central part of the study area (D2; Figs. 22, 25); (*ii*) contains volcanic and plutonic rocks that represent remnants of an intra-oceanic arc assemblage; and (*iii*) preserves a volcaniclastic assemblage, the Michie formation, which represents a late phase deposition of arc-proximal clastic rocks, quite possibly sourced from the Kutcho assemblage and its correlatives in British Columbia (Thorstad, 1984; Childe and Thompson, 1997; Mihalynuk et al., 2003; English et al., 2010; Schiarizza, 2012).

The structural history of the northern termination of the Cache Creek reveals two compressional phases resulting in two main thrusts in the study area. The first phase, D1, resulted in the southwestward emplacement of Cache Creek rocks over rocks of the Whitehorse trough along the Judas Mountain thrust. This thrust is poorly exposed in the map area (Fig. 5 and 22), but is identified in the Judas Mountain area where it has juxtaposed volcanic rocks of the Cache Creek terrane over clastic rocks of the Whitehorse trough. The D1 phase is most likely synchronous with initial south-west

verging accretion of Cache Creek rocks to the Stikine arc segments, a thrust similar to that of the Nahlin fault in northern British Columbia and southernmost Yukon (Hart and Radloff, 1990; Gabrielse, 1991; 1998; Mihalynuk, 1999; Mihalynuk et al., 2004; Evenchick et al., 2005). This phase occurred prior to deposition of the Cache Creek chert clast-bearing Tantalus and Inklin formations and after deposition of the footwall Richthofen formation; the activity on the fault, therefore, may be linked to the Bajocian aged unconformity between these two units (Fig. 4).

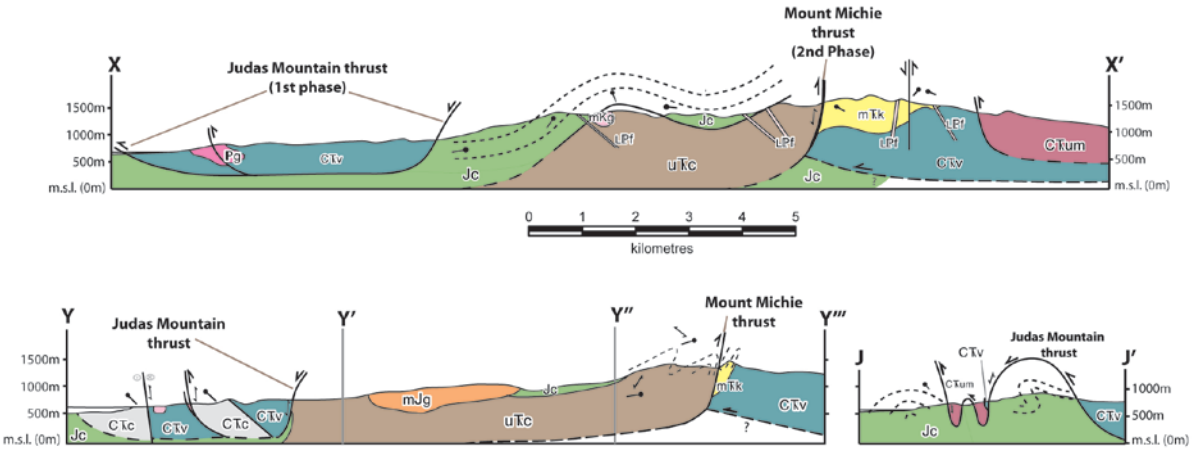

Figure 25. Structural cross sections of study area
Cross sections for section lines shown in Figure 6 and 20; the same legend applies in this figure as in Fig. 5; no vertical exaggeration.

The D2 phase of compression folded the Judas Mountain thrust contact, so that it appears as multiply repeating, and steeply dipping, fault contacts (Fig. 25). The main structure associated with the D2 phase of deformation is the north-northwest-striking, east-verging Mount Michie thrust fault, which is cross-cut by a pluton that may belong to the mid-Cretaceous Whitehorse suite (Fig. 5). Compressional structures similar to the D2 folds and the Mount Michie thrust are recorded in central Stikinia, particularly in the Bowser Basin, where rocks similar to those of the Whitehorse trough (e.g., English and Johnston, 2005) were folded and thrust eastward as early as Oxfordian to Albian time (Skeena fold and thrust belt; Evenchick, 1991; Evenchick et al., 2007). Northwest-trending structures in the northern portion of the Canadian Cordillera, however, appear to have been re-activated by transpression at ca. 115-95 Ma from movement on major strike-slip faults such as the Teslin and Braeburn (Gabrielse et al., 2006; White et al., 2013). Thus, the Mount Michie thrust likely developed following the accretionary

emplacement of the Cache Creek terrane above strata of Stikinia and the Whitehorse trough, and probably correlates to structural features such as the Skeena fold belt and/or mid-Cretaceous transpression that immediately predated intrusion of the Whitehorse suite.

From a regional Canadian Cordillera perspective, the first compressional event, represented by the Judas Mountain thrust and associated fabrics, relates to the obduction of Cache Creek terrane rocks onto the Stikinia arc along WSW-verging structures (Fig. 26C and D). This phase of obduction is recorded in a thrust panel within the French Range of northern British Columbia, which contains blueschist dated at ca. 172 for both peak metamorphism and exhumation cooling by U-Pb zircon and $^{40}Ar/^{39}Ar$ plateau ages, respectively (Mihalynuk et al., 2004). The second compressional phase results in the previous major fault contact being cross-cut by a fault with a similar trend. The Mount Michie thrust is more subtle than the Judas Mountain thrust and may correlate to eastward verging structures in the Skeena fold and thrust belt. In the more northerly portion of the Canadian Cordillera, structures of similar eastward vergence do not appear until the mid-Cretaceous (Nelson et al., 2013). The Mount Michie thrust, therefore, is most likely correlative to the mid-Cretaceous compressional features of the northern Canadian Cordillera.

Tectonic discrimination diagrams shown in Fig. 18 display the composition of mafic rocks at the northern termination in the Cache Creek relative to those in northern British Columbia that were published in the geochemical study of English et al. (2010). The British Columbia study revealed tectonically imbricated assemblages within the northern wedge of Cache Creek terrane ranging from island arc tholeiites and back arc basalts to enriched, within-plate basalts. The alkaline ocean island basalt (OIB) of the "carbonate assemblage" of English et al. (2010; Fig. 18) has been paleontologically determined to be Carboniferous-Permian (Monger, 1975), whereas the island arc, calc-alkaline, and back arc basin related rocks of the "oceanic crustal assemblage" have been dated to be mid-Late Permian to Middle Triassic (Childe et al., 1998; Devine, 2002; Mihalynuk et al., 2003).

The rocks of the Cache Creek terrane in the study area, north of the Crag Lake fault, are geochemically similar to those of the volcanic arc rocks in northern British

Columbia. Unlike the volcanic rocks of the thick carbonate sequence, which are found along with the arc volcanic rocks in northern BC, the mafic rocks north of the Crag Lake fault lack any OIB geochemical signatures. The geochemical signature of the mafic rocks in the most northerly exposed portion of the Cache Creek terrane characterizes the study area's rocks as having formed in an arc to back-arc setting. This arc affinity differs from what Cache Creek terrane lithological descriptions would include in the past (e.g. Monger and Price, 2002).

The Kutcho assemblage to the south of the field area, combined with arc and oceanic volcanic rocks of the Cache Creek terrane in the northern Cordillera have been regarded as the products of Middle-Upper Permian incipient arc magmatism by English and Johnston (2005). This arc magmatism is thought to have followed a reversal in subduction polarity in the Stikine arc; from eastward dipping subduction of the Panthalassa lithosphere to westward subduction of the Cache Creek terrane (English and Johnston, 2005). Data from the Michie formation, however, indicates it is an arc-flanking depositional sequence, which most likely was derived from a correlative to the Kutcho Assemblage to the south. The Early Triassic age of Cache Creek terrane ultramafic rocks east of the study area (245.4 ± 0.8 Ma; Gordey et al., 1998) is similar to the age populations obtained from the Michie formation and may represent an igneous portion to the Kutcho-correlative arc. The Michie formation zircon populations and the tectonic signature of surrounding volcanic and intrusive rocks represent a single juvenile arc with no detrital influence from more evolved rocks, such as Stikinia, in the early Middle Triassic. These observations further illustrate an accretion of an intra-oceanic arc to the Stikinia-Quesnellia subduction zone. This accretion should be included in the evaluation of theories such as the proposed oroclinal bending model which proposes an indented geometry of the once curvilinear Stikinia-Quesnellia arc and cessation of subduction at the proposed hinge of the orocline prior to the arrival of the larger seamount and (or) oceanic plateaux of the Panthalassic Ocean which contain exotic Tethyan fauna (Mihalynuk et al., 1994).

The enigmatic Intermontane terrane geometry in Canadian Cordillera is perhaps best explained as having evolved from oroclinal bending of the Stikinia-Quesnellia arc (Mihalynuk et al., 1994), entrapping the Cache Creek accretionary complex (Fig. 26, A-C). In this model, buoyant seamounts entered the trench and stalled subduction of

Panthalassic Ocean beneath the Stikinia-Quesnellia arc in the Late Triassic, triggering counter-clockwise oroclinal rotation of the Stikine portion of the terrane about a vertical axis. A modern analogue for the initial impingement proposed by this model may be found in the northwestern Pacific Ocean, where the Emperor seamount chain is slowing subduction at the cusp of the Aleutian and Kurile arcs (Vogt et al., 1976). The model of Mihalynuk et al., (1994) describes the evolution of the Stikinia-Quesnellia arc having resulted in subduction of the Panthalassic Ocean in opposing directions beneath Quesnellia to the east and Stikinia to the west (Fig. 26D). The doubly verging subduction between a continuous Stikinia-Quesnellia arc and the necessary rotation of Stikinia during the Late Triassic to Middle Jurassic is debated as being geodynamically problematic. This debate is valid, as the model provides a modern analogue with a weak correlation; the analogue describes doubly verging subduction of the Molucca Sea between two separate arcs, the Sangihe and Halmahera in southeast Asia, rather than a continuous arc, as is proposed by bending of the Stikinia/Yukon-Tanana/Quesnellia arc (Hamilton, 1979; Mihalynuk et al., 1999).

Permian limestones within the Cache Creek accretionary complex contain Tethyan macro- and microfauna, and non-North American Middle Triassic conodont and radiolarian populations occur in the Sowchea succession in central British Columbia (Orchard et al., 2001). The Middle Triassic conodont populations in the limestone indicate that portions of the Cache Creek terrane remained in the Panthalassa, far outboard of western North America at this time (Orchard et al., 2001). Similarly, we interpret the Michie formation to have been deposited from a unimodal intra-oceanic arc source, within Panthalassa, outboard of western North America, in the Early to Middle Triassic (e.g. paleogeographic reconstruction in Figure 3B). The intra-oceanic Kutcho arc most likely was ferried into the Cache Creek accretionary complex during the subduction of Panthalassic oceanic lithosphere during the Early to Middle Triassic. A modern analogue to the accretion of juvenile arc crust (and flanking Michie formation) to the Stikina forearc may be that of the buoyant Izu-Bonin-Mariana arc obliquely colliding with, and accreting to, the mature Honshu volcanic arc to the north in the west Pacific (Soh et al., 1991; Taira et al., 1992; 1998; Taira, 2001).

Following the doubly verging subduction of Panthalassic oceanic lithosphere, during the Early Jurassic, the northern apex of the Stikinia/Yukon-Tanana/Quesnellia

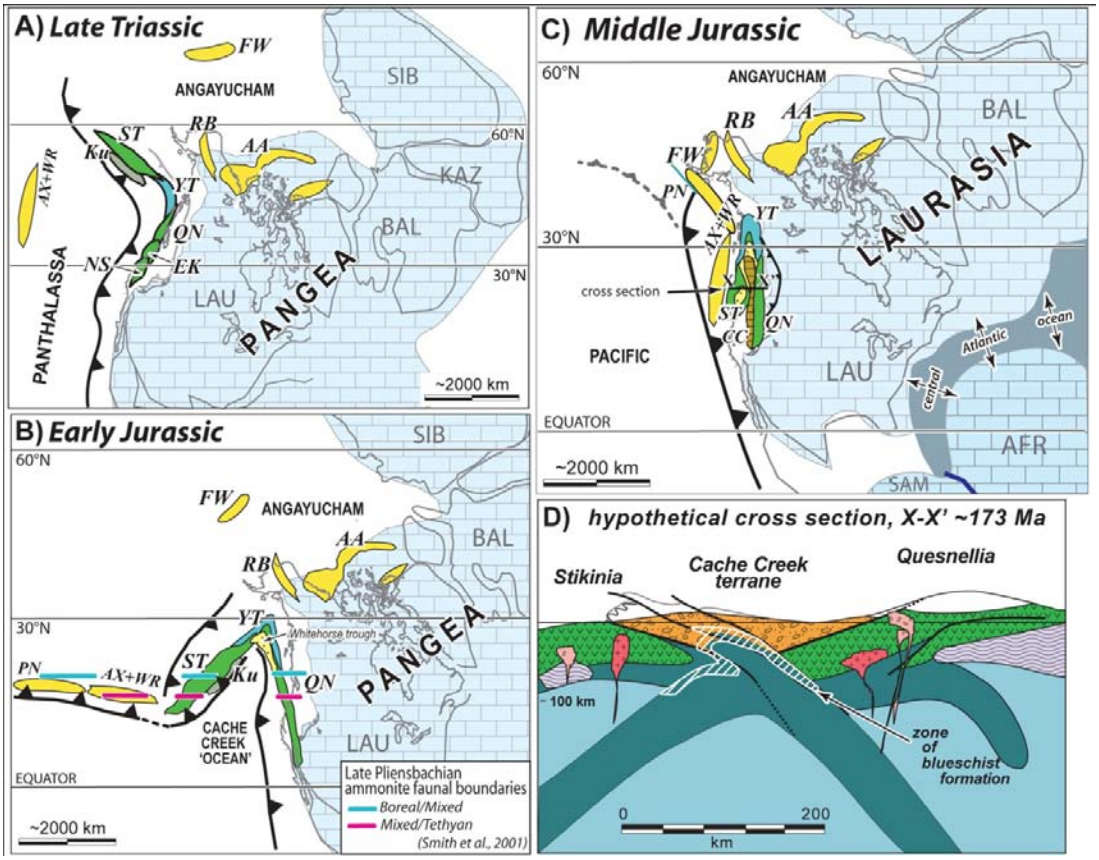

Figure 26. Late Triassic to Middle Jurassic paleogeographic reconstructions

Mesozoic paleogeographic reconstructions along the western margin of Laurentia, modified after Nelson et al. (2013) for (A) Late Triassic, (B) Early Jurassic and (C) Middle Jurassic. Reconstructions show rotation of Stikinia during oroclinal bending of the ST-YT-QN arc after model proposed by Mihalynuk et al. (1994). Fossil constraints from Smith et al. (2001) shown in (B), as well as onset of deposition in Whitehorse trough and exhumation of the Yukon-Tanana terrane (YT). (D) shows Middle Jurassic schematic cross section across Intermontane terranes and rupture of the doubly subducting slab, leading to exhumation and cooling of Cache Creek (CC) blueschist (after Mihalynuk et al., 2004). AA = Arctic Alaska, AX = Alexander, CC = Cache Creek, EK = Eastern Klamaths, FW = Farewell, Ku = Kutcho arc, NS = Northern Sierras, PN = Peninsular, QN = Quesnellia, RB = Ruby, ST = Stikinia, WR = Wrangellia, YT = Yukon-Tanana.

orocline was rapidly exhumed and was accompanied by the onset of marine deltaic sedimentation into the Whitehorse trough (Fig. 26B, Laberge Group; Lowey, 2004; Lowey et al., 2009; Colpron et al., 2007, White et al., 2012; Nelson et al., 2013). Provenance of the Laberge Group of the Whitehorse trough records this additional detrital source in the small detrital zircon pre-Jurassic age populations (Fig. 21).

Chapter 3. Conclusions

Prior to accretion of the Cache Creek terrane to the Stikinia-Quesnellia volcanic arc and oroclinal enclosure, oceanic crustal components of the Cache Creek terrane lay outboard of both the Kutcho volcanic arc and the Stikinia-Quesnellia arc, within the Panthalassic Ocean. In the current terrane geometry, rocks at the northern termination of the Cache Creek terrane in Yukon Territory most resemble a northern extension of Cache Creek terrane seen in the Atlin to Dease Lake region of northern British Columbia. The rocks at the northern termination consist of an igneous complex of mafic to intermediate metavolcanic rocks. The geochemical signature of mafic plutonic rocks which exclusively intrude volcanics in the study area is defined by high Th/Nb and Ce/Nb ratios as well as consistent LREE enrichment, indicating the rocks formed in a magmatic arc that was sourced from a slightly enriched mantle. These intrusive rocks are similar to those of the volumetrically dominant igneous rocks of the Cache Creek terrane in northern British Columbia which has a subalkaline geochemical signature with arc affinity (English et al., 2010).

Rocks overlying and locally intercalated with the Cache Creek terrane volcanics in the study area include a siliciclastic to volcaniclastic unit informally termed the Michie formation in this study. Based on unimodal U-Pb zircon ages of sharply faceted grains, this unit is interpreted to record proximal deposition of sediment derived from an igneous complex with a unimodal and narrow $^{206}Pb/^{238}U$ age-range of 245.85 ± 0.07 to 244.64 ± 0.08 Ma. The narrow age-range and intra-oceanic arc signature in the intrusive rocks which source the volcaniclastic rocks indicate the Michie formation was deposited on the flank of a volcanic arc. The $^{206}Pb/^{238}U$ ages from the Michie formation overlap with ages obtained from within the Kutcho arc assemblage in northern British Columbia (Childe et al., 1998; Schiarizza, 2012). A single detrital source for the Michie formation, which was deposited along the flank of a Kutcho equivalent arc, suggests that the arc which hosted the flanking basin was not interacting with other terranes (alternative detrital sources)

during the Early to Middle Triassic. Alternatively, the Kutcho equivalent arc was the only emergent arc in the vicinity of the Michie basin during the Early to Middle Triassic.

Accretion of the Cache Creek terrane with the Stikinia-Quesnellia arc and subsequent enclosure of the accretionary complex involved a record of northwest-trending, southwest-verging thrusting of rocks belonging to the Cache Creek terrane over those of Stikinia and its correlative forearc basin, the Whitehorse trough. This thrust juxtaposition led to syn-orogenic deposition into the Whitehorse trough by Early Jurassic. The initial phase of thrusting between these two terranes is represented in northern British Columbia and southern Yukon by the Nahlin fault (Fig. 2; Hart and Radloff, 1990; Mihalynuk, 1999). The Judas Mountain thrust, defined in this study at the northern termination of the Cache Creek terrane in Yukon Territory, is interpreted to represent an extension of the Nahlin fault. The Judas Mountain thrust is traced north of the Crag Lake fault (Fig. 5), which is a northeast trending, down-to-the-south normal fault. The Judas Mountain thrust had a relatively shallow dip before being folded by a second compressional event which led to east-verging folding and thrusting. The second compressional event transported rocks belonging to Stikinia and the Whitehorse trough, originally in the footwall of the Judas Mountain thrust, structurally above Cache Creek terrane rocks in its hanging wall. A consequence of the second compressional event was folding of the Judas Mountain thrust and exposure of a fenster of Laberge Group rocks at Judas Mountain (Fig. 5; Appendix A). This phase of compression may correlate to the Oxfordian to Albian east-verging folds and thrusts of the Skeena fold belt in the Bowser basin (Evenchick, 1991). The character of the Mount Michie thrust and related folds also share traits such as the axial planar strike in S2 structural orientations as well as the entire package of rocks being affected by the transpressional folding and faulting in the northern Whitehorse trough. These structures formed by re-activation along the Teslin Fault at ca. 115-95 Ma (Gabrielse et al., 2006; White et al., 2013) and led to further shortening at the termination of the Cache Creek terrane during the mid-Cretaceous.

References

Armstrong, R. L. 1988, Mesozoic and early Cenozoic magmatic evolution of the Canadian Cordillera: Geological Society of America Special Papers, **218**: 55-92.

Bambach, R. K. 1990, Late Palaeozoic provinciality in the marine realm: Memoirs of the Geological Society of London, **12**: 307-323.

Barrett, T. J. and MacLean, W. H. 1999, Volcanic sequences, lithogeochemistry, and hydrothermal alteration in some bimodal volcanic-associated massive sulfide systems. In Volcanic-Associated Massive Sulfide Deposits: Processes and Examples in Modern and Ancient Environments. Edited by Barrie, C. T. and M. D. Hannington. Society of Economic Geologists, Reviews in Economic Geology, **8**: 101-131.

Beck, M.E. 1976. Discordant paleomagnetic pole position as evidence of regional shear in the western Cordillera of North America: American Journal of Science, **276**: 694-712.

Belasky, P. and Stevens, C. H. 2006, Permian faunas of westernmost North America: Paleobiogeographic constraints on the Permian positions of Cordilleran terranes: Geological Association of Canada, Special Paper **46**: 71–80.

Bickerton, L., Colpron, M., and Gibson, D. 2013. Cache Creek terrane, Stikinia, and overlapassemblages of eastern Whitehorse (NTS 105D) and western Teslin (NTS 105C) map areas.In: Yukon Exploration and Geology 2012, K.E. MacFarlane, M.G. Nordling, and P.J. Sack (eds.), Yukon Geological Survey, p. 1-17.

Boutelier, D., Chemenda, A., and Burg, J. P. 2003, Subduction versus accretion of intra-oceanic volcanic arcs: insight from thermo-mechanical analogue experiments: Earth and Planetary Science Letters, **212**: 31-45.

Brayard, A., Bucher, H., Escarguel, G., Fluteau, F., Bourquin, S., and Galfetti, T. 2006, The Early Triassic ammonoid recovery: Paleoclimatic significance of diversity gradients: Palaeogeography, Palaeoclimatology, Palaeoecology, **239**: 374-395.

Canil, D., Mihalynuk, M., and Charnell, C. 2006, Sedimentary record for exhumation of ultrahigh pressure (UHP) rocks in the northern Cordillera, British Columbia, Canada: Geological Society of America Bulletin, **118**: 1171-1184.

Cawood, P. A., Kröner, A., Collins, W. J., Kusky, T. M., Mooney, W. D. and Windley, B. F. 2009. Accretionary orogens through Earth history. In Earth Accretionary Systems in Space and Time. Edited by Cawood, P. A. and A. Kröner: Geological Society of London, Special Publications **318**: 1-36.

Childe, F.C., Thompson, J.F.H., Mortensen, J.K., Friedman, R.M., Schiarizza, P., Bellefontaine, K., and Marr, J.M. 1998. Primitive Permo-Triassic volcanism in the Canadian Cordillera: Tectonic and metallogenetic implications: Economic Geology, **93**: 224–231.

Cloos, M. 1993, Lithospheric buoyancy and collisional orogenesis; subduction of continental margins, island arcs, and oceanic plateaus: Abstracts with Programs - Geological Society of America, **25**: 70-71.

Colpron, M. 2011. Geological compilation of Whitehorse trough - Whitehorse (105D), Lake Laberge (105E), and part of Carmacks (115I), Glenlyon (105L), Aishihik Lake (115H), Quiet Lake (105F) and Teslin (105C). Yukon Geological Survey, Geoscience Map 2011-1, 1:250 000.

Colpron, M. and Friedman, R.M. 2007. U-Pb zircon ages for the Nordenskiold formation (Laberge Group) and Cretaceous intrusive rocks, Whitehorse trough, Yukon. Yukon Exploration and Geology 2007: 139-152.

Colpron, M. and Nelson, J.L. 2011. A digital atlas of terranes for the northern Cordillera: Yukon Geological Survey, www.geology.gov.yk.ca/bedrock_terrane.html, accessed September 2013; also BC Geological Survey, BC GeoFile 2011-11, http://www.empr.gov.bc.ca/Mining/Geoscience/PublicationsCatalogue/GeoFiles/Pages/2011-11.aspx.

Colpron, M., Nelson, J.L. and Murphy, D.C. 2006. A tectonostratigraphic framework for the pericratonic terranes of the northern Canadian Cordillera, *in* Colpron, M. and Nelson, J.L., eds., Paleozoic Evolution and Metallogeny of Pericratonic Terranes at the Ancient Pacific Margin of North America, Canadian and Alaskan Cordillera: Geological Association of Canada Special Paper **45**: 1-23.

Coney, P. J., Jones, D.L., and Monger, J.W.H. 1980. Cordilleran suspect terranes: Nature, **288**-27: p. 8.

Cook, F.A., Clowes, R.M., Snyder, D.B., van der Velden, A.J., Hall, K.W., Erdmer, P., and Evenchick, C.A. 2004, Precambrian crust beneath the Mesozoic northern Canadian Cordillera discovered by Lithoprobe seismic reflection profiling: Tectonics, **23**: TC2010.

Cordey, F., Gordey, S.P., and Orchard, M.J. 1991. New biostratigraphic data from the northern Cache Creek terrane, Teslin map area, southern Yukon. In: Current Research part E, Geological Survey of Canada, p. 67-76.

Crowley, J.L., Schoene, B., Bowring, S.A. 2007, U-Pb dating of zircon in the Bishop Tuff at the millennial scale: Geology, **35**: 1123-1126.

Devine, F.A.M. 2002. U–Pb geochronology, geochemistry, and tectonic implications of oceanic rocks in the northern Cache Creek Terrane, Nakina area, northwestern British Columbia. B.Sc. thesis, The University of British Columbia, Vancouver, B.C.

Dickinson, W. R., 1970, Interpreting detrital modes of graywacke and arkose: Journal of Sedimentary Research, **40**: 695-707.

Dostal, J., Gale, V., and Church, B.N. 1999. Upper Triassic Takla Group volcanic rocks, Stikine Terrane, north-central British Columbia: geochemistry, petrogenesis, and tectonic implications: Canadian Journal of Earth Sciences, **36**: 1483–1494.

Dostal, J., Keppie, J. D., and Ferri, F. 2009, Extrusion of high-pressure Cache Creek rocks into the Triassic Stikinia-Quesnellia arc of the Canadian Cordillera: implications for terrane analysis of ancient orogens and palaeogeography: Geological Society, London, Special Publications, **327**: 71-87.

English, J. M., and Johnston, S. T. 2005, Collisional orogenesis in the northern Canadian Cordillera: Implications for Cordilleran crustal structure, ophiolite emplacement, continental growth, and the terrane hypothesis: Earth and Planetary Science Letters, **232**: 333-344.

English, J.M., Mihalynuk, M.G., and Johnston, S.T. 2010. Geochemistry of the northern Cache Creek terrane and implications for accretionary processes in the Canadian Cordillera: Canadian Journal of Earth Sciences, **47**: 13-34.

Evenchick, C.A., Gabrielse, H., Cook, F.A., Clowes, R.M., Snyder, D.B., van der Velden, A.J., Hall, K.W., and Erdmer, P. 2001, Highlights of SNORCLE Line 2A—The Cassiar-Stewart Highway (Highway 37, 37A), in Cook, F., and Erdmer, P., eds., Slave–Northern Cordillera Lithospheric Evolution (SNORCLE) Transect and Cordilleran Tectonics Workshop Meeting, Lithoprobe Report No. 79: Sydney, Pacific Geoscience Centre: 56–58.

Evenchick, C. A., Gabrielse, H., and Snyder, D. 2005, Crustal structure and lithology of the northern Canadian Cordillera: alternative interpretations of SNORCLE seismic reflection lines 2a and 2b: Canadian Journal of Earth Sciences, **42**: 1149-1161.

Evenchick, C.A., McMechan, M.E., McNicoll, V.J. and Carr, S.D., 2007, A synthesis of the Jurassic-Cretaceous tectonic evolution of the central and southeastern Canadian Cordillera: Exploring links across the orogen: Geological Society of America, Special Paper **433**: 117–145.

Gabrielse, H., 1985. Major dextral transcurrent displacements along the Northern Rocky Mountain Trench and related lineaments in north-central British Columbia: Geological Society of America Bulletin, **96**: 1-14.

Gabrielse, H. 1991, Late Paleozoic and Mesozoic terrane interactions in north-central British Columbia: Canadian Journal of Earth Sciences, **28**: 947-957.

Gabrielse, H., 1994. Geology of Dease Lake (104J/E) and Cry Lake (104I) map areas, north central British Columbia: Geological Survey of Canada, Open File 2779.

Gabrielse, H. 1998. Geology of Dease Lake (104J) and Cry Lake (104I) map areas, north-central British Columbia: Geological Survey of Canada, Bulletin **504**.

Gabrielse, H., Monger, J.W.H., Wheeler, J.O., and Yorath, C.J. 1991, Part A-Morphogeological belts, tectonic assemblages and terranes, Chapter 2, *in* Gabrielse, H., and Yorath, C.J., eds., Geology of the Cordilleran Orogen in Canada: Geological Survey of Canada, Geology of Canada, no.4:15–28

Gabrielse, H., Murphy, D.C. and Mortensen, J.K. 2006, Cretaceous and Cenozoic dextral orogen-parallel displacements, magmatism and paleogeography, north-central Canadian Cordillera, in Haggart, J.W., Monger, J.W.H., and Enkin, R.J., eds., Paleogeography of the North American Cordillera: Evidence For and Against Large-Scale Displacements: Geological Association of Canada Special Paper **46**: 255-276.

Gehrels, G.E., McClelland, W.C., Samson, S.D., and Patchett, P.J. 1991. U-Pb geochronology of detrital zircons from a continental margin assemblage in the northern Coast Mountains, southeastern Alaska: Canadian Journal of Earth Sciences, **28**: 1285-1300.

Gibson, S.A., Kirkpatrick, R.J., Emmerman, R., Schmincke, P.-H., Pritchard, G., Okay, P.J., Thorpe, R.S., Marriner, G.F. 1982. The trace element composition of the lavas and dykes from a 3 km vertical section through a lava pile of Eastern Iceland: Journal of Geophysical Research, **87**: 6532– 6546.

Gordey, S.P. and Stevens, R.A. 1994. Geology, Teslin, Yukon Territory. Geological Survey of Canada, Open File 2886, 1:250 000 scale.

Gordey, S.P. and Makepeace, A.J. 2001. Bedrock geology, Yukon Territory. Geological Survey of Canada, Open File 3754, 1:1 000 000. *also: Yukon Geological Survey,Open File 2001-1*.

Gordey, S.P., McNicoll, V.J., and Mortenson, J.K. 1998. New U-Pb ages from the Teslin area, southern Yukon, and their bearing on terrane evolution in the northern Cordillera. *In:* Radiogenic age and isotopic studies. Report 11, Geological Survey of Canada, Current Research no 1998-F, p. 129-148.

Gunning, M.H., Hodder, R.W.H., and Nelson, J.L. 2006. Contrasting volcanic styles and their tectonic implications for the Paleozoic Stikine assemblage, western Stikine Terrane, northwestern British Columbia. *In* Paleozoic Evolution and Metallogeny of Pericratonic Terranes at the Ancient Pacific Margin of North America, Canadian and Alaskan Cordillera, M. Colpron and J.L. Nelson (eds.): Geological Association of Canada, Special Paper **45:** 201-227.

Hamilton, W.B. 1979. Tectonics of the Indonesian region. U.S. Geological Survey Professional Paper, **1078**: 345 pp.

Hart, C.J.R. 1995. Magmatic and tectonic evolution of the Intermontane Superterrane and Coast Plutonic Complex in southern Yukon Territory. unpublished M.Sc. thesis, The University of British Columbia, 198 p.

Hart, C. J. R. 1997. A Transect Across Northern Strikinia: Geology of the Northern Whitehorse Map Area, Southern Yukon Territory (105D/13-16), Canada. Dept. of Indian Affairs Northern Development. Exploration Geological Services Division, Yukon Region.

Hart, C.J.R. and Radloff, J.K. 1990. Geology of the Whitehorse, Alligator Lake, Fenwick Creek, Carcross and part of Robinson map areas (105D/11,6,3,2&7),Yukon Territory. Exploration and Geological Services Division, Yukon Region, Indian and Northern Affairs Canada, Open File 1990-4, 113 p.

Helwig, J. 1974. Eugeosynclinal basement and a collage concept of orogenic belts. In Modern and Ancient Geosynclinal Sedimentation. Edited by Dott, R. H., Jr. and R. H. Shaver: Society of Economic Paleontologists and Mineralogists, Special Publication **19**: 359-380.

Ingersoll, R. V. 1978, Petrofacies and Petrologic Evolution of the Late Cretaceous Fore-Arc Basin, Northern and Central California: The Journal of Geology, **86**: 335-352.

Ingersoll, R. V. Fullard, T. F., Ford, R. L., Grimm, J. P., Pickle, J. D., and Sares, S. W., 1984, The effect of grain size on detrital modes; a test of the Gazzi-Dickinson point-counting method: Journal of Sedimentary Research, **54**: 103-116.

Jackson, J.L. 1992, Tectonic analysis of the Nisling, northern Stikine and northern Cache Creek Terranes, Yukon and British Columbia; unpublished Ph.D. thesis, *The University of Arizona*, Tucson, 200 pages.

Jackson, J. L., Gehrels, G. E., Patchett, P. J., and Mihalynuk, M. G. 1991, Stratigraphic and isotopic link between the northern Stikine terrane and an ancient continental margin assemblage, Canadian Cordillera: Geology, **19**: 1177-1180.

Jaffey, A.H., Flynn, K.F., Glendenin, L.E., Bentley, W.C., and Essling, A.M. 1971, Precision measurements of half-lives and specific activities of 235U and 238U, Physical Review C, 4:1889-1906.

Kobayashi, F. 1999, Tethyan uppermost Permian (Dzhulfian and Dorashamian) foraminiferal faunas and their paleogeographic and tectonic implications: Palaeogeography, Palaeoclimatology, Palaeoecology, **150**: 279-307.

Lallemand, S., Culotta, R., and Von Huene, R. 1989, Subduction of the Daiichi Kashima Seamount in the Japan Trench: Tectonophysics, **160**: 231-247.

LeBas, M.J., LeMaitre, R.W., Steckeisen, A., and Zanettin, B. 1985, A chemical classification of volcanics based on the total alkali-silica diagram: Journal of Petrology, **27**: 745-750.

Long, D. G. F. 2005. Sedimentology and hydrocarbon potential of fluvial strata in the Tantalus and Aksala formations, northern Whitehorse Trough, Yukon: Yukon Exploration and Geology 2005, p. 9.

Love, D.A., Clark, A.H., Hodgon, C.J., Mortensen, J.K., Archibald, D.A., and Farrar, E. 1998. The timing of adularia-sericite-type mineralization and alunite–kaolinite-type alteration, Mount Skukum epithermal gold deposit, Yukon Territory, Canada, 40Ar-39Ar and U–Pb geochronology: Economic Geology, **93**: 437–462.

Lowey, G. W. 2004. Sedimentology, stratigraphy and source rock potential of the Richthofen formation (Jurassic), northern Whitehorse Trough. In: Yukon Exploration and Geology 2004, D.S. Edmond, L.L. Lewis and G.D. Bradshaw (eds.), Yukon Geological Survey: 177-191.

Lowey, G. W., Long, D. G. F., Fowler, M. G., Sweet, A. R., and Orchard, M. J. 2009. Petroleum source rock potential of Whitehorse trough: a frontier basin in south central Yukon: Bulletin of Canadian Petroleum Geology, **57**: 350-386.

Ludwig, K.R. 2003, User's Manual for Isoplot 3.00. Berkeley Geochronology Center: Berkeley, CA, 70 p.

Mathews, W.H. and Watson, K.D. 1953. Spherulitic alkali rhyolite dikes in the Atsutla Range, northern British Columbia: American Mineralogist, **38**: 432–447.

Mattinson, J.M. 2005, Zircon U-Pb chemical abrasion ("CA-TIMS") method: combined annealing and multi-step partial dissolution analysis for improved precision and accuracy of zircon ages: Chemical Geology, **220**: 47-66.

McClelland, W.C. 1992, Permian and older rocks of the southwestern Iskut River map area, northwestern British Columbia: Current research, part A. Geological Survey of Canada, Paper, p. 303-307.

Mihalynuk, M.G. 1999. Geology and mineral resources of the Tagish Lake area (NTS 104M/8,9,10E, 15 and 104N/12W), Northwestern British Columbia. BCGS Bulletin 105, p. 293.

Mihalynuk, M. G., Smith, M. T., Gabites, J. E., Runkle, D. and Lefebure, D. 1992, Age of emplacement and basement character of the Cache Creek terrane as constrained by new isotopic and geochemical data: Canadian Journal of Earth Sciences, **29**: 2463-2477.

Mihalynuk, M. G., Nelson, J., and Diakow, L. J. 1994. Cache Creek Terrane entrapment; oroclinal paradox within the Canadian Cordillera: Tectonics, **13**: 575-595.

Mihalynuk, M. G., Erdmer, P., Ghent, E.D., Archibald, D.A., Friedman, R.M., Cordey, F., Johannson, G.G., and Beanish, J. 1999. Age constraints for emplacement of the northern Cache Creek terrane and implications of blueschist metamorphism: Geological Fieldwork 1998, 1: p. 14.

Mihalynuk, M. G., Johnston, S.T., English, J.M., Cordey, F., Villeneuve, M.E., Rui, L., and Orchard, M.J. 2003. Atlin TGI, Part II: Regional geology and mineralization of the Nakina area (NTS 104N/2W and 3). In: Geological fieldwork 2002; British Columbia Ministry of Energy and Mines: 9–37.

Mihalynuk, M. G., Erdmer, P., Ghent, E. D., Cordey, F., Archibald, D. A., Friedman, R. M., and Johannson, G.G. 2004. Coherent French Range blueschist: Subduction to exhumation in <2.5 m.y.?: Geological Society of America Bulletin, **116**: 910-922.

Miller, M. M. 1987. Dispersed remnants of a northeast pacific fringing arc: Unpper Paleozoic terranes of Permian McCloud faunal affinity: Western U.S. Tectonics, **6**: 807-830.

Miskovic, A. and Francis. D. 2004. The Early Tertiary Sifton Range volcanic complex, southwestern Yukon. In: Yukon Exploration and Geology 2003, D.S. Edmond and L.L. Lewis (eds.), Yukon Geological Survey, p. 143-155.

Miyashiro, A., and Shido, F. 1975, Tholeiitic and calc-alkalic series in relation to the behaviors of titanium, vanadium, chromium, and nickel: American Journal of Science, **275**: 265-277.

Monger, J.W.H. 1975. Upper Paleozoic rocks of the Atlin Terrane: Geological Survey of Canada, Paper 74-47, 63 p.

Monger, J.W.H. 1977. Upper Paleozoic rocks of the western Canadian Cordillera and their bearing on Cordilleran evolution: Canadian Journal of Earth Sciences, **14**: 1832-1859.

Monger, J.W.H. and Nokleberg, W.J. 1996. Evolution of the northern North American Cordillera: generation, fragmentation, displacement and accretion of successive North American plate margin arcs. *In* Geology and ore deposits of the American Cordillera. *Edited by* A.R. Coyner and P.L. Fahey. Geological Society of Nevada Symposium Proceedings, Reno–Sparks, Nev., April 1995: 1133–1152

Monger, J.W.H. and Price, R.A. 2002, The Canadian Cordillera: Geology and tectonic evolution: Canadian Society of Exploration Geophysicists Recorder, February 2002: 17–36.

Monger, J.W.H. and Ross, C. A. 1971. Distribution of fusulinaceans in the western Canadian Cordillera: Canadian Journal of Earth Sciences, **8**: 259-278.

Monger, J.W.H., Price, R.A., and Tempelman-Kluit, D. J. 1982. Tectonic accretion and the origin of the two major metamorphic and plutonic welts in the Canadian Cordillera: Geology (Boulder), **10**: 70-75.

Mortimer, N. 1986. Late Triassic, arc-related, potassic igneous rocks in the North American Cordillera: Geology, **14**: 1035-1038.

Nelson, J. L. and Mihalynuk, M. G. 1993, Cache Creek ocean: Closure or enclosure?: Geology, **21**: 173-176.

Nelson, J. L. and Friedman, R. 2004, Superimposed Quesnel (late Paleozoic-Jurassic) and Yukon-Tanana (Devonian-Mississippian) arc assemblages, Cassiar Mountains, northern British Columbia; field, U-Pb, and igneous petrochemical evidence: Canadian Journal of Earth Sciences, **41**: 1201-1235.

Nelson, J., and Colpron, M., 2007, Tectonics and metallogeny of the British Columbia, Yukon and Alaskan Cordillera, 1.8 Ga to the present, *in* Goodfellow, W.D., ed., Mineral Deposits of Canada: A Synthesis of Major Deposit-Types, District Metallogeny, the Evolution of Geological Provinces, and Exploration Methods: Geological Association of Canada, Mineral Deposits Division, Special Publication **5**: 755-791.

Nelson, J.L., Colpron, M., Piercey, S.J., Dusel-Bacon, C., Murphy, D.C. and Roots, C.F. 2006, Paleozoic tectonic and metallogenic evolution of the pericratonic terranes in Yukon, northern British Columbia and eastern Alaska, in Colpron, M. and Nelson, J.L., eds., Paleozoic Evolution and Metallogeny of Pericratonic Terranes at the Ancient Pacific Margin of North America, Canadian and Alaskan Cordillera: Geological Association of Canada, Special Paper, **45**: 323-360.

Nelson, J.L., Colpron, M. and Israel, S. 2013. The Cordillera of British Columbia, Yukon, and Alaska: Tectonics and metallogeny, In Colpron, M., Bissig, T., Rusk, B.G. and Thompson, J.F.H., eds., Tectonics, Metallogeny and Discovery: The North American Cordillera and Similar Accretionary Settings: Society of Economic Geologists, Inc., Special Publication, **17**: 53-103.

Nokleberg, W.J., Parfenov, L.M., Monger, J.W.H., Norton, I.O., Khanchuk, A.I., Stone, D.B., Scotese, C.R., Scholl, D.W. and Fujita, K. 2000. Phanerozoic tectonic evolution of the circum-North Pacific: U.S. Geological Survey Professional Paper 1626, 122 p.

Nokleberg, W.J., Bundtzen, T., Eremin, R.A., Ratkin, V.V., Dawson, K.M., Shpikerman, V.V., Goryachev, N.A., Byalobzhesky, S.G., Frolov, Y.F., Khanchuck, A.I., Koch, R.D., Monger, J.W.H., Pozdeev, A.A., Rozenblum, I.S., Rodionov, S.M., Parfenov, L.M., Scotese, C.R., and Sidorov, A.A. 2005, Metallogenesis and tectonics of the Russian Far East, Alaska and the Canadian Cordillera: U.S. Geological Survey, Professional Paper 1697: 397 p.

Orchard, M. J., Cordey, F., Rui, L., Bamber, E. W., Mamet, B., Struik, L. C., Sano, H., and Taylor, H. J. 2001. Biostratigraphic and biogeographic constraints on the Carboniferous to Jurassic Cache Creek Terrane in central British Columbia: Canadian Journal of Earth Sciences, **38**: 551-578.

Packer, D.R., and Stone, D.B. 1974. Paleomagnetism of Jurassic rocks from southern Alaska, and their tectonic implications: Canadian Journal of Earth Sciences, **11**: 976-997.

Paterson, I. A., and Harakal, J. E. 1974, Potassium-Argon Dating of Blueschists from Pinchi Lake, Central British Columbia: Canadian Journal of Earth Sciences, **11**: 1007-1011.

Pearce, J.A. 1983, Role of the sub-continental lithosphere in magma genesis at active continental margins. In: Hawkesworth, C.J. and Norry, M.J. eds. Continental basalts and mantle xenoliths, Nantwich, Cheshire: 230-249.

Pearce, J., and Peate, D. 1995, Tectonic implications of the composition of volcanic arc magmas: Annual Review of Earth and Planetary Sciences, **23**: 251-286.

Piercey, S. J., Murphy, D. C., Mortensen, J. K. and Creaser, R. A. 2004. Mid-Paleozoic initiation of the northern Cordilleran marginal back-arc basin: Geological, geochemical and neodymium isotopic evidence from the oldest mafic magmatic rocks in Yukon-Tanana terrane, Finlayson Lake district, southeast Yukon, Canada: Geological Society of America Bulletin, **116**: 1087-1106.

Price, R. A., and Charmichael, D. M. 1986, Geometric test for Late Cretaceous–Paleogene intracontinental transform faulting in the Canadian Cordillera: Geology, **14:** 468–471.

Ricketts, B. D., Evenchick, C.A., Anderson, R.G., and Murphy, D.C. 1992, Bowser basin, northern British Columbia: Constraints on the timing of initial subsidence and Stikinia-North America terrane interactions: Geology, **20**: p. 3.

Ruks, T. W., Piercey, S. J., Ryan, J. J., Villeneuve, M. E. and Creaser, R. A. 2006. Mid- to Late Paleozoic K-Feldspar Augen Granitoids of the Yukon Tanana Terrane, Yukon, Canada: Implications for Crustal Growth and Tectonic Evolution of the Northern Cordillera: Geological Society of America Bulletin, **118**: 1212-1231.

Samson, S.D., Patchett, P.J., McClelland, W.C., and Gehrels, G.E. 1991. Nd isotopic characterization of metamorphic rocks in the Coast Mountains, Alaskan and Canadian Cordillera: Ancient crust bounded by juvenile terranes: Tectonics, **10**: 770-780.

Schiarizza, P. 2011, Geology of the Kutcho Assemblage between Kutcho Creek and the Tucho River, Northern British Columbia (NTS 104I/01): Paper - Ministry of Energy, Mines and Petroleum Resources: 99-118.

Schiarizza, P. 2012. Bedrock geology of the upper Kutcho Creek area, parts of NTS 104-I/01, 02: Open-File Report - Geological Survey of Canada, 2012-08

Schiarizza, P. 2013, The Wineglass assemblage, lower Chilcotin River, south-central British Columbia: Late Permian volcanic and plutonic rocks that correlate with the Kutcho assemblage of northern British Columbia. In: Geological Fieldwork 2012, British Columbia Ministry of Energy, Mines and Natural Gas, British Columbia Geological Survey Paper 2013-1: 53-70.

Schmitz, M.D., Schoene, B. 2007, Derivation of isotope ratios, errors and error correlations for U-Pb geochronology using 205Pb-235U-(233U)-spiked isotope dilution thermal ionization mass spectrometric data: Geochemistry, Geophysics, Geosystems, **8**.

Scotese, C.R. 2002, Paleomap project: http://www.scotese.com/earth.htm.

Simard, R. -L. 2003, Geological map of southern Semenof Hills (part of NTS 105E/1,7,8), south-central Yukon (1:50 000 scale). Yukon Geological Survey, Open File 2003-12.

Simard, R-L., Dostal, J., and Roots, C.F. 2003. Development of Late Paleozoic volcanic arcs in the Canadian Cordillera: an example from the Klinkit Group, northern British Columbia and southern Yukon: Canadian Journal of Earth Sciences, **40**: 907–924.

Skinner, J. W., and Wilde, G. L. 1965. Permian biostratigraphy and fusulinid faunas of the Shasta Lake area, northern California, Paleontological Institute, University of Kansas, **6**: 1-98.

Smith, P.L., Tipper, H.W., and Ham, D.M. 2001. Lower Jurassic Amaltheidae (Ammonitina) in North America: paleobiogeography and tectonic implications: Canadian Journal of Earth Sciences, **38**: 1439–1449.

Smith, R. E., and Smith, S. E., 1976, Comments on the use of Ti, Zr, Y, Sr, K, P and Nb in classification of basalt: Earth and Planetary Science Letters, **32**: 114-120.

Souther, J. G. 1977, Volcanism and tectonic environments in the Canadian Cordillera; a second look: Special Paper - Geological Association of Canada, no. 16: 3-24.

Souther, J.G. 1991. Volcanic regimes, Chapter 14. In: Gabrielse, H., and Yorath, C. J. (eds.), Geology of the Cordilleran orogen in Canada: Ottawa. Geological Survey of Canada, Geology of Canada, **4**: 457–490.

Struik, L. C., Schiarizza, P., Orchard, M. J., Cordey, F., Sano, H., MacIntyre, D. G., Lapierre, H., and Tardy, M. 2001. Imbricate architecture of the upper Paleozoic to Jurassic oceanic Cache Creek Terrane, central British Columbia. Canadian Journal of Earth Sciences, **38**: 495-514.

Sun, S.-s., and McDonough, W. F. 1989, Chemical and isotopic systematics of oceanic basalts: implications for mantle composition and processes: Geological Society, London, Special Publications, **42**: 313-345.

Tempelman-Kluit, D.J. 1979. Transported cataclasite, ophiolite and granodiorite in Yukon: Evidence of arc-continent collision: Geological Survey of Canada Paper **79**, 27 pp.

Tempelman-Kluit, D.J. 1984. Geology, Laberge (105E) and Carmacks (105I), Yukon Territory. Geological Survey of Canada, Open File 1101, 1:250 000.

Tempelman-Kluit, D.J. 2009. Geology of Carmacks and Laberge map areas, central Yukon: Incomplete draft manuscript on stratigraphy, structure and its early interpretation (ca. 1986): Geological Survey of Canada, Open File 5982, 399 p.

Thorstad, L.E., and Gabrielse, H. 1986. The Upper Triassic Kutcho Formation, Cassiar Mountains, north-central British Columbia. Geological Survey of Canada, Paper 86-16.

Vogt, P. R., Lowrie, A., Bracey, D. R., and Hey, R. N. 1976. Subduction of aseismic oceanic ridges; effects on shape, seismicity, and other characteristics of consuming plate boundaries: United States. Geological Society of America (GSA) : Boulder, CO, United States.

Watson, K. D. and Mathews, W.H. 1944. The Tuya-Teslin area. British Columbia Department of Mines, Bulletin, **19**: 1-52.

Wernicke, B. and Klepacki, D. W. 1988, Escape hypothesis for the Stikine block: Geology, **16**: 461-464.

Wheeler, J.O. 1961. Whitehorse map-area, Yukon Territory (105D). Geological Survey of Canada, Memoir, 312: 156 p.

Wheeler, J.O. and McFeely, P. 1991, Tectonic assemblage map of the Canadian Cordillera and adjacent parts of the United States of America: Geological Survey of Canada, Map 1712A, 1:2 000 000.

White, D., Colpron, M. and Buffett, G. 2012. Seismic and geological constraints on the structure and hydrocarbon potential of the northern Whitehorse trough, Yukon, Canada: Bulletin of Canadian Petroleum Geology, **60**: 16 p.

Winchester, J.A. and Floyd, P.A. 1977. Geochemical discrimination of different magma series and their differentiation products using immobile elements: Chemical Geology, **20**: 325–343.

Appendix A.

1:50 000 scale Bedrock Geology Map of the Marsh Lake Area

Appendix B.

Petrographic Descriptions and Sample Locations

Notes:

Modal per cent estimates are by area. Sample location UTM coordinates (NAD 83) are listed below **(Easting, Northing)**.

List of abbreviations used: v.f.g., very fine-grained; f.g., fine-grained; m.g., medium-grained; c.g., coarse-grained.

Samples categorized based on units seen in legend of Appendix A.

CACHE CREEK TERRANE

11-LB-011 (539673, 6705610):

Highly fractured, highly altered clast-supported cataclasite (tectonized gabbro). Clasts consist of recrystallized (fibrous?) plagioclase (50%) and minor quartz with pleochroic blue/grey clinochlore (?) throughout. Matrix (30%) consists of opaque material with biotite/sericite between clasts. Within the recrystallized clasts, opaque minerals (10%) are dispersed. Some clasts contain chalcedony quartz (10%). A coarser chalcedony recrystallized variety of quartz infills fractures which are subsequently cut by veins infilled with biotite and opaques.

11-LB-012 (539673, 6705860):

Somewhat altered pyroxene-rich ultramafic. Orthopyroxene (40%) dominates crystal content but most are altered or recrystallized to epidote. Minor clinopyroxene present and opaque minerals are accessory (5%). Matrix (55%) consists of brown mafic glass. Fractures are infilled with calcite. Accessory minerals may include apatite with opaque inclusions and laden with fission tracks.

11-LB-015 (547206, 6693768):

Microcrystalline seriate textured basalt (somewhat trachytic). Plagioclase laths (40%) with polysynthetic twinning vary in size from v.f.g. to f.g. Dispersed throughout are pale brown coloured clinopyroxene (40%) interstitially enclosing plagioclase crystals. Also, interstitially in the section is pleochroic green biotite (10%), mostly altered to chlorite. Matrix (5%) of mafic glass and accessory opaque minerals (5%).

11-LB-027 (539116, 6706198):

M.g. to c.g. intergranular metapyroxenite. Groundmass (50%) shows alteration of dark grey coloured (non-pleochroic), low birefringent clays throughout. Subhedral, altered crystals of clinopyroxene (30%), some replaced by chlorite. Orthopyroxene present less

commonly (10%), and rarely olivine (5%). Accessory minerals include opaque minerals (5%).

11-LB-028 (539559, 6705782):

Cataclastic ultramafic. Altered orthopyroxene (10%), brecciated, clinopyroxene (5%), olivines altered to epidote/chlorite (15%). Opaques (10%), brecciated vein zone infilled with cryptocrystalline quartz and calcite. Matrix (60%) undivided, non-birefringent and grey/green/brown in colour.

11-LB-029 (539497, 6706071):

Glomerophyritic pyroxenite. Coarse clinopyroxene crystals (40%), euhedral to sub-euhedral with polysynthetic and Carlsbad twinning, some show zoning and some show skeletal texture (less commonly altered to chlorite +/- epidote). Groundmass (60%) composed of clinopyroxene, elongate crystals (hornblende), and elongate plagioclase. Accessory minerals are opaques.

11-LB-031 (539699, 6702536):

F.g. to m.g. hypidiomorphic quartz-bearing monzogabbro. Abundant plagioclase (30%), K-feldspar (60%, in places altered to sericite), some pleochroic green epidote (5%) with radial growth and commonly associated with calcite infilling fractures. Quartz present as accessory phases (5%) and, rarely, opaques.

11-LB-033 (544789, 6691255):

Intensely altered ultramafic – most minerals altered to clays, some coarser minerals completely replaced by biotite. Some hornblende remains unaltered (subhedral). C.g. biotite (15%), hornblende (5%). Matrix (80%) composed of hornblende-to-biotite, plagioclase, clays (sericite?), could be f.g. gabbro with xenocrystic hornblende +/- clinopyroxene replaced by biotite. Calcite present replacing minerals as well.

11-LB-035 (544368, 6691433):

M.g. to c.g. listwaenite. Completely altered by CO_3^{2-} , some preservation of epidote crystals (or alteration products?) and opaque minerals. Clear coloured mica with strong birefringence throughout (5%, muscovite, fucite?). Some cryptocrystalline quartz infilling fractures. Some microstructures reveal a shear sense in the fabric. More resistant opaque mineral giving σ-type porphyroclast (sample is unoriented)

11-LB-036 (544348, 6691668):

F.g. to m.g. altered hypidiomorphic gabbro. Sub-to-anhedral plagioclase laths (30%) with polysynthetic twinning. Inclusion laden quartz (10%), anhedral K-feldspar (30%), and minor biotite (5%, from hornblende). Matrix (25%) composed of chlorite, altered feldspar, sericite. Accessory minerals include opaque minerals (5%).

11-LB-039 (543837, 6691831):

Almost completely altered/replaced ultramafic (pyroxenite?). Most minerals replaced by colourless/yellowish clay with weak grey/blue birefringence and sweeping extinction (80%, chlorite?). Some crystals retain crystal shape but are completely replaced (once were olivine/pyroxene?). Some euhedral orthopyroxene present, pleochroic rose-to-clear with medium birefringence (hypersthene?; 10%). Opaque minerals (10%) range from f.g. and v.f.g. to c.g. translucent grains deep red in plane polarized light (rutile?)

12-LB-037 (553912, 6693749)

Brecciated mafic to ultramafic glassy volcanic with abundant CO_3^{2-} alteration. Chlorite alteration throughout as well, particularily in late fractures. Most of the mafic volcanic component is autobrecciated into clasts which are c.g. to m.g. Lithic clasts (100%). Of Lithic clasts: volcanic (70%), carbonate (30%), very altered and clasts are fg to vfg-vitric.

12-LB-118 (543931, 6717396)

Poikiolitic m.g.-c.g. biotite gabbronorite. Groundmass is composed of plagioclase and remaining crystals include bt, clinopyroxene, chlorite and less commonly orthopyroxene. Chlorite alteration occurs throughout (some replacing biotite). Plagioclase (45%), clinopyroxene (30%), biotite (15%), chlorite (10%); Accessory minerals: opaques, orthopyroxene, calcite, apatite.

12-LB-122 (544294, 6718931)

Heavily altered gabbronorite. Heavy calcic sausseritization (carbonate?) and minor chlorite alteration throughout. All that remains of phenocrysts are euhedral to anhedral crystal shapes. These appear to be mostly pyroxene and less commonly olivine. Chlorite in phenocryst/pophyroblast pressure shadows?

12-LB-126 (544883, 6719170)

F.g. to m.g. clinopyroxene gabbro. Sample appears to have a poikiolitic polycrystalline feldspar groundmass. Some augite phenocrysts are larger, more subhedral than the smaller crystals. Some alteration throughout and calcite infilling fractures. Some minor hornblende may be present as well. Chlorite appears to partially and wholly replace some phenocrysts. Feldspar (55%), clinopyroxene (augite) (35%), quartz (8%), hornblende (2%).

12-LB-146 (546215, 6721395):

C.g., highly altered harzburgite. Olivine rich cumulate rock. Remnant olivine crystals either partially or wholly replaced by serpentinite (→ chrysotile? Antigorite?). Mostly completely replaced by brown, low birefringent mineral aggregate (Iddingsite?). Remaining mineral assemblages are dominantly opaque, magnetite, chromite (?) +/-

rutile. Orthopyroxene may be hypersthene (pinkish colour). Olivine (60%), orthopyroxene (30%), opaques (10%).

12-LB-147 (545810, 6722047):

C.g. to v.c.g. cumulate harzburgite (much less altered than 12LB146). Crystals appear to share a cumulate texture and olivine is serpentinized along fractures and crystal contacts. The other dominant mineral is orthopyroxene (most likely enstatite?). Orthopyroxene is locally poikiolitic (encloses olivine) and some appear to have exsolution lamellae (clinopyroxene feature?). Olivine (70%) orthopyroxene (enstatite 30%), accessory: some opaques infill fractures as aggregates (magnetite?) and others appear as cg crystals among ol and orthopyroxene.

12-LB-188 (548321, 6711815):

F.g. amygdaloidal greenstone. Completely altered/replaced f.g. amygdaloidal greenstone. Amygdules completely infilled by chlorite and/or calcite. Groundmass appears to once have been fg crystals (plag?), now replaced by sericite, chlorite +/- brown/dark clays. Other areas infilled with quartz. Veins infilled with either SiO_2 or $CaCO_3$. Entirely chlorite+/-sericite

MARSH LAKE INTRUSIVE COMPLEX

11-LB-024 (532983, 6711901):

F.g. to m.g. ophitic gabbro. Anhedral K-feldspar (40%) makes up the groundmass with altered f.g. subhedral plagioclase laths (25%), subhedral clinopyroxene crystals (10%, altered to chlorite and epidote), olivine (5%) serpentinized and chloritized. Hornblende makes up a fraction (10%, altered) and pleochroic brown biotite (5%). Accessory minerals include opaque minerals (5%) and apatite(?). Fractures infilled with calcite.

12-LB-020 (533698, 6712671):

Porphyritic clinopyroxene-bearing gabbro. Mostly trachytic groundmass of microcrystalline to v.f.g. plagioclase laths which appear to take on an alteration near/around altered phenocrysts (leaching?). Phenocrysts range from m.g. to c.g., are dominantly subhedral to euhedral clinopyroxene. Ghost phenocrysts are completely replaced by epidote and sericite alteration +/- chlorite. Some clinopyroxene show polysynthetic twinning and zoning. Plagioclase (grndmass, 80%), clinopyroxene (20%), accessory minerals include reddish-brown opaques (Rutile?).

12-LB-040 (534638, 6711417):

M.g. intensely altered gabbronorite. Extensively altered cumulate to poikiolitic texture dominantly subhedral to euhedral equigranular crystals of feldspar, clinopyroxene, and minor hornblende. K-Feldspar displays poikiolitic texture, feldspars are completely

sausseritized, epidote alteration occurs throughout (yellow colour = Fe rich). Clinopyroxene shows embayment textures and inclusions at fractures. Plagioclase (completely altered, 50%), Clinopyroxene (30%), Hornblende (10%), K-Feldspar (10%), Accessory: opaques (magnetite?), apatite.

12-LB-045 (533900, 6711297):

M.g. to c.g. porphyritic gabbronorite. Porphyritic; groundmass consists of f.g. to v.f.g. feldspars (plag = anorthite?) with abundant alteration to epidote (?) and sericite. Phenocrysts are dominantly clinopyroxene, some of which are partially or completely altered to epidote. Clinopyroxene crystals are euhedral to subhedral, typically with zoning pattern and embayment + sieve textures. Plagioclase (60%), clinopyroxene (40%), accessory: opaques, alteration products.

12-LB-055 (535273, 6711338):

Porphyritic (m.g.-c.g.) gabbronorite. Porphyritic, groundmass is f.g. to microcrystalline feldspar with epi alteration throughout (+calcite vein). Groundmass also contains opaques. Phenocrysts vary from m.g. to c.g. plagioclase and mg to v.c.g. clinopyroxene. Almost all plagioclase phenos are altered to varying degrees, mostly sausseritic; some remnant zoning and polysynthetic twins are visible → phenos appear as stubby to elongate crystal laths. Clinopyroxene phenos are dominantly euhedral to subhedral, show zoning, normal twinning, are partially to wholly altered to epidote with embayment and sieve texture. Plagioclase (65%), clinopyroxene (35%), Accessory: opaques. Quartz veins overprinted by calcite veins.

12-LB-056 (535577, 6711398):

M.g. to c.g. gabbronorite. Cumulate texture between plagioclase and clinopyroxene. Most feldspar laths are sericitized, displaying sieve texture, but commonly zoning and polysynthetic twinning are still visible. Many clinopyroxene crystals are euhedral to subhedral, display normal twinning, zoning and (less commonly) polsynthetic twinning. Crystals are commonly partially or wholly replaced by epidote, display embayment and vacuolization texture. Some pyroxenes have reaction rims of sericite. Plagioclase (60%), clinopyroxene (40%), Accessory: opaques.

12-LB-214 (532382, 6714423):

Augite phyric granodiorite/basalt. Pyroxene porphyritic basalt (clinopyroxene →augite?). Phenocrysts are dominantly euhedral to subhedral, and occur as singular crystals among groundmass or as aggregates of crystals. Crystal size varies from 0.45mm (diameter down C-axis) to 4.5mm diameter. Crystals are relatively unaltered with the exception of a couple crystals completely replaced by chlorite. Groundmass contains abundant plagioclase and clinopyroxene (microcrystalline), as well as opaques and chlorite (+/- sausserite?). Clinopyroxene (55%), Plagioclase (45%), accessory: opaques, chlorite. Part of TS shows accumulation of clinopyroxene.

12-LB-217 (534403, 6711078):

F.g. to c.g. inequigranular augite-gabbronorite. Sericitized, cumulate texture shows coarse clinopyroxene phenocrysts, some with embayments among a groundmass of f.g. to m.g. plagioclase feldspar and finer clinopyroxene crystals. Few plag still have polysynthetic twinning but most do show sieve texture. Chlorite appears interstitially, replacing the microcrystalline groundmass. Plagioclase feldspar (75%), clinopyroxene (25%), accessory: opaques and chlorite.

12-LB-229 (531206, 6713606):

M.g. equigranular gabbronorite. Most plagioclase laths are altered and clinopyroxene crystals show concentric zoning and some are replaced by chlorite. Plagioclase (65%), Augite (35%), Accessory: opaques and chlorite.

MICHIE FORMATION (CACHE CREEK TERRANE)

10-MC-049 (549463, 6709262):

C.g. calc-litharenite. Immature, well-sorted calc-lithic sandstone. Carbonate clasts throughout, some replaced by quartz and calcified matrix is predominant. The other main clast content is volcanic, mostly plag rich basalt but other v.f.g. monzonite and granodiorite as well. Chlorite typically seen within fractures but also replaces some minerals within clasts. Elsewhere, chlorite is seen as large grains (~5 mm). Lithic clasts (90%), quartz (5%), feldspar (5%), accessory: opaques, chlorite and calcite (alteration?). Of the Lithic Clasts: Carbonate (55%), Volcanic (43%), sedimentary (2%).

12-LB-059 (537743, 6725023):

Volcanic arenite. Immature, moderately sorted volcaniclastic rock. Clast content is heterogeneous, ranging in size from v.f.g. to c.g. and in composition from detrital quartz to chert and volcanic fragments. Extensively altered. Matrix composed of microcrystalline mafic volcanic/glass material. Clasts also represent altered orthopyroxene, clinopyroxene, metamorphic rocks, as well as chert fragments and calcite infill. Lithic Clasts (90%) Quartz (5%), Feldspar (5%). Of the lithic clasts: volcanic (70%), sedimentary (15%), metamorphic (15%).

12-LB-134 (545614, 6719856):

M.g. to c.g., moderately sorted, submature calclithite (Folk, 1968) or lithic arenite (Dott, 1964). Sandstone/wacke with a calcite rich matrix, calcite may also be replacing minerals within the lithic clasts. Rock is moderately sorted and submature. Lithic clasts include volcanics (mafic), chert, sedimentary, calcareous (mostly recrystallized → maybe some remnant coral fragments? Speckled appearance, dolomite?). Quartz and feldspars are relatively rounded. Lithic clasts (including chert, 75%), quartz (15%), feldspar (10%). Of lithic clasts: sedimentary (60%), volcanic (40%), accessory metamorphic grains.

12-LB-139 (545479, 6718632):

Aphanitic andesite. Phenocrysts are c.g. to v.c.g., quartz and plagioclase. Groundmass is most likely f.g. to v.f.g. plag and looks somewhat altered throughout. Some crystals look euhedral with minor resorption, other (typically the larger) are anhedral with extensive resorption. Plag phenos are altered but still display polysynthetic twinning. Plag (75% - including groundmass), quartz (25%), accessory: red mineral (in PPL and XPL, hematite?).

12-LB-142 (545785, 6719700):

C.g., well-sorted, immature calclithite (lithic arenite). Calcareous sandstone. Clast content is dominantly carbonate clasts followed by lithic and lesser quartz + feldspar. Lithic clasts which are not $CaCO_3$ are dominantly chert and volcanics with lesser metamorphic grains. Grain size is dominantly medium to coarse sand (0.5-0.55 mm). Some calcite may just be cement fill. Lithic clasts (75%), quartz (15%), feldspar (10%), accessory: opaques. Of Lithics: carbonate (60%), sedimentary (20%), volcanic (15%), metamorphic (5%).

12-LB-159 (549342, 6709526):

Moderately sorted, submature f.g.-m.g. carbonate litharenite. Rock has significant lithic clast content as well as rounded to sub-rounded quartz grains with lesser feldspar. Some of the calcite may be cement but a majority are recrystallized carbonate clasts. Lithic clasts are dominantly chert (aside from carbonate) and volcanics (mafic). Some feldspars have zoning with myrmekitic texture in rims, most quartz grains have planar extinction. Lithic clasts (75%), quartz (15%), feldspar (10%). Of Lithic clasts: Sedimentary (carbonate – 50%, chert – 25%), Volcanic (25%), metamorphic clasts appear accessory.

12-LB-173 (549043, 6710068):

Poorly sorted, submature m.g.-c.g. calc-litharenite. Volcanic rich sandstone. Rock is extensively altered to sericite/calcite with minor chlorite throughout. Although calcite is replacing clasts and alteration throughout, there may also be a carbonate clast content. Most quartz present is polycrystalline. Kinknig and deformation in chlorite from compaction (? More likely to be a deformation event?). Lithic Clasts (65%), quartz (15%), chlorite (10%), Feldspar (10%). Of lithic clasts: volcanics (45%), carbonate (40%), metamorphic (10%), chert (5%). Accessory: secondary apatite.

12-LB-181 (548763, 6711204):

Poorly sorted, immature f.g.-v.c.g. volcanic-litharenite (volcaniclastic). Rock is dominantly volcanic clasts with cg angular quartz and plag/feldspar. Alteration is relatively minimal but some feldspars exhibit minor sieve texture. Lithic clasts include volcanics (mafic and felsic?), chert +/- igneous (plag rich?). Minor deformed mica content (chlorite?) appears interstitially between grains. Some lithic grains filled with

rounded quartz inclusions. Lithic clasts (60%), Quartz (20%), plagioclase (20%), accessory: secondary opaques, chlorite, zircon.

12-LB-223 (545387, 6719659):

M.g., poorly sorted, immature volcanic litharenite (volcaniclastic, mafic). Rock has abundant volcanic clasts, angular quartz (planar extinction) and lesser feldspar clasts. Some carbonate clasts but calcic alteration occurs throughout. Prenhite (?) also occurs throughout (alteration). Amphibole occurs as a minor constituent but is extensively altered. Some mafic volcanic glass in situ among clast content. Volcanic lithics (42%), quartz (30%), feldspar (10%), calcareous clasts (10%), opaques (5%), Amphibole (3%), accessory: prenhite?

12-LB-225 (537248, 6725249):

F.g. to m.g. moderately sorted, submature calcareous litharenite (sandstone). Extensive alteration throughout (dominantly $CaCO_3$). Some lithic clasts may be CO_3^{2-} to begin with, along with chert, minor volcanic, sedimentary and metamorphic. One mineral occurs as aggregate clasts and singular colourless, non-pleochroic, blue birefringent, elongate crystals (high relief), cleavage difficult to see (chlorite?). Chlorite occurs normally as alteration (?) throughout. Lithic clasts (85%), feldspar (10%), quartz (5%), accessory: opaques, zircon, rutile(?). Of Lithic clasts: Carbonate (50%), Sedimentary (30%), Metamorphic (15%), volcanic (5%).

12-LB-226 (537360, 6725081):

F.g.-c.g., poorly sorted, submature carbonaceous volcanic wacke. Matrix (f.g.-v.f.g.) appears dominantly volcanic (?). Most feldspar is extensively altered with sieve texture, quartz which is present usually is subrounded with either planar extinction or polycrystalline texture. Clasts of chlorite (m.g.-c.g.) could be from schist source, some appear to host accessory zircon(?) and apatite. Calcite mostly alteration product but also seen recrystallizing carbonate clasts throughout. Lithic clasts (60%), Feldspar (15%), quartz (10%), chlorite (metamorphic clast? 5%), accessory: opaques, zircon, apatite. Of Lithic Clasts: Volcanic (52%), sedimentary (40%), metamorphic (8%).

12-LB-227 (537656, 6724932): Volcanic clast in Michie

Quartz porphyritic rhyolites clast. v.f.g. to c.g. aphyric felsic volcanic. Quartz phenocrysts (c.g.) are mostly resorbed with planar extinction (+ fluid inclusion trails, + some armouring accessory zircon). Groundmass mostly microcrystalline quartz(?) with some feldspar. Other phenocrysts appear completely altered (dark clay?) but some may have been plag and others clinopyroxene (or hornblende?). Quartz (70%), Plagioclase (30%), accessory: opaques, zircon, clinopyroxene?.

CASCA FORMATION (LEWES RIVER GROUP)

12-LB-091 (541636, 6716068):

F.g., well sorted, submature feldspathic arenite. Well sorted, submature feldspar rich sandstone with abundant sericite alteration in matrix. Grain size is overall f.g. sand (0.2 – 0.3 mm). Most feldspar is relatively unaltered, some grains show polysynthetic twinning. Sericite (?) infills most spaces. Of quartz present, some show polycrystalline texture, others with undulose extinction. Relatively minor lithic component. Feldspar (70%), Quartz (20%), Lithic clasts (10%), Accessory: opaques, calcite, zircon, chlorite.

12-LB-113 (543488, 6718688):

Well-sorted, submature, f.g. to m.g. lithic arkose. Well sorted, submature, feldspar rich sandstone, dominantly. Most grains have undergone minor alteration and most feldspars still display twinning. Most hornblende present is intact, however, some are partially or wholly replaced by chlorite. Quartz present can be polycrystalline, but chert fragments are also present. Feldspar (50%), Lithic fragments (30%), Quartz (20%), Accessory: opaques, zircon, muscovite (sericte alteration?).

12-LB-154 (549163, 6709238):

Moderately sorted, immature f.g. to m.g. lithic arkose (sandstone). Rock is relatively heterogeneous clast content from feldspar, quartz, chert, volcanics, hornblende, chlorite, chloritized volcanics, lithics, to minor carbonate clasts and CO3. Appears to be very little interstitial v.f.g. matrix. Most hornblende present are strongly pleochroic green. Feldspar (40%), Lithic (sedimentary and minor volcanic) clasts (35%), Amphibole (15%), Quartz (10%), accessory: opaques, zircon, chlorite, $CaCO_3$.

12-LB-163 (549826, 6708650):

Well sorted, submature m.g.-c.g. lithic arkose sandstone (feldspathic). Most feldspar clasts are somewhat sericitized, other clasts include lithics (mostly sedimentary or volcanic), quartz and some amphibole (hornblende → some of these altered to chlorite). Most lithic grains are well rounded, quartz and feldspar are subangular to subrounded. Plagioclase (40%), K-Feldspar (15%), Lithics (30%), quartz (10%), Amphibole (5%), accessory: opaques, $CaCO_3$. Of Lithic clasts: Volcanic (55%), sedimentary (40%), metamorphic (5%)

1**2-LB-210 (545391, 6705984):**

Moderately sorted, submature, m.g.-c.g. arkosic arenite (sandstone). Altered throughout, affects mostly the matrix, although some clasts of feldspar are partially replaced by calcite and/or chlorite. Other clasts appear to be recrystallized quartz (derived from a quartzite?). Feldspar (45%), Quartz (40%), Lithic clasts (mostly altered, 15%).

LABERGE GROUP

11-LB-018 (543508, 6691500):

Quartz-rich f.g. to m.g. sandstone. Quartz grains (40%) vary in size and are dominantly plain extinctive with some rarer cryptocrystalline extinctions. Matrix (55%) consists of lithic clasts composed mostly of altered feldspars, recycled and recrystallized detrital and volcanic material (+/- biotite and hornblende?). Accessory opaque minerals (5%).

11-LB-040 (543759, 6691826):

Sand to silt sized quartz-feldspar sandstone. Quartz clasts (20%) are anhedral with undulatory extinction and some show syn-kinematic microfractures/fluid inclusion tracts which align with shear fabric. Plagioclase (10%) shows alteration and fragmentation of laths with polysynthetic twinning (most commonly found as f.g. fragments). The matrix (65%) consists primarily of micas that preserve shear fabric, clear in colour and have medium birefringence (sericite?). Matrix also consists of altered feldspar (volcanic fragments?) and rarely amphibole fragments (hornblende?). Accessory minerals include opaque minerals (pyrite?, 5%)

11-LB-045 (574804, 6680965):

F.g.-m.g. volcaniclastic rock. Immature angular quartz grains (15%) with normal extinction (igneous derived). Hornblende grains (15%) pleochroic green/brown and some replaced by chlorite. Plagioclase (5%) altered and replaced by brown coloured, pleochroic hornblende/chlorite(?) with somewhat radial growth. Clinopyroxene (5%) less common. Matrix (60%) includes lithic fragments and abundant chlorite alteration with biotite fragments. Accessory phases include opaque minerals and zircon.

12-LB-011 (544539, 6692913):

F.g. to c.g., poorly sorted arkose sandstone. Angular to sub-rounded grains ranging from f.g. to c.g. plagioclase and K-feldspar(?) with quartz. Most feldspar have sieve texture and vacuolization but albite twinning still visible. Alteration is dominantly to chlorite with some sericite alteration (+biotite, may be authigenic?). Quartz and lithic clasts are typically larger and more immature. More mafic portions see chlorite alteration and minor amphibole (?) content completely altered with matrix sericitized. Plagioclase (40%), Quartz (35%), K-Feldspar (Orthoclase, 15%), Lithic Clasts (10%); accessory include zircon, opaques (magnetite?), amphibole.

12-LB-031 (545642, 6692200):

Moderately sorted, v.f.g. to m.g. submature feldspathic litharenite. Clast composition is relatively heterogeneous, but significant lithic clast content indicates a feldspathic litharenite. Calcite appears as alteration throughout and dominates the groundmass, along with epidote and chlorite alteration, plus presence of biotite (authigenic?). Some quartz with cryptocrystalline texture. Lithic clasts (40%), K-feldspar (mix of Orthoclase

and Sanidine 20%), quartz (10%), biotite (5%), plagioclase (8%), Hornblende (7%). Accessory minerals: opaques, apatite, zircon.

12-LB-087 (541412, 6714731):

F.g. to m.g. feldspathic litharenite. Submature, moderately sorted sandstone with a majority of clast content being angular to sub-angular quartz grains and dominantly volcanic to sedimentary lithic fragments. Matrix and grains have sericite plus minor epidote (?) and chlorite alteration. Sericitized feldspar grains show sieve texture and some remaining polysynthetic twinning throughout. Grain sizes are fine to medium, some quartz fragments are cryptocrystalline, others are actually chert (counted as lithic), matrix is f.g. to v.f.g. sediment. Lithic (45%), Quartz (30%), Orthoclase (15%), Plagioclase (10%). Of Lithics: Volcanic (80%), sedimentary (includes chert, 20%). Accessory: opaques, mica (biotite), calcite, zircon +/- hornblende fragments.

12-LB-111 (542661, 6718611):

Poorly sorted, immature volcanic litharenite. Lithic fragments are most common, matrix appears mostly volcanic, containing feldspar, quartz, hornblende, biotite (minor); some grains angular, others rounded. Most volcanic grains have euhedral outline, except quartz (which looks resorbed in most places). Most feldspars have a well defined polysynthetic twinning, volcanic matrix looks dominantly mafic. Rock fragments (50%), Feldspar (35%), Quartz (10%), Hornblende (5%). Of lithic clasts: volcanic/igneous (80%), sedimentary (15%), metamorphic (5%), accessory: opaques, abundant volcanic minerals throughout.

12-LB-186 (546317, 6712937):

Moderate to poorly sorted, immature, f.g. to m.g. lithic arkose sandstone. Rock also contains, to a lesser extent(?), quartz, lithic clasts and hornblende. Some minor alteration of feldspars (mostly angular) throughout, quartz dominantly has planar extinction and is rounded to subangular. Matrix is relatively minor, but some compaction evident between grains. Lithic clasts include volcanics, minor chert, and minor metamorphic (polycrystalline quartz). Feldspar (45%), quartz (30%), Lithic clasts (20%), and hornblende (5%), accessory: opaques and zircon.

12-LB-220 (548209, 6708340):

C.g., well sorted, submature feldsarenite (arkose). Rock dominantly contains feldspar with minor lithic clasts and quartz. Chlorite appears to be replacing volcanic grains (amphibole? pyroxene?) throughout. Most feldspars show sieve texture and sericitization. Plagioclase (50%), K-Feldspar (35%), Lithics (10%), quartz (5%), accessory: opaques.

WHITEHORSE SUITE

11-LB-023 (532258, 6712952):

Porphyritic hornblende basalt. M.g. to c.g. hornblende crystals showing zonation and Carlsbad twinning (35%), clear in plane-polarized light. Some of these crystals are partially resorbed, some are partially or wholly replaced by chlorite. Groundmass (60%) consists of microcrystalline plagioclase, elongate green-coloured crystals (hornblende-to-chlorite?), and opaques. Accessory minerals include m.g. opaque sulphides (pyrite?; 5%)

11-LB-014 (540224, 6704889):

Holocrystalline, m.g.-c.g., hypidiomorphic inequigranular diorite. Somewhat altered, Carlsbad twinned oligoclase (60%) with sieve texture and replacement by clays (sericite?). Clinopyroxene (10%) throughout, some with rims altered to amphibole. Amphiboles (10%) in rock include actinolite which has grown with radially fibrous texture. Some olivine and orthopyroxene crystals are intensely altered to chlorite throughout (5%) and rimmed by pleochroic brown hornblende. Interstitial orthopyroxene (10%) can be seen enveloping oligoclase crystals. Acessory minerals include opaques (5%).

12-LB-078 (538406, 6722230):

Biotite-quartz-monzonite. C.g. to v.c.g. equigranular rock dominated by anhedreal K-feldspar and plagioclase. Relatively unaltered, some plagioclase laths show sieve texture as well as polysynthetic twinning. Quartz (anhedral) occurs throughout the section and is typically loaded with fluid inclusion tracks. Other major mineral is biotite, but chlorite appears as well (rare- alteration of biotite?). K-Feldspar (35%), Plag (40%), Quartz (20%), Biotite (5%). Accessory: opaques, zircon.

ALKALINE INTRUSION

12-LB-211 (544768, 6705316):

Pegmatitic biotite-muscovite-syenite. Pegmatitic biotite and muscovite (phlogopite?) bearing syenite. Feldspars are somewhat altered throughout with minor sieve texture (sausserite?) but polysynthetic and normal twinning is still visible. Crystals are largely hypidiomorphic (?); some micas may be the result of alteration of brown/dark amphibole. Orthoclase (57%), Plagioclase (20%), muscovite (15%), biotite (8%), accessory, opaques.

UNKNOWN VOLCANICS (EOCENE?)

11-LB-044 (548486, 6712015):

F.g. dacite, strongly overprinted and altered by carbonaceous alteration. Very little remains unaltered, some quartz crystals and plagioclase being replaced by calcite. Veins infilled with calcite and cryptocrystalline quartz. Microcrystalline opaque mineralization dispersed throughout and especially concentrated in veins. Some altered orthopyroxene may be present as well (?).

12-LB-112 (542989, 6718604):

F.g. quartz-hornblende-monzogabbro. Sample is altered throughout with extensive chlorite alteration and colourless birefringent blue mineral (epizoisite?). Most feldspars are partially or wholly sausseritized (?). Most amphiboles are subhedral with reaction rims. Growth appears interstitial and crystallization is relatively rapid. Feldspar (40%), Hornblende (40%), Epi (15%), Quartz (5%), accessory: opaques.

12-LB-117 (543837, 6717658):

Spherulitic alkali feldspar rhyolites. Alkali-feldspar spheruoles typically grow around smaller crystals of quartz or feldspar and often show myrmekitic intergrowths near nuclei. These dominate the section, while vugs are filled with quartz, feldspar, acicular mineral (musc?) and in the cores of vugs (sometimes), hematite (?). Alkali feldspar (80%), Quartz (15%), Musc (sericite? 5%).

Appendix C.

Geochronology Methods: LA-ICPMS

Zircon grains were separated from rocks using standard techniques and annealed at 900^{o}C for 60 hours in a muffle furnace. They were mounted in epoxy and polished until the centers of the grains were exposed. Cathodoluminescence (CL) images were obtained with a JEOL JSM-1300 scanning electron microscope and Gatan MiniCL. Zircon was analyzed by laser ablation inductively coupled plasma mass spectrometry (LA-ICPMS) using a ThermoElectron X-Series II quadrupole ICPMS and New Wave Research UP-213 Nd:YAG UV (213 nm) laser ablation system. In-house analytical protocols, standard materials, and data reduction software were used for acquisition and calibration of U-Pb dates and a suite of high field strength elements (HFSE) and rare earth elements (REE). Data were collected from two samples in two sessions conducted in May 2011 (session 1, sample 10MC049) and March 2013 (session 2, sample 12LB220). Zircon grains were ablated with a laser spot of 25 µm diameter using fluence and pulse rates of 5 J/cm^2 and 5 Hz (session 1) or 10 Hz (session 2), respectively, during a 45 second analysis (15 sec gas blank, 30 sec ablation) that excavated a pit ~25 µm deep. Ablated material was carried by a 1.2 L/min He gas stream to the nebulizer flow of the plasma. Dwell times for experiment 1 were 5 ms for Si and Zr, 100 ms for ^{49}Ti and ^{207}Pb, 40 ms for ^{202}Hg, ^{204}Pb, ^{206}Pb, ^{208}Pb, ^{238}U, ^{232}Th and 10 ms for all other HFSE and REE. Dwell times for session 2 were 5 ms for Si and Zr, 200 ms for ^{49}Ti and ^{207}Pb, 80 ms for ^{238}U and ^{206}Pb, 40 ms for ^{232}Th, ^{202}Hg, ^{204}Pb, ^{208}Pb, and 10 ms for all other HFSE and REE. Background count rates for each analyte were obtained prior to each spot analysis and subtracted from the raw count rate for each analyte. Ablations pits that appear to have intersected glass or mineral inclusions were identified by time-resolved data that show large fluctuations in Ti or P, and were rejected. Similarly, pits that appear contaminated by common Pb were rejected based on an intensity of mass 204 above baseline. For concentration calculations, background-subtracted count rates for each analyte were internally normalized to ^{29}Si and calibrated with respect to NIST SRM-610 and -612 glasses as the primary standards. Temperature was calculated from the Ti-in-zircon thermometer (Watson et al., 2006). Because there are no constraints on the activity of TiO_2 in the source rocks, an average value in crustal rocks of 0.6 was used.

For U-Pb and ^{207}Pb/^{206}Pb dates, instrumental fractionation of the background-subtracted ratios was corrected and dates were calibrated with respect to interspersed measurements of the Plesovice zircon standard (Sláma et al., 2008). Two analyses of Plesovice were done for every 10 analyses of unknown zircon; a polynomial fit to the standard analyses yields each sample-specific fractionation factor. Signals at mass 204 were indistinguishable from zero following subtraction of mercury backgrounds measured during the gas blank (<1000 cps 202Hg), and thus dates are reported without common Pb correction. Radiogenic isotope ratio and age error propagation for all analyses includes uncertainty contributions from counting statistics and background subtraction. For spot analyses that are individually interpreted (e.g., detrital zircon analyses), the uncertainty from the standard calibration is propagated into the error on each date. This uncertainty is the standard deviation of the time-varying U/Pb fractionation factor and the standard error of the mean of the time-invariant, smaller

$^{207}Pb/^{206}Pb$ fractionation factor. For groups of analyses that are collectively interpreted from a weighted mean date, a weighted mean date is first calculated using Isoplot 3.0 (Ludwig, 2003) using errors on individual dates that do not include the standard calibration uncertainties, and then the standard calibration uncertainty is propagated into the error on the weighted mean date. Standard calibration uncertainties for $^{207}Pb/^{206}Pb$ dates are 0.7 and 0.5% (2σ) for sessions 1 and 2, respectively. Standard calibration uncertainty for $^{206}Pb/^{238}U$ dates are 2.0 and 3.2% (2σ for experiments 1 and 2, respectively. Age interpretations are based on $^{206}Pb/^{238}U$ dates. Errors on the $^{207}Pb/^{206}Pb$ and $^{206}Pb/^{238}U$ dates from individual LA-ICPMS analyses are given at 2σ, as are the errors on the weighted mean dates.

Two zircon secondary reference materials were treated as unknowns to assess accuracy, interspersed as groups of two analyses for every 20 unknown analyses. FC1 zircon (1098 Ma from unpublished chemical abrasion thermal ionization mass spectrometry (CA-TIMS) data, Boise State University) yielded weighted mean $^{207}Pb/^{206}Pb$ dates of 1086 ± 13 (MSWD=0.6, n=25) and 1100 ± 15 (MSWD=1.6, n=8) from sessions 1 and 2, respectively. Weighted mean $^{206}Pb/^{238}U$ dates are 1120 ± 22 Ma (MSWD=1.0, n=22), and 1102 ± 35 (MSWD=0.4, n=8) from sessions 1 and 2, respectively. Seiland zircon (530 Ma from unpublished CA-TIMS data, Boise State University) yielded a weighted mean $^{206}Pb/^{238}U$ dates of 515 ± 18 (MSWD=1.5, n=6) from session 2. These results show that accurate $^{207}Pb/^{206}Pb$ and $^{206}Pb/^{238}U$ dates were obtained.

References:

Ludwig, K.R., 2003, User's Manual for Isoplot 3.00. Berkeley Geochronology Center: Berkeley, CA, 70 p.

Sláma, J., Košler, J, Condon, D.J., Crowley, J.L., Gerdes, A., Hanchar, J.M., Horstwood, M.S.A., Morris, G.A., Nasdala, L., Norberg, N., Schaltegger, U., Schoene, B. Tubrett, M.N, Whitehouse, M.J. 2008. Plešovice zircon — A new natural reference material for U–Pb and Hf isotopic microanalysis. Chemical Geology, **249**: 1-35.

Watson EB, Wark DA, Thomas JB (2006) Crystallization thermometers for zircon and rutile, Contributions to Mineral Petrology, **151**: 413–433.

Appendix D.

Geochronology Methods: CA-TIMS

U-Pb dates were obtained by chemical abrasion isotope dilution thermal ionization mass spectrometry (CA-TIMS) on single zircon grains (Table 4). Zircon grains were separated from rocks using standard techniques and mounted in epoxy and polished until the centers of the grains were exposed. Cathodoluminescence (CL) images were obtained with a JEOL JSM-1300 scanning electron microscope and Gatan MiniCL. Zircon was removed from the epoxy mounts and subjected to a modified version of the chemical abrasion method of Mattinson (2005), reflecting analysis of single grains or fragments of grains. Grains or fragments of grains were selected for dating based on CL images.

Zircon grains were placed in a muffle furnace at 900°C for 60 hours in quartz beakers. Single grains were then transferred to 3 ml Teflon PFA beakers and loaded into 300 µl Teflon PFA microcapsules. Fifteen microcapsules were placed in a large-capacity Parr vessel, and the crystals partially dissolved in 120 µl of 29 M HF for 12 hours at 180°C. The contents of each microcapsule were returned to 3 ml Teflon PFA beakers, the HF removed and the residual grains immersed in 3.5 M HNO3, ultrasonically cleaned for an hour, and fluxed on a hotplate at 80°C for an hour. The HNO_3 was removed and the grains were rinsed twice in ultrapure H_2O before being reloaded into the same 300 µl Teflon PFA microcapsules (rinsed and fluxed in 6 M HCl during sonication and washing of the grains) and spiked with the Boise State University mixed ^{233}U-^{235}U-^{205}Pb tracer solution. These chemically abraded grains were dissolved in Parr vessels in 120 µl of 29 M HF with a trace of 3.5 M HNO_3 at 220°C for 48 hours, dried to fluorides, and then re-dissolved in 6 M HCl at 180°C overnight. Uranium and Pb were separated from the zircon matrix using a HCl-based anion-exchange chromatographic procedure (Krogh, 1973), eluted together and dried with 2 µl of 0.05 N H_3PO_4.

Lead and U were loaded on a single outgassed Re filament in 5 µl of a silica-gel/phosphoric acid mixture (Gerstenberger and Haase, 1997), and U and Pb isotopic measurements made on a GV Isoprobe-T multicollector thermal ionization mass spectrometer equipped with an ion-counting Daly detector. Pb isotopes were measured by peak-jumping all isotopes on the Daly detector for 100 to 160 cycles, and corrected for 0.18 ± 0.03%/a.m.u. (1 sigma error) mass fractionation. Transitory isobaric interferences due to high-molecular weight organics, particularly on ^{204}Pb and ^{207}Pb, disappeared within approximately 30 cycles, while ionization efficiency averaged 104 cps/pg of each Pb isotope. Linearity (to ≥1.4 x 106 cps) and the associated deadtime correction of the Daly detector were monitored by repeated analyses of NBS982, and have been constant since installation. Uranium was analyzed as UO_2^+ ions in static Faraday mode on 1011 ohm resistors for 200 to 250 cycles, and corrected for isobaric interference of $^{233}U^{18}O^{16}O$ on $^{235}U^{16}O^{16}O$ with an $^{18}O/^{16}O$ of 0.00206. Ionization efficiency averaged 20 mV/ng of each U isotope. Uranium mass fractionation was corrected using the known $^{233}U/^{235}U$ ratio of the Boise State University tracer solution.

Weighted mean $^{206}Pb/^{238}U$ dates were calculated from equivalent dates using Isoplot 3.0 (Ludwig, 2003). Errors on the weighted mean $^{206}Pb/^{238}U$ date are the internal

errors based on analytical uncertainties only, including counting statistics, subtraction of tracer solution, and blank and initial common Pb subtraction. They are given at the 2σ confidence interval. These errors should be considered when comparing our dates with $^{206}Pb/^{238}U$ dates from other laboratories that used the same Boise State University tracer solution or a tracer solution that was cross-calibrated using EARTHTIME gravimetric standards. When comparing our dates with those derived from other geochronological methods using the U-Pb decay scheme (e.g., laser ablation ICPMS), a systematic uncertainty in the tracer calibration should be added to the internal error in quadrature. When comparing our dates with those derived from other decay schemes (e.g., $^{40}Ar/^{39}Ar$, ^{187}Re-^{187}Os), systematic uncertainties in the tracer calibration and ^{238}U decay constant (Jaffey et al., 1971) should be added to the internal error in quadrature. These errors are given as $^{206}Pb/^{238}U$ date ± x / y / z Ma, where x is the internal error, y includes the uncertainty in the tracer calibration, and z includes the uncertainties in the tracer calibration and ^{238}U decay constant. Errors on the $^{206}Pb/^{238}U$ dates from individual grains are also given at the 2σ confidence interval.

U-Pb dates and uncertainties were calculated using the algorithms of Schmitz and Schoene (2007), $^{235}U/^{205}Pb$ of 77.93 and $^{233}U/^{235}U$ of 1.007066 for the Boise State University tracer solution, and U decay constants recommended by Jaffey et al. (1971). $^{206}Pb/^{238}U$ ratios and dates were corrected for initial ^{230}Th disequilibrium using a Th/U[magma] = 3.0 ± 0.3 using the algorithms of Crowley et al. (2007), resulting in an increase in the $^{206}Pb/^{238}U$ dates of ~0.09 Ma. All common Pb in analyses was attributed to laboratory blank and subtracted based on the measured laboratory Pb isotopic composition and associated uncertainty. Uranium blanks are difficult to precisely measure, but are estimated at 0.07 pg.

Seven aliquots of the EARTHTIME 100 Ma synthetic solution were measured during this experiment using the Boise State University tracer solution and the same mass spectrometry methods described above. Each aliquot was 4-6 pg of radiogenic Pb, slightly smaller than the average analysis measured during the experiment. The weighted mean $^{206}Pb/^{238}U$ and $^{207}Pb/^{235}U$ dates are 100.08 ± 0.03 / 0.10 and 100.04 ± 0.13 / 0.16 Ma, respectively. These dates agree with the known dates determined by analysis of large aliquots measured with the EARTHTIME mixed ^{233}U-^{235}U-^{202}Pb-^{205}Pb tracer solution (D. Condon, unpublished data).

References:

Crowley, J.L., Schoene, B., Bowring, S.A., 2007, U-Pb dating of zircon in the Bishop Tuff at the millennial scale: Geology **35**:1123-1126.

Gerstenberger, H., Haase, G., 1997, A highly effective emitter substance for mass spectrometric Pb isotope ratio determinations: Chemical Geology **136**:309-312.

Jaffey, A.H., Flynn, K.F., Glendenin, L.E., Bentley, W.C., and Essling, A.M., 1971, Precision measurements of half-lives and specific activities of ^{235}U and ^{238}U: Physical Review C, **4**:1889-1906.

Krogh, T.E., 1973, A low contamination method for hydrothermal decomposition of zircon and extraction of U and Pb for isotopic age determination: Geochimica et Cosmochimica Acta **37**:485-494.

Ludwig, K.R., 2003, User's Manual for Isoplot 3.00. Berkeley Geochronology Center: Berkeley, CA, 70 p.

Mattinson, J.M., 2005, Zircon U-Pb chemical abrasion ("CA-TIMS") method: combined annealing and multi-step partial dissolution analysis for improved precision and accuracy of zircon ages: Chemical Geology **220**:47-66.

Schmitz, M.D., Schoene, B., 2007, Derivation of isotope ratios, errors and error correlations for U-Pb geochronology using ^{205}Pb-^{235}U-(^{233}U)-spiked isotope dilution thermal ionization mass spectrometric data: Geochemistry, Geophysics, Geosystems (G^3) 8, Q08006, doi:10.1029/2006GC001492.